

AN ABSTRACT OF THE DISSERTATION OF

Karla M. Jarecke for the degree of Doctor of Philosophy in Forest Ecosystems and Society presented on December 2, 2021.

Title: Spatial Patterns of Soil Moisture and the Relative Importance of Atmospheric Water Demand Versus Soil Moisture Availability in Limiting Late-summer Growth of Douglas-fir Under a Changing Climate

Abstract approved: _____

Steven M. Wondzell

Kevin D. Bladon

The rapid pace of climate change is increasing tree mortality and highlighting the need to improve the mechanistic understanding of plant function under increased water stress. However, the processes that control soil moisture availability in steep mountainous terrain are poorly understood, as are the relative effects of atmospheric and soil conditions that regulate tree water stress. This dissertation describes the factors controlling the spatial patterns and temporal persistence in soil moisture distributions at hillslope scales and how interactions between climate, soils, and hydrology influenced Douglas-fir (*Psuedotsuga menziesii*) water stress in the Pacific Northwest's seasonally dry climate.

In Chapter 2, I tested the influence of topography on soil moisture across steep, highly dissected terrain of an even-aged Douglas-fir forest in the western Cascade Mountains of Oregon. I found that terrain-based metrics were poor predictors of shallow soil moisture whereas soil properties were stronger predictors. These results suggest that the horizontal redistribution of water along topographic gradients is unlikely to influence shallow soil moisture in areas with steep, quick-draining, and deep (> 2 m) soils. Chapter 3 examined how interannual climate variability affects seasonal growth of Douglas-fir. We found that latewood growth decreased

with increasing vapor pressure deficit (VPD) in early summer. In contrast, latewood growth did not appear to be sensitive to the timing of rainfall. Chapter 4 complements Chapter 3 by disentangling the relative effects of VPD and precipitation on Douglas-fir gross primary productivity and transpiration. I found that gross primary productivity showed greater decline with increased VPD than decreased rainfall when varying VPD and rainfall over ranges expected from climate projections for the Pacific Northwest. However, transpiration over the growing season declined significantly with decreased rainfall while cumulative transpiration increased with elevated VPD.

My work has important implications for forest management practices aimed at improving drought resilience in forests. Management choices such as thinning need to be evaluated for their impact both to increased atmospheric aridity and to soil moisture availability. Simply put, thinning forests to reduce competition for soil moisture may not increase drought resilience if either soil moisture is not limiting or if thinning increases canopy exposure to a hotter and drier atmosphere.

©Copyright by Karla M. Jarecke
December 2, 2021
All Rights Reserved

Spatial Patterns of Soil Moisture and the Relative Importance of Atmospheric Water Demand
Versus Soil Moisture Availability in Limiting Late-summer Growth of Douglas-fir Under a
Changing Climate

by
Karla M. Jarecke

A DISSERTATION

Submitted to

Oregon State University

in partial fulfillment of
the requirements for the
degree of

Doctor of Philosophy

Presented December 2, 2021
Commencement June 2022

Doctor of Philosophy dissertation of Karla M. Jarecke presented on December 2, 2021

APPROVED:

Co-Major Professor, representing Forest Ecosystems and Society

Co-Major Professor, representing Forest Engineering, Resources & Management

Head of the Department of Forest Ecosystems and Society

Dean of the Graduate School

I understand that my dissertation will become part of the permanent collection of Oregon State University libraries. My signature below authorizes release of my dissertation to any reader upon request.

Karla M. Jarecke, Author

ACKNOWLEDGEMENTS

Thank you to my advisers, Steve Wondzell and Kevin Bladon. Steve, thank you for your outstanding mentorship, helping me improve as a science writer and communicator, and many great memories of pressing cider. Kevin, thank you for your welcoming me as a member of your lab and helping me become a better writer, colleague, and educator. Thank you to my committee members, Rick Meinzer, Lisa Ganio, Chris Still, and Jeff Hatten. Their support and conversations helped inform my research and made me a better scientist. Thank you to Ariel Muldoon for support with data visualization and statistics, Linnia Hawkins for helping me build foundational skills with modelling, and Andrew Merschel and James Johnston for their guidance with tree ring analysis.

I am grateful for the H.J. Andrews community especially the support from Lina DiGregorio, Michael Nelson, Mark Schulze, Suzanne Remillard, and the many people who helped me in the field and lab. I especially appreciate the hard work and friendship of Adrian Gallo, Aaron Rachels, Ryan Cole, Lauren Roof, Haley Weir, Ellen Luedloff, and Melissa Mauk.

I thank my amazing friends who have made this journey possible. I especially want to thank Allison Swartz for her unwavering support and humor. Thank you to Andrew Hadland for encouraging me throughout graduate school. To Adam Haley and my PhD writing groups, thank you for helping me improve (and enjoy) writing. Thank you to Eric Hunt for his positive attitude and encouragement. Thank you to my friends and colleagues in the College of Forestry who gave me a sense of community including the FEWS Lab, Segura Lab, Hatten Lab, Snell Crew, Jessica Bagley, Michelle Greene, and many others. A big thanks to Adam who brings me so much joy and whose support fueled me through the end of my PhD journey. Finally, I thank my family, especially my parents, whose work ethic inspires me.

CONTRIBUTION OF AUTHORS

In Chapter 2 and 3, Karla M. Jarecke participated in study design, data collection, data analysis, data archival, and writing of the manuscript. Dr. Steve Wondzell and Dr. Kevin Bladon participated in the study design and writing of the manuscript.

For Chapter 4, Karla M. Jarecke participated in the experimental design, modelling, data analysis, and writing of the manuscript. Dr. Linnia Hawkins participated in the modelling and writing of the manuscript. Dr. Steve Wondzell and Dr. Kevin Bladon participated in the experimental design and writing of the manuscript.

TABLE OF CONTENTS

	<u>Page</u>
CHAPTER 1	1
1.1 GENERAL INTRODUCTION	1
1.2 CHAPTER OVERVIEWS	3
1.3 FIGURES	6
1.4 REFERENCES	7
CHAPTER 2 THE INFLUENCE OF LOCAL AND NONLOCAL FACTORS ON SOIL WATER CONTENT IN A STEEP FORESTED CATCHMENT	9
ABSTRACT	10
2.1 INTRODUCTION	11
2.2 SITE DESCRIPTION.....	15
2.3 METHODS.....	16
2.3.1 Topographic Analysis	16
2.3.2 Quantification of Soil Water Content	17
2.3.3 Measurements of Soils and Vegetation.....	18
2.3.4 Data Analysis	21
2.4 RESULTS	23
2.4.1 Nonlocal and Local Controls	23
2.4.2 Persistent Spatial Patterns	25
2.4.3 Variability in Volumetric Water Content.....	26
2.5 DISCUSSION	27
2.5.1 Nonlocal Controls	27
2.5.2 Local Controls.....	30
2.5.3 Temporal Persistence	33
2.5.4 Relationship Between Local Factors and Topographic Metrics	34
2.5.5 Study Limitations and Future Work	37
2.6 CONCLUSIONS	38
2.7 ACKNOWLEDGMENTS AND DATA.....	39
2.8 REFERENCES	40
2.9 FIGURES	48
2.10 TABLES	56

TABLE OF CONTENTS (continued)

	<u>Page</u>
CHAPTER 3 CLIMATE SENSITIVITY OF LATEWOOD GROWTH OF DOUGLAS-FIR IN THE WESTERN CASCADE MOUNTAINS OF OREGON	58
ABSTRACT	58
3.1 INTRODUCTION	60
3.2 METHODS.....	63
3.2.1 Study Site.....	63
3.2.2 Climate Variables and Field Data Collection	63
3.2.3 Lab Processing of Tree Cores	65
3.2.4 Moving Window Analysis	65
3.2.5 Mixed Effects Model	68
3.3 RESULTS	69
3.3.1 Moving Window Analysis to Detect Climate Signals in Latewood Growth.....	69
3.3.2 Differences in Climate-growth Relationship Among Sites	70
3.4 DISCUSSION	71
3.4.1 Latewood Growth Sensitivity to Climate.....	71
3.4.2 Climate-growth Relationships Among Sites.....	74
3.4.3 Timing of Radial Growth Phases and Sensitivity to Climate	75
3.4.4 Study Limitations.....	77
3.5 ACKNOWLEDGMENTS AND DATA.....	79
3.6 REFERENCES	80
3.7 FIGURES	85
3.6 TABLES	91
CHAPTER 4 MODELLING THE EFFECTS OF DECREASED RAINFALL AND INCREASED VAPOR PRESSURE DEFICIT ON DOUGLAS-FIR CARBON AND WATER FLUXES IN A MEDITERRANEAN CLIMATE	92
ABSTRACT	92
4.1 INTRODUCTION	94
4.2 METHODS.....	97
4.2.1 Site Description.....	97
4.2.2 Model Description	98
4.2.3 Model Parameterization and Meteorological Drivers	100

TABLE OF CONTENTS (continued)

	<u>Page</u>
4.2.4 Climate Scenarios	101
4.3 RESULTS	103
4.3.1 Model Agreement with Observations	103
4.3.2 Effects of Increased VPD and Decreased Rainfall	104
4.3.3 Temporal Dynamics of Water Stress with Decreased Rainfall.....	106
4.3.4 Temporal Dynamics of Water Stress with Increased VPD.....	107
4.3.5 Effect of VPD and Rainfall Scenarios on Cumulative GPP and Transpiration	108
4.4 DISCUSSION	110
4.4.1 Effects of Increased VPD vs. Decreased Rainfall on GPP and Transpiration.....	110
4.4.2 Interactive Effects of Increased VPD and Decreased Rainfall on GPP and Transpiration	113
4.5 CONCLUSION.....	115
4.6 ACKNOWLEDGEMENTS.....	116
4.7 REFERENCES	116
4.8 FIGURES	121
4.9 TABLES	129
4.10 APPENDICES	131
CHAPTER 5	133
5.1 SUMMARY OF CONCLUSIONS	133
5.2 REFERENCES	137

LIST OF FIGURES

<u>Figure</u>	<u>Page</u>
FIGURE 1.1 H.J. ANDREWS EXPERIMENTAL FOREST	6
FIGURE 2.1 STUDY AREA	48
FIGURE 2.2 TERRAIN METRICS.....	49
FIGURE 2.3 SEASONAL RELATIONSHIPS	50
FIGURE 2.4 ANTECEDENT RAINFALL	51
FIGURE 2.5 CORRELATIONS BETWEEN TERRAIN METRICS AND SOIL PROPERTIES.....	52
FIGURE 2.6 STANDARD DEVIATION OF AVERAGE RANK.....	53
FIGURE 2.7 STANDARD DEVIATION ACROSS WETNESS STATES	54
FIGURE 2.8 DIFFERENCE IN SOIL WATER CONTENT BETWEEN DEPTHS	55
FIGURE 3.1 SITE MAP	85
FIGURE 3.2 CHRONOLOGY OF BASAL AREA INCREMENT	86
FIGURE 3.3 MOVING WINDOW ANALYSIS	87
FIGURE 3.4 CLIMATE-GROWTH RELATIONSHIPS	88
FIGURE 3.5 MODEL ESTIMATES	89
FIGURE 3.6 RELATIONSHIP BETWEEN SLOPES ESTIMATES AND SITE ATTRIBUTES	90
FIGURE 4.1 SITE MAP	121
FIGURE 4.2 SOIL WATER CONTENT FOR CALIBRATION	122
FIGURE 4.3 CLIMATE SCENARIOS	123
FIGURE 4.4 MONTHLY CLIMATE.....	124
FIGURE 4.5 SOIL WATER CONTENT AND WATER POTENTIAL	125
FIGURE 4.6 TEMPORAL DYNAMICS OF GROSS PRIMARY PRODUCTION AND TRANSPIRATION	126
FIGURE 4.7 CHANGE IN CUMULATIVE GROSS PRIMARY PRODUCTION AND TRANSPIRATION.....	127

LISTER OF FIGURES (Continued)

<u>Figure</u>	<u>Page</u>
FIGURE 4.8 INTERACTIVE EFFECTS OF CLIMATE MODIFICATIONS.....	128

LIST OF TABLES

<u>Table</u>	<u>Page</u>
TABLE 2.1 STATISTICS FOR SOIL AND VEGETATION PROPERTIES	56
TABLE 2.2 DIFFERENCES IN SOIL WATER CONTENT BETWEEN DEPTHS.....	57
TABLE 3.1 RESULTS FROM MOVING WINDOW ANALYSIS	91
TABLE 4.1 MODEL PARAMETERS.....	129
TABLE 4.2 MONTHLY RAINFALL	130
TABLE 4.3 MONTHLY VAPOR PRESSURE DEFICIT AND TEMPERATURE	130

LIST OF APPENDIX FIGURES

<u>Figure</u>	<u>Page</u>
APPENDIX 4.1 SOIL WATER RETENTION CURVE	131
APPENDIX 4.2 MEASURED VERSUS PREDICTED SOIL WATER CONTENT	132

CHAPTER 1

1.1 General Introduction

Increased heat and drought stress from global climate change are causing widespread tree mortality and reducing forest productivity (Allen et al., 2010; Brodribb et al., 2020).

Approximately 65% of water supplied to communities in the western USA originates on forested land (Brown et al., 2008). The timing, amount, and quality of water that is transported from forested headwater streams to downstream river and estuarine ecosystems is inextricably linked to forest vegetation and soils. Thus, if the resulting changes in forest composition and structure from forest die-off are large enough, they are likely to have cascading effects on water resources (Guardiola-Claramonte et al., 2011), and ecosystem services like wood resources, wildlife habitat, and clean water (Anderegg et al., 2012; Dalton et al., 2013).

Drought-related threats to forest health are well-recognized, especially in areas with seasonally dry climates. Thus, forest managers are faced with the urgent task to develop strategies to increase drought resilience and reduce tree water stress across varying topography, soils, climates, and forest types (Grant et al., 2013). However, predicting the consequences of climate change on forest ecosystems remains a major challenge for scientists because the physiological mechanisms that underpin how trees respond to water stress in a heterogeneous forested landscape are not well understood.

Soil moisture availability may be a critical determinant in how a given tree species responds to climate change. Changes in soil moisture available to vegetation over highly dissected terrain may mitigate or intensify the effect of drought in different landscape positions within the same catchment (Hawthorne and Miniati, 2016). In general, increases in soil moisture in downslope positions have been shown to increase growth and transpiration (Adams et al.,

2014; Swetnam et al., 2017). However, few studies have examined the influence of complex topography and associated soil and hydrologic processes on the spatial patterns of soil moisture available to vegetation. Thus, interaction between soils, topography, and climate are poorly understood, as are implications for vegetation growing in different landscape positions (Hoylman et al., 2018).

In addition to soil moisture supply, the atmospheric demand for water (aka atmospheric vapor pressure deficit or VPD) is a critical driver of plant function. However, the relative role of atmospheric versus soil water stress on vegetation productivity and transpiration during periods of water stress remains poorly understood in forest ecosystems (Grossiord et al., 2020). A growing body of evidence suggests that an increase in VPD during warm, dry periods significantly reduces forest productivity even when soil moisture is plentiful (Jiang et al., 2019; Novick et al., 2016). However more studies are needed to examine the relative effect of high atmospheric demand versus soil drought on seasonal growth and physiological water stress in seasonally dry climates. For example, trees are known to have a wide range of strategies to deal with temporary heat and water stress including growing deeper roots, modifying the size of xylem conduits, and adjusting their water use efficiency (Venturas et al., 2017). However, a warmer and drier climate could severely increase water stress in some species while active acclimation may mitigate the impacts of climate change for others (Anderegg et al., 2019).

The overarching goal of this work was to improve our fundamental understanding of the interplay between the physical environment and biotic response of vegetation to improve our ability to predict future change in forest ecosystems in the Pacific Northwest, USA. The dry summer season associated with Mediterranean climates makes the Pacific Northwest (PNW), USA particularly sensitive to projected climate warming. Winters in this region are cool and wet

while summers are warm and dry. Annual precipitation typically exceeds 2000 mm from the coast to the Cascade crest. However, the summer period (June–September) receive less than 10% of the annual rainfall (Daly et al., 2019). The specific objectives of our study were to: (a) determine the factors controlling patterns of soil moisture in topographically complex terrain, (b) examine the time of year when tree growth is most sensitive to climate variability, and (c) disentangle the relative effect of soil vs. atmospheric water stress on gross primary productivity and transpiration. My research took place at the H.J. Andrews Experimental Forest located in the Cascade Mountains in Oregon (Figure 1.1). The Andrews Forest, established in 1948 by the U.S. Forest Service, is an important site for ecohydrology research in the Pacific Northwest. My study watershed (Watershed 1) is characterized by steep, highly dissected hillslopes and, at the time of this study, the overstory was dominated by ~50-year-old Douglas-fir (*Pseudotsuga menziesii*) trees.

1.2 Chapter overviews

In Chapter 2, I examined the influence of topography and soil properties on soil moisture in a steep forested catchment of the H.J. Andrews Experimental Forest in the western Cascade Mountains of Oregon, USA. When soils saturate, excess water may move downslope, leading to more water in hillslope hollows. However, in places where soils do not become saturated, the factors controlling the spatial patterns in soil water availability are less well understood. I designed my study to test if the redistribution of water, following surface topography, controlled the spatial patterns of soil moisture across a steep forested hillslope with well-drained soils. I found that spatial patterns of soil moisture were persistent throughout the year, but the downslope movement of water was not responsible for these patterns because soils were drier in

hillslope hollows and wetter on the intervening ribs. Instead, I found that the amount of water in the soil was primarily controlled by the spatial heterogeneity in soil properties.

Chapter 3 examined how interannual variability in climate influenced latewood growth in the ~50-year-old Douglas-fir trees at my study site in the western Cascade Mountains of Oregon. Climate factors that affect seasonal latewood formation can be different from those that affect earlywood and annual growth (Levesque et al., 2013), and may be important to understanding the vulnerability of Douglas-fir to projected increases in summertime water stress in the Pacific Northwest. We tested the effect of vapor pressure deficit (VPD), relative humidity, temperature, and precipitation on the latewood growth using a moving window analysis to identify the period of time that climate variables were most strongly correlated with latewood growth. We found that Douglas-fir was highly sensitive to the average daytime VPD, relative humidity, and temperature in early summer and less sensitive to the timing and amounts of precipitation. We also found evidence that the sensitivity of latewood growth to VPD differed among hillslope positions and was apparently mediated by soil moisture availability during the summer.

Chapter 4 examined the relative role of atmospheric and soil water stress on Douglas-fir growing on the western Cascade Mountains of Oregon. I used the process-based model of the soil-plant-atmosphere continuum (SPA). Disentangling the role of atmospheric demand and soil moisture deficit on tree growth and tree physiology are critical to understanding the underlying causes of, and potential solutions to, tree water stress. Although other studies have documented the combined effects of soil drought (low plant-available soil water) and atmospheric aridity (high VPD and temperature) on tree function, the independent physiological effect of atmospheric water stress without soil drought has been less explored (Grossiord et al., 2020). We found that the effects of atmospheric drought on carbon assimilation may outweigh the effect of

soil drought in Douglas-fir growing in this region. Climate scenarios showed that transpiration was highly sensitive to decreases in rainfall especially in late spring and early summer (April–June), whereas transpiration was less sensitive to increases in maximum daily VPD during the summer. In contrast, increasing the VPD during summer reduced gross primary productivity much more than did decreasing the total rainfall amount. Our results suggest that elevated VPD, under climate change, is likely to reduce primary productivity in Douglas-fir forests in the Pacific Northwest while simultaneously increasing water loss through transpiration.

1.3 Figures



Figure 1.1 H.J. Andrews Experimental Forest

The H.J. Andrews Experimental Forest is located on the west slopes of the Cascade Mountains near Blue River, Oregon. Our study area in Watershed 1 was characterized by steep, complex terrain. Forty to fifty-year-old Douglas-fir trees dominate the overstory.

1.4 References

- Adams, H.R., Barnard, H.R., Loomis, A.K., 2014. Topography alters tree growth-climate relationships in a semi-arid forested catchment. *Ecosphere* 5, 1–16.
<https://doi.org/10.1890/ES14-00296.1>
- Allen, C.D., Macalady, A.K., Chenchouni, H., Bachelet, D., McDowell, N., Vennetier, M., Kitzberger, T., Rigling, A., Breshears, D.D., Hogg, E.H. (Ted), Gonzalez, P., Fensham, R., Zhang, Z., Castro, J., Demidova, N., Lim, J.H., Allard, G., Running, S.W., Semerci, A., Cobb, N., 2010. A global overview of drought and heat-induced tree mortality reveals emerging climate change risks for forests. *For. Ecol. Manage.* 259, 660–684.
<https://doi.org/10.1016/j.foreco.2009.09.001>
- Anderegg, W.R.L., Anderegg, L.D.L., Huang, C., 2019. Testing early warning metrics for drought-induced tree physiological stress and mortality. *Glob. Chang. Biol.* 25, 2459–2469.
<https://doi.org/10.1111/gcb.14655>
- Anderegg, W.R.L., Kane, J.M., Anderegg, L.D.L., 2012. Consequences of widespread tree mortality triggered by drought and temperature stress. *Nat. Clim. Chang.* 3, 30–36.
<https://doi.org/10.1038/nclimate1635>
- Brodribb, T.J., Powers, J., Cochard, H., Choat, B., 2020. Hanging by a thread? Forests and drought. *Science* (80-.). 368, 261–266. <https://doi.org/10.1126/science.aat7631>
- Brown, T.C., Hobbins, M.T., Ramirez, J.A., 2008. Spatial distribution of water supply in the coterminous United States. *J. Am. Water Resour. Assoc.* 44, 1474–1487.
<https://doi.org/10.1111/j.1752-1688.2008.00252.x>
- Dalton, M.M., Mote, P.W., Snover, A.K. (Eds.), 2013. *Climate change in the Northwest. Implications for our landscapes, waters, and communities.* Washington, DC: Island Press.
- Daly, C., Schulze, M., McKee, W., 2019. Meteorological data from benchmark stations at the HJ Andrews Experimental Forest, 1957 to present. *Long-Term Ecological Research.*
<https://doi.org/10.6073/pasta/c021a2ebf1f91adf0ba3b5e53189c84f>
- Grant, G.E., Tague, C.L., Allen, C.D., 2013. Watering the forest for the trees: An emerging priority for managing water in forest landscapes. *Front. Ecol. Environ.* 11, 314–321.
<https://doi.org/10.1890/120209>
- Grossiord, C., Buckley, T.N., Cernusak, L.A., Novick, K.A., Poulter, B., Siegwolf, R.T.W., Sperry, J.S., McDowell, N.G., 2020a. Plant responses to rising vapor pressure deficit. *New Phytol.* nph.16485. <https://doi.org/10.1111/nph.16485>
- Grossiord, C., Buckley, T.N., Cernusak, L.A., Novick, K.A., Poulter, B., Siegwolf, R.T.W., Sperry, J.S., McDowell, N.G., 2020b. Plant responses to rising vapor pressure deficit. *New Phytol.* <https://doi.org/10.1111/nph.16485>

- Guardiola-Claramonte, M., Troch, P.A., Breshears, D.D., Huxman, T.E., Switanek, M.B., Durcik, M., Cobb, N.S., 2011. Decreased streamflow in semi-arid basins following drought-induced tree die-off: A counter-intuitive and indirect climate impact on hydrology. *J. Hydrol.* 406, 225–233. <https://doi.org/10.1016/j.jhydrol.2011.06.017>
- Hawthorne, S., Miniati, C.F., 2016. Topography may mitigate drought effects on vegetation along a hillslope gradient. *Ecohydrology* 11. <https://doi.org/10.1002/eco.1825>
- Hoylman, Z.H., Jencso, K.G., Hu, J., Martin, J.T., Holden, Z.A., Seielstad, C.A., Rowell, E.M., 2018. Hillslope topography mediates spatial patterns of ecosystem sensitivity to climate. *J. Geophys. Res. Biogeosciences* 123, 353–371. <https://doi.org/10.1002/2017JG004108>
- Jiang, Y., Kim, J.B., Trugman, A.T., Kim, Y., Still, C.J., 2019. Linking tree physiological constraints with predictions of carbon and water fluxes at an old-growth coniferous forest. *Ecosphere* 10. <https://doi.org/10.1002/ecs2.2692>
- Levesque, M., Saurer, M., Siegwolf, R., Eilmann, B., Brang, P., Bugmann, H., Rigling, A., 2013. Drought response of five conifer species under contrasting water availability suggests high vulnerability of Norway spruce and European larch. *Glob. Chang. Biol.* 19, 3184–3199. <https://doi.org/10.1111/gcb.12268>
- Novick, K.A., Ficklin, D.L., Stoy, P.C., Williams, C.A., Bohrer, G., Oishi, A.C., Papuga, S.A., Blanken, P.D., Noormets, A., Sulman, B.N., Scott, R.L., Wang, L., Phillips, R.P., 2016. The increasing importance of atmospheric demand for ecosystem water and carbon fluxes. *Nat. Clim. Chang.* 6, 1023–1027. <https://doi.org/10.1038/nclimate3114>
- Swetnam, T.L., Brooks, P.D., Barnard, H.R., Harpold, A.A., Gallo, E.L., 2017. Topographically driven differences in energy and water constrain climatic control on forest carbon sequestration. *Ecosphere* 8. <https://doi.org/10.1002/ecs2.1797>
- Venturas, M.D., Sperry, J.S., Hacke, U.G., 2017. Plant xylem hydraulics: What we understand, current research, and future challenges. *J. Integr. Plant Biol.* 59, 356–389. <https://doi.org/10.1111/jipb.12534>

CHAPTER 2

THE INFLUENCE OF LOCAL AND NONLOCAL FACTORS ON SOIL WATER CONTENT IN A STEEP FORESTED CATCHMENT

Karla M. Jarecke, Forest Ecosystems and Society, Oregon State University

Kevin D. Bladon, Forest Engineering, Resources, and Management, Oregon State University

Steven M. Wondzell, US Forest Service, Pacific Northwest Research Station

Water Resources Research

<https://agupubs.onlinelibrary.wiley.com/journal/19447973>

Volume 57, Issue 5

<https://doi.org/10.1029/2020WR028343>

Received 9 July 2020

Accepted 20 April 2021

Abstract

Surface topography can influence flow pathways and the location of runoff source areas and water transport in steep headwater catchments. However, the influence of topography on spatial patterns of residual soil moisture is less well understood. We measured soil volumetric water content (VWC) on 14 dates at 0–30 and 30–60 cm depth at 54 sites on a steep, 10-ha north-facing forested slope in the west-central Cascade Mountains of Oregon, USA. Spatial patterns in VWC were persistent over time, and contrary to expectations—VWC at 30–60 cm depth was greater on divergent than convergent slopes, especially during wet periods ($R^2 = 0.27$, $p < 0.001$). Vegetation characteristics were assessed for all VWC monitoring locations and soil properties were determined for 13 locations as local factors that affect spatial patterns in VWC. Mean VWC over all dates was negatively correlated to gravimetric rock content ($R^2 = 0.28$, $p = 0.03$) and positively correlated to water storage at field capacity ($R^2 = 0.56$, $p < 0.01$). The variability in rock content in quick-draining soils influenced soil-water retention, and by extension, created spatially heterogeneous but temporally persistent patterns in VWC. While spatial patterns were persistent, they were not easily explained by surficial topography in a steep, mountainous landscape with rocky, well-drained soils. Further research is needed to understand if combined soil-terrain metrics would be a more useful proxy for VWC than terrain-based wetness metrics alone.

2.1 Introduction

Surface topography is commonly used as a proxy for soil water availability (Swetnam et al., 2017). This stems from our classic understanding that soil water is redistributed and organized in space via lateral and downslope movement of water. This can occur as saturation-excess surface runoff (Grayson et al., 1997; Western et al., 1999) or as subsurface flow along a bedrock-soil interface or an interface between soil horizons (Lin et al., 2006). Consequently, terrain-based wetness metrics are widely used to identify likely runoff flow paths at hillslope and catchment scales (Jencso & McGlynn, 2011; McDonnell et al., 1996). While these projections are commonly used to inform our understanding of streamflow source areas in montane forests (Nippgen et al., 2015), few studies have examined if and how terrain-mediated flow paths impact soil volumetric water content (VWC) available to vegetation in steep, topographically complex terrain (Liang et al., 2017).

The influence of topography on surface and subsurface paths of lateral water movement, or the nonlocal control on VWC (Grayson et al., 1997), depends on overall catchment wetness/seasonality (Ali et al., 2014; Beven & Kirkby, 1979; McNamara et al., 2005), soil permeability (Rinderer et al., 2014), soil depth (Liang & Chan, 2017), and the spatial distribution of bedrock weathering (St. Clair et al., 2015). Nevertheless, the use of terrain-based wetness metrics as a proxy for water availability has become widespread for understanding ecosystem productivity, structure, and photosynthetic activity (Helman et al., 2017; Hoylman et al., 2018; Milledge et al., 2013). Terrain metrics include topographic wetness index (TWI), upslope accumulated area (UAA), Euclidean distance from stream, slope, slope curvature, and topographic position index (TPI). In many instances, these metrics have been useful for predicting VWC in the rooting zone where seasonal subsurface water movement is influenced by

gradients in water potential that follow the surface topography. Terrain-based wetness metrics have also been used to predict catchment wetness in regions where water transport can occur as overland flow (Grayson et al. 1997; Western et al. 1999), and in semi-arid montane ecosystems where subsurface water flow is thought to occur along impermeable boundaries (Gómez-Plaza et al., 2001; Kaiser & McGlynn, 2018; McNamara et al., 2005; Williams et al., 2009). However, surface terrain can be a poor predictor of saturated flow paths where water flows along bedrock topography or within fractured geology, where the bedrock surface does not mirror surface topography (Freer et al., 2002). Further, if soils are deep and well-drained, near-surface soils may not receive laterally redistributed water. In those situations, the spatial patterning of VWC may be more strongly controlled by local factors, such as soil properties and vegetation (Grayson et al., 1997) than by topography.

When soils are dominated by vertical water fluxes, topography may exert considerable control on spatial patterns of VWC by indirectly controlling the organization of soil hydraulic properties and soil thickness (Baggaley et al., 2009; Lin et al., 2006; Pelletier et al., 2013). For example, terrain metrics can explain spatial variability in soil-water retention (Pachepsky and Timlin, 2001), predict soil morphological units with distinct water table regimes (Gannon et al., 2014; Gillin et al., 2015), and dictate permeability and distribution of bedrock fractures (St. Clair et al., 2015). Differences in evapotranspiration along topographic gradients may also create spatial patterns in VWC depending on vegetation species and rooting depths (Fatichi et al., 2015; Gómez-Plaza et al., 2001; Gwak & Kim, 2016; Ivanov et al., 2010; Traff et al., 2014; Tromp-van Meerveld & McDonnell, 2006a).

Understanding the mechanisms by which topography affects variability in VWC is important for future prediction of soil water availability in forest ecosystems. There is strong

evidence that terrain-based wetness metrics can serve as a useful tool for predicting spatial patterns of near-surface VWC if boundary conditions and soil properties permit saturated water transport in shallow soils (Gevaert et al., 2014) or if soil hydraulic properties are mediated by surface topography (Lin et al., 2006). Our knowledge of the topographic controls on VWC was originally developed in a gently sloping grassland (Grayson et al., 1997). Since then, the concept has been extended to forest catchments with moderately sloped terrain (e.g., Kaiser & McGlynn, 2018, average = 10°, Gwak & Kim, 2016, average = 16°, Lin et al., 2006, range = 14–26°, and Penna et al., 2009, range = 12–42°). However, relatively few studies have investigated the controls on soil VWC in forest catchments where the average slope exceeds 30° (e.g., Liang et al., 2017, range = 6–64°, average = 41° and Kim et al., 2007, range = 30–45°). Thus, the degree to which terrain mediates VWC in steep, montane forests remains poorly understood.

Topography may not be useful in predicting near-surface VWC if lateral flow is negligible, if vertical movement via infiltration and evaporation controls soil moisture dynamics in the top meter of soil, or if soil hydraulic properties are not organized along topographic gradients (Hu & Si, 2014). In mountainous regions, high densities of roots and rocks can lead to well-drained, highly permeable soils in which vertical preferential flow dominates (Beven & Germann 1982; Bundt et al. 2001; Liu & Lin 2015; Wiekenkamp et al. 2016). Where soils drain quickly, saturation may be constrained to deeper subsurface soil layers (>1 m) (Zimmer & Gannon, 2018) or in fractured bedrock (Gabielli et al. 2012). Water in forest soil layers below one meter can be a critical water source for vegetation, especially in regions that experience seasonal drought (Rempe & Dietrich, 2018). However, most direct measurement of VWC have occurred in the upper meter of soil due to the difficulty in accessing deeper soil layers. Liang et al. (2017) investigated the influence of topography, soil properties, and vegetation on VWC in

the upper 20 cm of soil in a steep, humid catchment. They found that patterns in VWC were explained by the local saturated hydraulic conductivity of soils and vegetation density where rocky soils were underlain by fractured bedrock.

Understanding the relative effect of local and nonlocal factors can help determine the dominant mechanisms controlling near-surface soil water in steep, mountainous regions. The overall objectives of our study were to test whether common terrain metrics used in catchment scale hydrological models—topographic position index, topographic wetness index, upslope accumulation area, slope, and Euclidean distance from stream—explained the spatial patterns of VWC and how antecedent rainfall and soil depth altered the spatial patterns in VWC.

Specifically, we asked:

1. How do attributes of topography, soils, and vegetation affect VWC across a range of antecedent rainfall amounts?
2. Are there spatial patterns in VWC and are these patterns persistent over time?
3. How does the variability of VWC change as a function of the spatial mean?

We hypothesized that topographic position would control VWC when antecedent rainfall was greatest. Specifically, we postulated that VWC would be greater along convergent slopes compared to divergent slopes due to downslope and lateral flows of water from adjacent areas. Additionally, we assumed this relationship would weaken during dry periods because soil properties and evapotranspiration would have a greater effect on spatial patterns of VWC when soils are below field capacity.

2.2 Site Description

Our study was located in Watershed 1, a 96-ha catchment at the H. J. Andrews Experimental Forest on the west slope of the central Cascade Mountains of Oregon, USA (44°12'18.8" N, 122°15'16.2" W). The average elevation of the study area is 576 m and the average slope is 37 degrees. The study catchment was 100 % clearcut from 1962–1966 and logging residues were burned in 1966 to expose a mineral soil seedbed. There were several efforts to re-establish vegetation in the watershed. The watershed was aerially seeded with Douglas-fir (*Pseudotsuga menziesii*) in 1967 and 10 ha were re-seeded in 1968. In 1969, 2-yr-old Douglas-fir trees were planted across the entire watershed, and in 1971, 40 ha were re-planted with 2- and 3-yr-old trees (Halpern, 1988). Today, forty to fifty-year-old Douglas-fir trees dominate the overstory. While much less common, both bigleaf maple (*Acer macrophyllum*) and western hemlock (*Tsuga heterophylla*) are also present. The understory includes vine maple (*Acer circinatum*), Oregon grape (*Mahonia aquifolium*), and sword fern (*Polystichum munitum*).

The average depth of the forest floor and organic horizon was 5 cm at our soil measurement points. Mineral soil in the top 100 cm was generally gravelly, silty clay loam with A and B horizons, which had gradual and poorly defined boundaries. Soils were underlain by unconsolidated, highly weathered saprolite and fractured bedrock (Gabrielli et al. 2012). Soil thickness ranged from 20 cm to more than 5 m. Parent materials primarily include tuffs and breccias, but basalts and andesites are also present (Halpern, 1988).

2.3 Methods

2.3.1 Topographic Analysis

We used a map of classified Topographic Position Index (TPI) to guide the placement of soil monitoring sites. The TPI was estimated from a 1x1 m digital elevation model (Spies, 2016) by subtracting the elevation of a grid cell from the mean elevation of all cells within a 30 m radius (Jenness, 2006). This method allowed us to classify slope position and landforms following the method of Weiss (2001). Positive TPI values represented divergent slope positions where the elevation of a pixel was high relative to the average surrounding locations. Conversely, negative TPI values represented convergent slope positions where the elevation of a pixel was low relative to surroundings. Locations where TPI was close to zero were relatively planar. Individual hillslopes were distinguished by a switch between negative and positive TPI along the same elevation contour (Figure 2.1A).

We used additional DEM-derived terrain metrics to test the effect of topography on soil water content. Other metrics used in our analysis were: slope gradient, upslope accumulated area (UAA), topographic wetness index (TWI), and distance from stream. UAA represents the amount of land draining to each pixel and was estimated with the triangular multiple flow-direction algorithm developed by Seibert & McGlynn (2007). TWI was calculated as $\ln\left(\frac{UAA}{\tan(\text{slope})}\right)$, as proposed by Beven & Kirkby (1979) in an effort to characterize the potential for nonlocal water subsidies and lateral water redistribution. Distance from stream was calculated as Euclidean distance from the site to the headwater perennial stream. We analyzed and visualized all terrain metrics using ArcGIS 10.5.1.

2.3.2 Quantification of Soil Water Content

We established 54 permanent soil water monitoring sites along alternating convergent and divergent hillslopes within a 10-ha north-facing area of the catchment in July 2016 (Jarecke et al., 2021). Sites were spaced roughly 30 m apart along transects. Once sites were established, we determined the GPS coordinates of each site using a Trimble GGeoXT Global Positioning System. The TPI values at individual sites (Figure 2.1B) were representative of the range in TPI values estimated for each 1x1 m grid cell across the catchment (Figure 2.1C).

We measured soil volumetric water content (VWC) using time domain reflectometry (TDR; model No. 1502C, Tektronix Inc., Beaverton, OR). TDR is a standard method for obtaining VWC; it measures the propagation of electromagnetic waves in a pair of 3 mm diameter stainless steel rods. VWC was measured over two depths of mineral soil, 0–30 and 0–60 cm. We replicated measurements points at each site so there were two VWC measurements for each depth. A measurement point consisted of a pair of TDR rods installed vertically, 5 cm apart, in mineral soil (see Gray & Spies 1995 for additional details on methods). The replicate measurement points were, on average, 2.5 m apart and the measurement volume of each point was 30 cm or 60 cm deep and 10 cm in diameter (Topp et al. 1980). There were multiple attempts to insert rods at approximately half of the sites because we encountered rocks that prevented the rods from penetrating the soil. We could not install the 60 cm rods at eight of the 54 sites due to high rock content below 30 cm. Rods remained in place over the entire study period.

We measured VWC on 18 dates from August 2016 to October 2017. The forest floor was removed prior to taking measurements and replaced between sampling dates. We converted the reflection trace from TDR to VWC using a calibration equation developed in a nearby watershed

(Gray & Spies, 1995). We estimated VWC at 30–60 cm using the VWC from adjacent 0–30 and 0–60 cm probes after accounting for differences in volume sampled: $VWC_{30-60cm} = 2 \times VWC_{0-60cm} - VWC_{0-30cm}$. The sensitivity of the instrument was $0.01 \text{ cm}^3 \text{ cm}^{-3}$ as determined from repeat measurements less than one minute apart. Prior to analysis, we averaged VWC from the two replicate measurement points at each site. We chose to use the average because the difference between the two measurement points (average = $0.01 \text{ cm}^3 \text{ cm}^{-3}$) was small relative to the variability among sites (standard deviation = $0.07 \text{ cm}^3 \text{ cm}^{-3}$). Poor quality data occurred on four sampling dates during wet and cold conditions in winter and early spring; these data were not included in the analysis.

We also installed 10 shallow groundwater wells along two convergent hillslopes to understand the timing and duration of subsurface flows by driving a solid steel rod into the soil until refusal, which was generally ~2–2.5 m below the surface. We then inserted a 3.8 cm diameter screened PVC pipe. Wells were installed in late summer and all wells were dry at the time of installation. We used pressure transducers (Solinst Levellogger Junior Edge, model 3001) recording at an hourly time interval to identify if the soils became saturated, and if they did, the date, duration, and depth of soil saturation.

2.3.3 Measurements of Soils and Vegetation

We quantified soil hydraulic properties—saturated hydraulic conductivity and soil water retention—on intact soil cores collected at 13 of the 54 soil moisture monitoring sites (Figure 2.1A). Selection of the 13 sites was based on preliminary findings of high and low VWC measured on divergent and convergent slopes. Persistently wet and dry sites were selected to capture potential differences in soil properties that could control VWC on convergent versus

divergent slopes. Soils were collected by digging a shallow pit and exposing an undisturbed soil face. Soils overlying each sampling depth, 15 and 45 cm, were removed and a 250 cm³ metal cylinder (5 cm tall and 8 cm diameter) was pounded vertically into the soil. The intact soil cores were capped on both ends to preserve the soil structure and delivered to laboratory where they were stored at 4 °C.

Saturated hydraulic conductivity (K_s) was measured in the laboratory using the falling head method on the KSAT device (METER Group Inc.). See details on methods in Sarkar et al. (2019). The K_s was averaged from five repeated measurements from each soil core. Soil water retention was measured using the simplified evaporation method (Schindler et al., 2010) with HYPROP and WP4C Dewpoint Potentiometer instruments (METER Group Inc.). The HYPROP system uses two tensiometers installed vertically into the soil core at 1.25 and 3.75 cm to measure matric potential. Change in the mass of the soil core is measured simultaneously for VWC, and measurements were recorded every 30 minutes. Measurements were stopped when air entered the lower tensiometer, which typically occurred around -81 kPa. After HYPROP measurements were complete, we immediately extracted five soil samples in 1 cm increments starting at the surface of the soil core. We then placed soil samples in the WP4C instrument to measure water potential of the dry soils using the chilled-mirror dewpoint technique (Scanlon et al., 2002). Data from the HYPROP and the WP4C were combined using HYPROP-Fit software and the data were fit using the unimodal constrained hydraulic function developed by van Genuchten (1980).

Soils from individual cores were subsequently dried at 105 °C for 24 hours and the oven-dried weight was divided by the sample volume to determine the bulk density. We used the dried soil sample to quantify gravimetric coarse content and particle size. Coarse material consisted of

2–5 mm rock fragments, weathered saprolite fragments, roots, and wood. We placed the sample in a mortar and lightly tapped the soil with a pestle to break soil aggregates but preserve saprolite fragments. We then passed the sample through a 2 mm sieve to remove coarse material, including saprolite fragments. The sieved soil was mixed, a 5–7 g subsample was collected, and then organic carbon was removed from the subsample using the hydrogen peroxide method (Mikutta et al., 2005). The subsample was sent to the Critical Zone Lab at Virginia Tech for particle size analysis using laser diffractometry on a CILAS 1190 laser particle size analyzer (Miller & Schaeztl, 2012).

We measured depth to bedrock at 38 of the 54 soil moisture monitoring sites using a dynamic cone penetrometer, which is also known as a knocking pole (Shanley et al., 2003; Yoshinaga & Ohnuki, 1995). The pole consisted of 0.5 m graduated steel rod segments and a 20 mm long and 24 mm diameter cone tip, which was driven into the soil by repeated drops of a 5 kg weight onto a platform threaded on the upper segment of the pole. When the resistance to penetration became large (moving less than 1 cm in 15 or more knocks), we assumed the cone tip had reached bedrock. We calculated soil depth to bedrock at each site from the average of 2–3 repeat measurements taken approximately 5–10 m apart.

Vegetation, especially trees, is a local factor that can influence VWC through root uptake or canopy interception. We attempted to limit the influence of root water uptake and canopy interception by locating our soil monitoring sites along a uniform slope, with uniform aspect, in a single-aged, mono-specific stand with relatively uniform tree size and density. We calculated the total basal area and total distance-weighted basal area in a 5 m radius plot around each measurement point. Distance-weighted basal area was calculated using an equation from Trompvan Meerveld & McDonnell (2006a) and Liang et al. (2017):

$$\text{Distance-weighted basal area} = \sum A_i \exp(-\delta d_i)$$

where A_i is the basal area of a tree (m^2), d_i is the corresponding distance to tree (m) measured with an IMPULSE laser (Laser Inc. Technologies), and δ is a constant set to 0.2 that determines the weight of the distance, such that the trees closer to the measurement point had greater weight than trees further away. We chose a 5 m radius plot around each measurement because this was the approximate crown radius of trees in our study area. We assumed that trees more than 5 m away would not be able to extend their roots to measurement points because the horizontal root systems of Douglas-fir, the dominant tree species at our site, do not typically reach beyond the crown projection of the tree (Mauer & Palátová, 2012).

2.3.4 Data Analysis

We assessed the effectiveness of terrain metrics for predicting VWC using regression relationships between VWC and the following terrain metrics: topographic position index (TPI), topographic wetness index (TWI), upslope accumulated area (UAA), slope, and Euclidean distance from stream. Topographic position index and UAA were weakly correlated (Pearson correlation = -0.5); however, other terrain metrics were not correlated to one another. The magnitude and range of the terrain metrics was highly variable, making direct comparisons of these metrics' effects on VWC difficult. Thus, we standardized the terrain metrics by subtracting the mean and dividing by the standard deviation. The resulting standardized slopes represented the change in VWC for a one standard deviation shift of the terrain metric. We compared the magnitude of the slopes to determine which of the terrain metrics might be most useful for explaining differences in VWC over our study area. We chose the terrain metrics with the greatest absolute slope to then repeat the regression analysis with the original/unstandardized

metrics. We also used regression analysis to identify which local variables—soil and vegetation properties—were correlated to VWC.

We graphically assessed the relationship between VWC and each soil and vegetation property on each sampling date to identify which, if any, variables were correlated to VWC. Additionally, we were interested to know if the slope of the relationships depended on the antecedent rainfall amount. To determine this, we correlated 2-week antecedent rainfall to the predicted change in VWC for a one standard deviation (SD) shift for each local or nonlocal variable of interest. We also visually checked the pairwise relationship and Pearson correlation between these local and nonlocal variables.

We tested the spatial patterns of VWC for persistence over time. We first ranked sites from driest (1) to wettest (54) on each of the 14 measurement dates. We calculated the SD of the rank for each site over the study period, then compared the observed SDs to the expected SDs if the spatial patterns were entirely random. To do this, we randomly selected a rank from 1 to 54 for each site on each date, without replacement, and used these ranks to calculate a predicted SD from the random rankings. We repeated this process 1,000 times to create a distribution of predicted SD values. We then compared the observed SD at each site to the distribution of predicted SD of rank. If the observed SD of rank was less than the predicted values generated from random spatial patterns, the VWC at those sites had a persistent or stable rank over the study period. We set a threshold at the 5th percentile of the predicted distribution and considered observed values below that threshold to show evidence of stability in VWC over time.

We examined how the variability of VWC across sites ($n = 54$) and difference in VWC between depths ($n = 2$) changed with overall catchment wetness. To characterize variability over space, we calculated the standard deviation (SD) of mean VWC on each measurement date ($n =$

14) and used a nonparametric smoothed spline regression to observe how the SD changed as the overall mean VWC increased. Additionally, we used a paired t-test to determine if the average difference in VWC between 0–30 and 30–60 cm at individual sites changed depending on 2-week antecedent rainfall, which ranged from 0 to 25 cm across measurement dates. We completed all data analysis using R statistical software (R Core Team, 2019) along with the R packages dplyr (Wickham et al., 2019), tidyr (Wickham & Henry, 2019), raster (Hijmans, 2019), ggplot2 (Wickham, 2016), cowplot (Wilke, 2019), GGally (Schloerke et al., 2020), and gridExtra (Auguie, 2017).

2.4 Results

2.4.1 Nonlocal and Local Controls

We found that topographic attributes were weakly correlated with spatial patterns of VWC across a range of antecedent rainfall amounts. VWC at 0–30 cm was not related to terrain metrics. However, VWC at the 30–60 cm changed by 0.01–0.03 cm³ cm⁻³ for one standard deviation (SD) change in topographic position index (TPI) and Euclidean distance from stream (Figure 2.2). When 2-week antecedent rainfall was high, VWC increased by 0.03 cm³ cm⁻³ for a one SD increase in TPI, which represents a 2 m increase in elevation (more divergent) over the surrounding terrain (Figure 2.2). Conversely, VWC decreased 0.03 cm³ cm⁻³ for a 39 m increase in distance from the stream during a period of intermediate wetness (Figure 2.2). We found a small decrease in VWC at 30–60 cm (0.01 to 0.02 cm³ cm⁻³) for one SD increase in TWI, but no detectable relationship between VWC and slope gradient or upslope accumulated area (UAA). While these changes in the absolute VWC may seem small, we note that the change in the

average VWC at 30–60 cm from the driest to the wettest sampling dates was only $0.10 \text{ cm}^3 \text{ cm}^{-3}$. Thus, a $0.01 \text{ cm}^3 \text{ cm}^{-3}$ change in VWC was equivalent to 10% of the annual range in average VWC at our sites.

We further tested the strength and directionality of the relationship between VWC, TPI, and distance from stream. There was a significant positive linear relationship between TPI and VWC at 30–60 cm on 9 of 14 sampling dates ($p < 0.05$, Figure 2.3), suggesting divergent locations (positive TPI) were wetter, on average, than convergent (negative TPI) locations. The greatest slope and coefficient of determination occurred when 2-week antecedent rainfall was $> 10 \text{ cm}$ (Figure 2.3 panels f, g, h, m, n). VWC increased, on average, $0.01 \text{ cm}^3 \text{ cm}^{-3}$ (mean 95% CI = 0.001 to 0.02) for one standard deviation increase in TPI—this slope was strongly correlated to the 2-week antecedent rainfall ($R^2 = 0.69$, Figure 2.4a). Conversely, the relationship was weakest when antecedent rainfall was low (3–6 cm) during fall and spring (e.g., Figure 2.3 panels c, d, i). In contrast, low antecedent rainfall conditions created the strongest relationship between VWC and distance from stream ($p < 0.05$, Figure 2.3 panels c, d, e). VWC decreased, on average, $0.01 \text{ cm}^3 \text{ cm}^{-3}$ for one standard deviation increase in distance from stream (mean 95% CI = -0.02 to 0.001, Figure 2.4b).

Linear regression of VWC with each local factor (Table 2.1) indicated that gravimetric rock content and VWC at field capacity (-33 kPa) explained more of the variability in VWC at 0–30 cm ($R^2 = 0.11$ – 0.20 ; data not shown) and at 30–60 cm ($R^2 = 0.28$ – 0.72 ; Figure 2.3) than the other soil and vegetation properties ($R^2 = 0.001$ – 0.10 ; data not shown). Statistically, there was evidence that for 9 of 14 sampling dates VWC at 30–60 cm was related to the gravimetric rock content of soils and, for all sampling dates, was also related to the laboratory measurement of field capacity VWC ($p < 0.05$, Figure 2.3). While the estimated slopes were greater than those

estimated from the regressions with TPI and Euclidean distance from stream, the 95% confidence intervals were much wider due to the relatively small number of sites where we measured soil properties ($n = 13$). VWC at field capacity and gravimetric rock content were highly correlated (Figure 2.5), and therefore, regression of VWC with these variables produced a similar, but directionally opposite, effect. VWC at 30–60 cm decreased, on average, $0.05 \text{ cm}^3 \text{ cm}^{-3}$ for one SD increase in rock content (mean 95% CI = -0.09 to -0.004 Figure 2.4c) and increased on average, $0.06 \text{ cm}^3 \text{ cm}^{-3}$ for one SD increase in field capacity VWC (mean 95% CI = 0.02 to 0.11, Figure 2.4d). Unlike TPI, the estimated slopes were poorly correlated to 2-week antecedent rainfall.

Soil properties were not correlated to TPI across the 13 sites (Figure 2.5). However, several soil properties were correlated with Euclidean distance from the stream. Soil clay content and water held at field capacity decreased with increased distance from the stream while sand content, bulk density, and rock content increased at locations further from the stream (Figure 2.5). Total depth to bedrock was not well correlated to any of the terrain metrics. However, we found the average depth to bedrock was 0.9 m greater on convergent slopes compared to divergent slopes (Table 2.1). Total soil depth to bedrock was also 0.8 m greater at locations within 80 m of the stream compared to locations further upslope.

2.4.2 Persistent Spatial Patterns

We found persistent spatial patterns in VWC across all sampling dates—some locations remained consistently wetter than the spatial average, while other locations remained consistently drier. When ranking individual sites according to VWC, the average rank, or relative wetness, of most sites varied little despite large seasonal differences in rainfall.

The SD of ranks for individual sites were distinct from those estimated from the permutation test on randomly assigned ranks. The SD of only five sites at 0–30 cm fell into the range of SDs that would be expected if ranking were entirely random (Figure 2.6). These few sites where rank was not as stable over time as the other sites, all had intermediate average rankings. For most sites, however, SDs of average ranks were lower than the SDs generated by random assignment at both soil depths (SD at 5th percentile = 11.9 at 0–30 cm and 10.2 at 30–60 cm). The sites that were most stable in VWC over time—indicated by standard deviation < 3—were either on the extreme dry or extreme wet end of the distribution of VWC, as indicated by high and low average rank.

2.4.3 Variability in Volumetric Water Content

VWC was spatially more variable at the deeper soil depth, 30–60 cm, compared to 0–30 cm. At both depths, the SD increased with mean VWC (Figure 2.7). The smallest variability in VWC occurred late in the dry season when 2-week antecedent rainfall was zero and soils were driest. The greatest variability occurred in October 2016 when 2-week antecedent rainfall was 24.9 cm and soils were at intermediate wetness. This led to a positive, convex relationship between the mean and SD at 30–60 cm (Figure 2.7).

We observed small differences in VWC between 0–30 and 30–60 cm at individual sites where VWC was measured at both depths. The differences were, on average, greater during dry sampling dates (2-week antecedent rainfall < 1 cm) than wet sampling dates (2-week antecedent rainfall > 1 cm). Over all dates, VWC was, on average, $0.01 \text{ cm}^3 \text{ cm}^{-3}$ greater at 30–60 cm than 0–30 cm ($t_{642} = -3.22$, $p = 0.02$, 95% CI = 0.012 to 0.003). However, during dry sampling dates, we found VWC was, on average, 0.02 to 0.03 $\text{cm}^3 \text{ cm}^{-3}$ greater at 30–60 cm than 0–30 cm ($p \leq$

0.02; Table 2.2). In contrast, during wet sampling dates, VWC differed between depths for one date in April 2017 when it was $0.02 \text{ cm}^3 \text{ cm}^{-3}$ greater at 0–30 than 30–60 cm ($p = 0.03$; Table 2.2). While the differences in VWC between depths at individual sites were generally small, a few sites had large differences—the maximum difference in VWC between the two depths at an individual site was $0.28 \text{ cm}^3 \text{ cm}^{-3}$ (Figure 2.8).

2.5 Discussion

Our results showed the importance of soil properties in controlling the spatial variability of volumetric water content (VWC) in steep, quick-draining hillslopes. We expected spatial patterns in VWC would result from lateral redistribution of subsurface flow and therefore, be highly correlated to surface topography. Instead, we found that soil properties were an important control on VWC on all sampling dates. The temporal persistence of these relationships, as well as the overall spatial patterns during wet and dry seasons, suggested the effect of soil hydraulic properties may outweigh seasonally dynamic fluxes such as subsurface water redistribution from saturated flows in this watershed. Our results emphasized that spatial patterns in VWC, while persistent, are not easily explained by surface topography in steep, upland soils that are rocky and well-drained.

2.5.1 Nonlocal Controls

In our study in Watershed 1 at the H.J. Andrews Experimental Forest, soils at 30–60 cm depth on convergent slopes were, on average, drier than soils on divergent slopes. Conversely, we found no relationship between surface topography and VWC at the 0–30 cm soil depth.

While the relationship at 30–60 cm was strongest when 2-week antecedent rainfall was high and soils were wet, it persisted across all sampling dates, including both dry and wet seasons (Figures 3 and 4). This relationship was opposite of our expectations, and clearly demonstrated that redistribution of soil water via subsurface flows, following flowpaths derived from the surface topography, could not explain the persistent spatial patterns in VWC in the top 60 cm of the soil.

The spatial redistribution of water by surface runoff or lateral subsurface flow following topographical features was previously defined as a nonlocal control on soil moisture by Grayson et al. (1997). Similarly, Western et al. (1999) found that surface soils became saturated and generated overland flow that accumulated in convergent areas. However, while saturation excess surface runoff has been described in some forested watersheds (e.g., Gomi et al., 2008), it is unlikely to have occurred at our field site because saturated hydraulic conductivity exceeded 200 cm hr⁻¹, which is far greater than precipitation intensity, even during the most intense rainstorms.

We expected subsurface lateral flows would be an important causal mechanism for spatial patterns of VWC at our study site. Subsurface flows have been observed in a nearby catchment (Gabrielli et al., 2012) and shown to influence spatial patterns in near-surface VWC especially during wet periods (Famiglietti et al., 1998; Grayson et al., 1997; Hoylman et al., 2019; Kaiser & McGlynn, 2018; McNamara et al., 2005; Takagi & Lin, 2011; Williams et al., 2009). Others have indicated that zones of saturation were better predicted by the topography of the bedrock than by surficial topography (Freer et al., 2002; Liang & Chan, 2017; Tromp-van Meerveld & McDonnell, 2006b). In either case, however, subsurface flows must occur relatively near the surface to lead to a measurable relationship between topography and VWC. However, high rates of infiltration and hydraulic conductivity at our site allowed for rapid drainage through the first 60 cm of soil. Additionally, soils were, on average, more than 2 m deep and, in most

locations, were underlain by highly weathered saprolite. Further, we never observed saturation in our 10 monitoring wells that penetrated over 2 m below the soil surface during more than two years of continuous monitoring. Thus, while saturation most likely occurred at our site, it occurred at depths too deep to influence spatial patterns of VWC in the upper 60 cm of soil.

We observed a significant relationship between VWC and distance from the stream, in which, soils closer to the stream were wetter than soils further upslope. We also found that upland soils within 80 m of the stream were approximately a meter deeper (mean depth = 2.7 m) than soils further upslope (mean depth = 1.9 m). Indeed, in our study area, the near-surface soils may be more likely to saturate where depth to bedrock was shallow. However, evidence of deep soils and lack of saturation in our 2-m deep hillslope wells suggested that saturated lateral flow and water table formation occurred much deeper than our measurement depths. Gabrielli et al. (2012) also found that subsurface saturation primarily occurred within highly weathered saprolite or fractured bedrock in a nearby watershed. Moreover, this is likely to occur during the wettest times of the year. However, we observed that VWC was most correlated with distance from stream during the fall when 2-week antecedent rainfall was low, soils were at intermediate wetness (Figures 3 and 4), and overall spatial variability in VWC was highest (Figure 2.7).

The spatial extent and scale of our study may be another reason why our results do not corroborate those of most studies, where convergent topographic positions are typically wetter than divergent ones. We used a 30 m radius to calculate TPI to represent hydrologic landforms in a 10 ha area while minimizing the effects of buried logs, tree tips, or other factors that create finer-scale surface roughness. Comparatively, TPI was estimated with a much larger radius in other studies where slope positions were classified (De Reu et al., 2013). For example, Hoylman et al. (2018) used a 150 m radius to classify slope positions in an 1,800 ha catchment in

Montana. While their study design was similar to ours, the hydrologic landforms spanned a much larger spatial extent, resulting in larger upslope areas draining to the base of convergent slopes. Thus, the spatial extent used to test for relationships between terrain metrics and VWC can be quite variable depending on catchment structure and surface roughness. As a result, different studies might identify different hydrologic mechanisms as the primary control on patterns of VWC simply because of the differences in the spatial scale of the investigation.

The question of spatial scale is not independent of the landscape in which our study occurred. We expect that lithology and climate influence landform development—especially the size of hillslope hollows, the drainage area at which channels first form, and the overall drainage density (Montgomery & Dietrich, 1989). These factors interact with vegetation to control soil development, especially soil hydraulic properties and, along with disturbance, influence surface roughness. If these factors work together in such a way to promote water flow along hydraulic gradients that follow surface topography measured at the scale of a given study, then topographic metrics should be highly correlated with VWC (Ali et al., 2014; Bracken et al., 2013).

Conversely, topographic metrics are unlikely to be well correlated with VWC at shallow depths if water flow is vertical rather than lateral in the upper meter of soil or if the mechanisms work at a scale substantially different than that measured in a given study.

2.5.2 Local Controls

The volumetric water content at our site was persistently and strongly influenced by soil physical properties—gravimetric rock content and water storage at field capacity—during both wet and dry seasons. When percent rock content increased by one standard deviation, VWC decreased by $\sim 0.05 \text{ cm}^3 \text{ cm}^{-3}$. In contrast, VWC changed only $0.01 \text{ cm}^3 \text{ cm}^{-3}$ when TPI and

distance from stream changed by one standard deviation (Figure 2.4). Previous studies have illustrated that the amount and density of rocks can influence the storage and availability of water to plants after free drainage (Naseri et al., 2019; Parajuli et al., 2017). In general, rock content can be considered hydraulically inactive in soils. The presence of rocks decreases the pore space available to store water when soils have drained to field capacity. This also explains why the amount of water in the soil, following free drainage to field capacity, was highly correlated to the measured VWC at our sites over the duration of our study (Figure 2.3).

Porous, highly weathered rocks are likely to hold some water, and if ignored, could lead to underestimation of VWC particularly during dry conditions (Parajuli et al., 2017; Rempe & Dietrich, 2018). Because fragments of weathered rock or saprolite were observed when digging soil pits at our sites, rocks may have contributed to measured VWC when located near TDR probes. We know neither the amount nor the mobility of the water stored in these rocks, so we do not know exactly how rock moisture influenced our measurements of VWC. Nevertheless, we measured lower VWC in rocky soils, suggesting that the volume of bulk soil occupied by rocks limited the water storage capacity of the soil after free drainage and that these effects can persist over time.

None of the vegetation metrics we employed appeared to be related to the spatial patterns in VWC. However, we controlled for vegetation factors in our study design to isolate the effects of topography. We established our study area in a ~50-yr old plantation forest on a north-facing hillslope with uniform aspect where tree density and size were also relatively uniform. Thus, it was not surprising that VWC was not influenced by the average distance to the nearest tree, tree density, or either total, or distance-weighted total basal area at our sites. Additionally, these vegetative metrics did not change with changes in TPI and distance from the stream. Although

we did not measure canopy cover at our sites, interception can decrease VWC under canopies compared to nearby soils under canopy gaps (Gray et al., 2002).

Evapotranspiration from trees can interact with soil moisture availability and soil depth to change spatial patterns in VWC. This was demonstrated by Tromp-van Meerveld & McDonnell (2006a) who found that trees transpired more soil water during the growing season at sites with deep soils ($\bar{x} = 93$ cm) than sites with shallow soils ($\bar{x} = 51$ cm). However, despite greater ET losses at the sites with deep soils, VWC measured at 30 cm depth decreased more slowly than at sites with shallow soils (Tromp-van Meerveld & McDonnell, 2006a). They attributed this to differences in soil depth, which determined the total amount of water that was available for transpiration during the growing season. However, our data suggest the spatial patterns in VWC at 30–60 cm were not likely to result from differences in total soil depth or from differences in ET. First, soils at our site are much deeper than those studied by Tromp-van Meerveld & McDonnell (2006a), averaging 1.8 m deep on divergent and 2.7 m deep on convergent slopes. Thus, root water uptake from deep soils or the hydraulic redistribution of deeper soil moisture to shallower soil layers (Brooks et al., 2006) would likely be similar between slope types. Further, convergent slopes, which had deeper soils were drier at 30–60 cm than divergent slopes, which is opposite of Tromp-van Meerveld & McDonnell's (2006a) results. Second, spatial patterns in VWC were persistent across both wet and dry seasons even though most plant water uptake occurs during the dry summer months, suggesting that the spatial patterns in VWC were not determined by ET, but rather dictated by differences in soil properties among sites.

2.5.3 Temporal Persistence

We observed strong temporal stability in spatial patterns of volumetric water content at our field site. Despite large seasonal changes in mean VWC from the wet winter season to the long, dry summer, the wettest sites were the wettest sites on every sampling date and the driest sites were the driest sites on every sampling date. Temporal stability of spatial patterns in soil water content has been observed in numerous studies and, in general, is attributed to feedbacks between soil water fluxes and water storage (Vanderlinden et al., 2012). This can occur due to nonlocal water redistribution (Takagi & Lin, 2011), local plant water uptake (Gómez-Plaza et al., 2001), and local soil properties such as bulk density and texture (Cosh et al., 2008). However, these factors either seem not to apply (nonlocal water redistribution) or are insufficient to explain the persistence of the spatial patterns we observed over the extreme seasonality in both precipitation and mean soil moisture (Figure 2.6). Moreover, results from other studies suggest that the combined effects of controlling factors rather than single factors are responsible for the temporal stability of VWC patterns (Vanderlinden et al., 2012).

We would expect spatial patterns of VWC to change seasonally because the relative influence of local and nonlocal factors also changes with season. For example, differences in rock content should generate spatial patterns in VWC that persist over the wet season when soil moisture remains at or near field capacity with frequent rainfall events. Conversely, the interaction of soil properties, soil depth, and ET would be expected to influence the development of a new spatial pattern during the dry season (Gómez-Plaza et al., 2001; Hu & Si, 2014; Tromp-van Meerveld & McDonnell, 2006a; Western et al., 1999). Given that we did not observe shifts in the spatial pattern in VWC, suggests that differences in ET across our sites were not large enough to influence spatial patterns of relative soil wetness among sites. This is notable because

it is widely accepted that soil moisture availability is often a critical control on evapotranspiration (Feddes et al., 2001; Jassal et al., 2009; Klein et al., 2014). As such, without substantial precipitation over the long dry summer, we would expect that total ET would be greater in the wettest locations and lesser in the driest locations, which would obscure existing spatial patterns in VWC (or produce new ones).

Evapotranspiration responds to two primary controls—soil moisture availability and atmospheric water demand. Research by Novick et al. (2016) showed that ET from Douglas-fir forests in the Pacific Northwestern USA was more strongly regulated by atmospheric water demand than by soil moisture availability. We would expect similar atmospheric conditions across the full extent of our study site because it was small (10 ha), had relatively uniform slope and aspect, and the range in elevation was relatively modest. If both atmospheric conditions and the forest canopy are uniform, then regulation of tree water use by atmospheric water demand could lead to similar magnitude and timing of plant water uptake among our sites. Under these conditions, the spatial patterns in VWC that were present at the end of the wet season could persist through the long summer dry season.

2.5.4 Relationship Between Local Factors and Topographic Metrics

While we found strong and persistent correlations between local soil properties and VWC, the local factors did not appear to differ strongly between convergent and divergent hillslopes as measured by TPI (Figure 2.5). Thus, we were unable to explain why divergent locations were wetter than convergent locations. Unfortunately, we did not have sufficient resources to dig soil pits and sample and analyze the soil at all 54 VWC monitoring sites. Rather, we chose to compare the wettest and driest sites, expecting that this contrast would most likely

demonstrate the mechanisms controlling differences correlated to topography. However, with only 13 sample locations for soil properties, our statistical power was low. Despite that, we saw no evidence that rock content differed between convergent and divergent slopes (Table 2.1, Figure 2.5). Thus, while others find soil properties and surface topography may jointly control VWC (Hu & Si, 2014), soil properties do not appear to be an explanation for the observed differences in VWC with TPI. We did, however, find that rock content, sand content, and bulk density was greater at sites further from the stream at 45 cm depth (Figure 2.5). Additionally, VWC at field capacity and clay content decreased with increased distance from stream (Figure 2.5). This suggested that soil physical and hydraulic properties may vary along hillslope lengths.

Total depth to bedrock was measured at 38 of our 54 VWC monitoring sites and results indicated that soils were slightly shallower at divergent locations than at convergent ones (Table 2.1). However, soil depth itself, was unrelated to VWC. We commonly encountered an increase in resistance with the knocking pole before reaching an impenetrable bedrock layer. Thus, we assumed most soils were underlain by highly weathered saprolite with a porous and friable consistency whereas a few locations were underlain with andesitic intrusions that were resistant but still highly fractured (Gabielli et al., 2012). In both cases, the underlying bedrock likely contributed to deep drainage and prevented formation of shallow saturated zones. Thus, the difference in total depth to bedrock among our measurement sites do not appear to be sufficient to control spatial patterns in VWC.

The mean and range in the values of our vegetation metrics also did not differ among convergent and divergent hillslopes. As described above, this study was designed to isolate topographic effects from potential confounding factors such as vegetation—by selecting a study site located in a relatively uniform plantation forest. The comparison of vegetation metrics

between convergent and divergent locations suggests that we were, in fact, successful. But consequently, there were no differences in vegetation metrics measured with the spatial grain and extent of our study.

Our results clearly showed that the effect of rock content on soil hydraulic properties altered VWC in measurable ways (Figures 3 and 4). Furthermore, the change in soil properties including bulk density, rock content, and soil texture with change in distance from the stream (Figure 2.5) may partially explain the positive linear relationship between VWC and distance from the stream (Figures 3). The delineation of landforms based on pedology and hydrologic processes could be a useful, albeit complex, framework for exploring the mechanisms that control VWC patterns (Baggaley et al., 2009; Gillin et al., 2015; Lin, 2010). Unfortunately, we often lack detailed soil maps that could otherwise be used to understand variability in soil properties and how soils alter hydrological processes at pedon and landscape scales. Thus, the spatial extent at which soils and topography interact to modify hydrological processes remain poorly understood in many landscapes (Western & Blöschl, 1999). While we did not have enough information to confidently discern how soil properties (e.g., rock content) are distributed in space, others have shown through model simulation that accounting for the effect of rock content on soil hydraulic properties improved predications of VWC (Lai et al., 2018). Thus, improved understanding of how rock content changes across horizontal and vertical space would likely be necessary to predict spatial patterns of VWC in our study area and in other steep mountainous catchments with rocky soils.

2.5.5 Study Limitations and Future Work

Given the high variability in the fraction of coarse material including rocks, roots, and buried wood (Table 2.1), the small measurement volume of our TDR sensors may exacerbate the effects of these factors on the observed spatial variability in VWC among sites. For example, if the TDR probes were inserted next to large pores created by rocks and roots, then macropores would likely decrease VWC relative to nearby soils free of large air-filled pores once soils drained to field capacity. Conversely, large pieces of decomposing wood can remain wetter than the adjacent soil and result in measurements of unusually high VWC. It was common to find buried wood and charcoal when extracting soil samples at 15 and 45 cm. This may explain why VWC differed by as much as $0.3 \text{ cm}^3 \text{ cm}^{-3}$ between the 0–30 and 30–60 cm depths at a few sites (Figure 2.8). However, because TDR probes were installed vertically from the surface, it was impossible to know the specific local conditions that each pair of probes encountered.

Nevertheless, we expected to observe high spatial variance in VWC relative to other studies given the abundance of rocks, coarse roots, and buried wood. However, we found that the range in the standard deviations over 14 sampling dates ($SD = 0.02$ to $0.07 \text{ cm}^3 \text{ cm}^{-3}$, Figure 2.7) was well within the range reported in other studies (Tague et al., 2010; Takagi & Lin, 2011). We also found the positive convex relationship between the mean and SD of VWC was reported in other studies (Brocca et al., 2010; Famiglietti et al., 2008; Tague et al., 2010). Thus, while these issues might account for some of the extreme variability among sites or between soil depths, the spatial variability appears typical of most soils and is an unlikely explanation for greater VWC on divergent slope positions versus convergent ones, or greater VWC at sites near the stream versus those further away. Additionally, we have no reason to expect that our site selection would have biased our results, especially with a sample of 54 soil moisture sites. We recommend that a

subset of sites be evaluated for small-scale variability in VWC given the heterogeneity of macropore structure found to be influential in forest soil hydrology (De Vries & Chow, 1978). This is a potential limitation of our study as we had only two measurement points for each depth, which were spaced roughly 2 m apart at each site. However, the variability between points was usually small relative to the variability among sites on any given sample date.

We recommend future work couple measurements of soil properties and hydraulic properties with measures of VWC at multiple spatial extents, and ideally, use a combination of point and spatially continuous measurements techniques to assess relative soil wetness. We also recommend researchers identify how soil hydraulic properties influence the temporal stability of spatial patterns at multiple depths. Doing so, could improve models of soil water storage and soil moisture availability for plants in landscapes with deep, fast-draining soils such as the ones studied here.

2.6 Conclusions

Our study was designed to test if the horizontal redistribution of water, following surface topography, controlled the spatial patterns of VWC across steep, highly dissected terrain. Spatial patterns of VWC are often characterized with metrics like the Topographic Position Index (TPI) or the Topographic Wetness Index (TWI). Most of the relationships between terrain metrics and VWC have been described for catchments with gentle to moderate slopes and, to a lesser extent, in catchments with steep terrain (Liang et al., 2017). Terrain metrics were developed to characterize source areas for streamflow generation models and, more recently, have been related to the volumetric water content (VWC) of the soil and used as a proxy to determine the potential

availability of water for plant growth. In our study, we found persistent spatial patterns in VWC, which were weakly related to topography. However, contrary to expectations, divergent hillslopes were actually wetter than convergent hollows. VWC was more strongly related to soil properties—specifically, the abundance of coarse fragments and the amount of water stored in the soil after draining to field capacity. Soils at the site were relatively deep ($\bar{x} = 2.3$ m), well-drained, and underlain by porous, highly weathered saprolite. Moreover, we did not find saturated conditions within 2 m of the soil surface over two winters during which we continuously monitored 10 hillslope wells. These conditions are unlikely to be conducive to the horizontal redistribution of water at depths sufficiently shallow to influence VWC of the upper soil profile. The conditions at our site are common in steep, mountainous terrain worldwide. Unfortunately, we lack detailed information on soil properties and their spatial variability in most locations, which challenges our ability to understand how soils alter hydrological processes from pedon to landscape scales. Thus, we recommend that future research test the spatial extent and depths at which soils and topography interact to modify hydrological processes in steep, complex topography.

2.7 Acknowledgments and Data

We thank the HJ Andrews staff for their support with project logistics and use of facilities. Data were provided by the HJ Andrews Experimental Forest research program, funded by the National Science Foundation's Long-Term Ecological Research Program (LTER7 DEB 1440409), USDA Forest Service Pacific Northwest Research Station, and Oregon State University. We thank Aaron Rachels and Lauren Roof for their help with field measurements

and Adrian Gallo and Ryan Stewart for their assistance with soil particle size analysis. Soil data are publicly available via the Andrews Forest database

(<http://andlter.forestry.oregonstate.edu/data/abstract.aspx?dbcode=SP036>) in addition to the LiDAR-based DEM (<http://andlter.forestry.oregonstate.edu/data/abstract.aspx?dbcode=GI010>) and meteorological data

(<http://andlter.forestry.oregonstate.edu/data/abstract.aspx?dbcode=MS001>). The use of trade or firm names in this publication is for reader information and does not imply endorsement by the U.S. Department of Agriculture of any product or service.

2.8 References

- Ali, G., Birkel, C., Tetzlaff, D., Soulsby, C., McDonnell, J. J., & Tarolli, P. (2014). A comparison of wetness indices for the prediction of observed connected saturated areas under contrasting conditions. *Earth Surface Processes and Landforms*, 39(3), 399–413. <https://doi.org/10.1002/esp.3506>
- Auguie, B. (2017). gridExtra: Miscellaneous functions for “grid” graphics. Retrieved from <https://cran.r-project.org/package=gridExtra>
- Baggaley, N., Mayr, T., & Bellamy, P. (2009). Identification of key soil and terrain properties that influence the spatial variability of soil moisture throughout the growing season. *Soil Use and Management*, 25(3), 262–273. <https://doi.org/10.1111/j.1475-2743.2009.00222.x>
- Beven, K., & Germann, P. F. (1982). Macropores and water flows in soils. *Water Resources Research*, 18(5), 1311–1325. <https://doi.org/10.1029/WR018i005p01311>
- Beven, K. J., & Kirkby, M. J. (1979). A physically based, variable contributing area model of basin hydrology. *Hydrological Sciences Bulletin*, 24(1), 43–69. <https://doi.org/10.1080/02626667909491834>
- Bracken, L. J., Wainwright, J., Ali, G. A., Tetzlaff, D., Smith, M. W., Reaney, S. M., & Roy, A. G. (2013). Concepts of hydrological connectivity: Research approaches, pathways and future agendas. *Earth-Science Reviews*, 119, 17–34. <https://doi.org/10.1016/j.earscirev.2013.02.001>
- Brocca, L., Melone, F., Moramarco, T., & Morbidelli, R. (2010). Spatial-temporal variability of soil moisture and its estimation across scales. *Water Resources Research*, 46, 1–14. <https://doi.org/10.1029/2009WR008016>

- Brooks, J. R., Meinzer, F. C., Warren, J. M., Domec, J. C., & Coulombe, R. (2006). Hydraulic redistribution in a Douglas-fir forest: Lessons from system manipulations. *Plant, Cell and Environment*, 29(1), 138–150. <https://doi.org/10.1111/j.1365-3040.2005.01409.x>
- Bundt, M., Widmer, F., Pesaro, M., Zeyer, J., & Blaser, P. (2001). Preferential flow paths: biological “hot spots” in soils. *Soil Biology & Biochemistry*, 33(6), 729–738. [https://doi.org/10.1016/S0038-0717\(00\)00218-2](https://doi.org/10.1016/S0038-0717(00)00218-2)
- St. Clair, J., Moon, S., Holbrook, W. S., Perron, J. T., Riebe, C. S., Martel, S. J., et al. (2015). Geophysical imaging reveals topographic stress control of bedrock weathering. *Science*, 350(6260), 534–538. <https://doi.org/10.1126/science.aab2210>
- Cosh, M. H., Jackson, T. J., Moran, S., & Bindlish, R. (2008). Temporal persistence and stability of surface soil moisture in a semi-arid watershed. *Remote Sensing of Environment*, 112(2), 304–313. <https://doi.org/10.1016/j.rse.2007.07.001>
- Daly, C., Schulze, M., & McKee, W. (2019). Meteorological data from benchmark stations at the HJ Andrews Experimental Forest, 1957 to present. Long-Term Ecological Research. Forest Science Data Bank, Corvallis, OR: Available: <http://andlter.forestry.oregonstate.edu/data/abstract.aspx?dbcode=MS001>. <https://doi.org/10.6073/pasta/c021a2ebf1f91adf0ba3b5e53189c84f>
- Famiglietti, J. S., Rudnicki, J. W., & Rodell, M. (1998). Variability in surface moisture content along a hillslope transect: Rattlesnake Hill, Texas. *Journal of Hydrology*, 210(1–4), 259–281. [https://doi.org/10.1016/S0022-1694\(98\)00187-5](https://doi.org/10.1016/S0022-1694(98)00187-5)
- Famiglietti, J. S., Ryu, D., Berg, A. A., Rodell, M., & Jackson, T. J. (2008). Field observations of soil moisture variability across scales. *Water Resources Research*, 44(1), 1–16. <https://doi.org/10.1029/2006WR005804>
- Fatichi, S., Katul, G. G., Ivanov, V. Y., Pappas, C., Paschalis, A., Consolo, A., et al. (2015). Abiotic and biotic controls of soil moisture spatiotemporal variability and the occurrence of hysteresis. *Water Resources Research*, 51(5), 3505–3524. [https://doi.org/10.1016/0022-1694\(68\)90080-2](https://doi.org/10.1016/0022-1694(68)90080-2)
- Feddes, R. A., Hoff, H., Bruen, M., Dawson, T., De Rosnay, P., Dirmeyer, P., et al. (2001). Modeling root water uptake in hydrological and climate models. *Bulletin of the American Meteorological Society*, 82(12), 2797–2809. [https://doi.org/10.1175/1520-0477\(2001\)082<2797:MRWUIH>2.3.CO;2](https://doi.org/10.1175/1520-0477(2001)082<2797:MRWUIH>2.3.CO;2)
- Freer, J., McDonnell, J. J., Beven, K. J., Peters, N. E., Burns, D. A., Hooper, R. P., et al. (2002). The role of bedrock topography on subsurface storm flow. *Water Resources Research*, 38(12), 5-1-5–16. <https://doi.org/10.1029/2001wr000872>
- Gabrielli, C. P., McDonnell, J. J., & Jarvis, W. T. (2012). The role of bedrock groundwater in rainfall–runoff response at hillslope and catchment scales. *Journal of Hydrology*, 450–451, 117–133. <https://doi.org/10.1016/j.jhydrol.2012.05.023>
- Gannon, J. P., Bailey, S. W., & McGuire, K. J. (2014). Organizing groundwater regimes and response thresholds by soils: A framework for understanding runoff generation in a headwater catchment. *Water Resources Research*, 1–17. <https://doi.org/10.1002/2014WR015498>.Received

- van Genuchten, M. T. (1980). A closed-form equation for predicting the hydraulic conductivity of unsaturated soils. *Soil Science Society of America Journal*, 44, 892–898.
- Gevaert, A. I., Teuling, A. J., Uijlenhoet, R., DeLong, S. B., Huxman, T. E., Pangle, L. A., et al. (2014). Hillslope-scale experiment demonstrates the role of convergence during two-step saturation. *Hydrology and Earth System Sciences*, 18(9), 3681–3692. <https://doi.org/10.5194/hess-18-3681-2014>
- Gillin, C. P., Bailey, S. W., McGuire, K. J., & Gannon, J. P. (2015). Mapping of hydropedologic spatial patterns in a steep headwater catchment. *Soil Science Society of America Journal*, 79(2). <https://doi.org/10.2136/sssaj2014.05.0189>
- Gómez-Plaza, A., Martínez-Mena, M., Albaladejo, J., & Castillo, V. M. (2001). Factors regulating spatial distribution of soil water content in small semiarid catchments. *Journal of Hydrology*, 253(1–4), 211–226. [https://doi.org/10.1016/S0022-1694\(01\)00483-8](https://doi.org/10.1016/S0022-1694(01)00483-8)
- Gomi, T., Sidle, R. C., Miyata, S., Kosugi, K., & Onda, Y. (2008). Dynamic runoff connectivity of overland flow on steep forested hillslopes: Scale effects and runoff transfer. *Water Resources Research*, 44(8), 1–16. <https://doi.org/10.1029/2007WR005894>
- Gray, A. N., & Spies, T. A. (1995). Water content measurement in forest soils and decayed wood using time domain reflectometry. *Canadian Journal of Forest Research*, 25(3), 376–385. <https://doi.org/10.1139/x95-042>
- Gray, A. N., Spies, T. a., & Easter, M. J. (2002). Microclimatic and soil moisture responses to gap formation in coastal Douglas-fir forests. *Canadian Journal of Forest Research*, 32(Tilman 1988), 332–343. <https://doi.org/10.1139/x01-200>
- Grayson, R. B., Western, A. W., Chiew, F. H. S., & Blöschl, G. (1997). Preferred states in spatial soil moisture patterns: Local and nonlocal controls. *Water Resources Research*, 33(12), 2897. <https://doi.org/10.1029/97WR02174>
- Gwak, Y., & Kim, S. (2016). Factors affecting soil moisture spatial variability for a humid forest hillslope. *Hydrological Processes*, 31(2), 431–445. <https://doi.org/10.1002/hyp.11039>
- Halpern, C. B. (1988). Early successional pathways and the resistance and resilience of forest communities. *Ecological Society of America*, 69(6), 1703–1715.
- Helman, D., Osem, Y., Yakir, D., & Lensky, I. M. (2017). Relationships between climate, topography, water use and productivity in two key Mediterranean forest types with different water-use strategies. *Agricultural and Forest Meteorology*, 232, 319–330. <https://doi.org/10.1016/j.agrformet.2016.08.018>
- Hijmans, R. J. (2019). raster: Geographic data analysis and modeling. Retrieved from <https://cran.r-project.org/package=raster>
- Hoylman, Z. H., Jencso, K. G., Hu, J., Martin, J. T., Holden, Z. A., Seielstad, C. A., & Rowell, E. M. (2018). Hillslope topography mediates spatial patterns of ecosystem sensitivity to climate. *Journal of Geophysical Research: Biogeosciences*, 123(2), 353–371. <https://doi.org/10.1002/2017JG004108>
- Hoylman, Z. H., Jencso, K. G., Hu, J., Holden, Z. A., Martin, J. T., & Gardner, W. P. (2019). The climatic water balance and topography control spatial patterns of atmospheric demand, soil moisture, and shallow subsurface flow. *Water Resources Research*, 55, 2370–2389.

<https://doi.org/10.1029/2018WR023302>

- Hu, W., & Si, B. C. (2014). Revealing the relative influence of soil and topographic properties on soil water content distribution at the watershed scale in two sites. *Journal of Hydrology*, *516*, 107–118. <https://doi.org/http://dx.doi.org/10.1016/j.jhydrol.2013.10.002>
- Ivanov, V. Y., Faticchi, S., Jenerette, G. D., Espeleta, J. F., Troch, P. A., & Huxman, T. E. (2010). Hysteresis of soil moisture spatial heterogeneity and the “homogenizing” effect of vegetation. *Water Resources Research*, *46*(9), 1–15. <https://doi.org/10.1029/2009WR008611>
- Jarecke, K., Wondzell, S., & Bladon, K. (2021). Soil moisture and soil properties in Watershed 1 of the HJ Andrews Experimental Forest, 2016–2020. Long-Term Ecological Research. Forest Science Data Bank, Corvallis, OR: Available: <http://andlter.forestry.oregonstate.edu/data/abstract.aspx?dbcode=SP036>. <https://doi.org/10.6073/pasta/d4764b05a9aa95f7cfc5514dfcacc6a3>
- Jassal, R. S., Black, T. A., Spittlehouse, D. L., Brümmer, C., & Nestic, Z. (2009). Evapotranspiration and water use efficiency in different-aged Pacific Northwest Douglas-fir stands. *Agricultural and Forest Meteorology*, *149*(6–7), 1168–1178. <https://doi.org/10.1016/j.agrformet.2009.02.004>
- Jencso, K. G., & McGlynn, B. L. (2011). Hierarchical controls on runoff generation: Topographically driven hydrologic connectivity, geology, and vegetation. *Water Resources Research*, *47*. <https://doi.org/10.1029/2011WR010666>
- Jenness, J. (2006). Topographic Position Index (tpi_jen.avx) Extension for ArcView. *Jenness Enterprises*.
- Kaiser, K. E., & McGlynn, B. L. (2018). Nested scales of spatial and temporal variability of soil water content across a semiarid montane catchment. *Water Resources Research*, *54*. <https://doi.org/10.1029/2018WR022591>
- Kim, S., Lee, H., Woo, N. C., & Kim, J. (2007). Soil moisture monitoring on a steep hillside. *Hydrological Processes*, 2910–2922. <https://doi.org/10.1002/hyp>
- Klein, T., Rotenberg, E., Cohen-Hilaleh, E., Raz-Yaseef, N., Tatarinov, F., Preisler, Y., et al. (2014). Quantifying transpirable soil water and its relations to tree water use dynamics in a water-limited pine forest. *Ecohydrology*, *7*(2), 409–419. <https://doi.org/10.1002/eco.1360>
- Lai, X., Zhu, Q., Zhou, Z., & Liao, K. (2018). Rock fragment and spatial variation of soil hydraulic parameters are necessary on soil water simulation on the stony-soil hillslope. *Journal of Hydrology*, *565*(April), 354–364. <https://doi.org/10.1016/j.jhydrol.2018.08.039>
- Liang, W., & Chan, M. (2017). Spatial and temporal variations in the effects of soil depth and topographic wetness index of bedrock topography on subsurface saturation generation in a steep natural forested headwater catchment. *Journal of Hydrology*, *546*, 405–418. <https://doi.org/10.1016/j.jhydrol.2017.01.033>
- Liang, W., Li, S., & Hung, F. (2017). Analysis of the contributions of topographic, soil, and vegetation features on the spatial distributions of surface soil moisture in a steep natural forested headwater catchment. *Hydrological Processes*, *31*, 3796–3809. <https://doi.org/10.1002/hyp.11290>

- Lin, H. (2010). Earth's Critical Zone and hydrogeology: Concepts, characteristics, and advances. *Hydrology and Earth System Sciences*, *14*(1), 25–45. <https://doi.org/10.5194/hess-14-25-2010>
- Lin, H., Kogelmann, W., Walker, C., & Bruns, M. (2006). Soil moisture patterns in a forested catchment: A hydrogeological perspective. *Geoderma*, *131*(3–4), 345–368. <https://doi.org/10.1016/j.geoderma.2005.03.013>
- Liu, H., & Lin, H. (2015). Frequency and control of subsurface preferential flow: From pedon to catchment Scales. *Soil Science Society of America Journal*, *79*(2), 362–377. <https://doi.org/10.2136/sssaj2014.08.0330>
- Mauer, O., & Palátová, E. (2012). Root system development in Douglas fir (*Pseudotsuga menziesii* [Mirb.] Franco) on fertile sites. *Journal of Forest Science*, *58*(9), 400–409. <https://doi.org/10.17221/94/2011-jfs>
- McDonnell, J. J., Freer, J., Hooper, R., Kendall, C., Burns, D., Beven, K., & Peters, J. (1996). New method developed for studying flow on hillslopes. *Eos*, *77*(47). <https://doi.org/10.1029/96EO00306>
- McNamara, J. P., Chandler, D., Seyfried, M., & Achet, S. (2005). Soil moisture states, lateral flow, and streamflow generation in a semi-arid, snowmelt-driven catchment. *Hydrological Processes*, *19*(20), 4023–4038. <https://doi.org/10.1002/hyp.5869>
- Mikutta, R., Kleber, M., Kaiser, K., & Jahn, R. (2005). Review : Organic matter removal from soils using hydrogen peroxide, sodium hypochlorite, and disodium peroxodisulfate. *Soil Science Society of America Journal*, *69*, 120–135. <https://doi.org/10.2136/sssaj2005.0120>
- Milledge, D. G., Warburton, J., Lane, S. N., & Stevens, C. J. (2013). Testing the influence of topography and material properties on catchment-scale soil moisture patterns using remotely sensed vegetation patterns in a humid temperate catchment, northern Britain. *Hydrological Processes*, *27*(8), 1223–1237. <https://doi.org/10.1002/hyp.9292>
- Miller, B. A., & Schaetzl, R. J. (2012). Precision of soil particle size analysis using laser diffractometry. *Soil Science Society of America Journal*, *76*(5), 1719–1727. <https://doi.org/10.2136/sssaj2011.0303>
- Montgomery, D. R., & Dietrich, W. E. (1989). Source areas, drainage density, and channel initiation. *Water Resources Research*, *25*(8), 1907–1918.
- Naseri, M., Iden, S. C., Richter, N., & Durner, W. (2019). Influence of stone content on soil hydraulic properties: experimental investigation and test of existing model concepts. *Vadose Zone Journal*, *18*. <https://doi.org/10.2136/vzj2018.08.0163>
- Nippgen, F., McGlynn, B. L., & Emanuel, R. E. (2015). The spatial and temporal evolution of contributing areas. *Water Resources Research*, *51*, 4550–4573. <https://doi.org/10.1002/2015WR017273>. Received
- Novick, K. A., Ficklin, D. L., Stoy, P. C., Williams, C. A., Bohrer, G., Oishi, A. C., et al. (2016). The increasing importance of atmospheric demand for ecosystem water and carbon fluxes. *Nature Climate Change*, *6*(11), 1023–1027. <https://doi.org/10.1038/nclimate3114>
- Pachepsky, Y., & Timlin, D. (2001). Soil water retention as related to topographic variables. *Soil Science Society of America Journal*, *65*, 1787–1795. <https://doi.org/10.2136/sssaj2001.1787>

- Parajuli, K., Sadeghi, M., & Jones, S. B. (2017). A binary mixing model for characterizing stony-soil water retention. *Agricultural and Forest Meteorology*, 244–245, 1–8. <https://doi.org/10.1016/j.agrformet.2017.05.013>
- Pelletier, J. D., Barron-Gafford, G. A., Breshears, D. D., Brooks, P. D., Chorover, J., Durcik, M., et al. (2013). Coevolution of nonlinear trends in vegetation, soils, and topography with elevation and slope aspect: A case study in the sky islands of southern Arizona. *Journal of Geophysical Research: Earth Surface*, 118(2), 741–758. <https://doi.org/10.1002/jgrf.20046>
- Penna, D., Borga, M., Norbiato, D., & Fontana, G. D. (2009). Hillslope scale soil moisture variability in a steep alpine terrain. *Journal of Hydrology*, 364(3–4), 311–327. <https://doi.org/10.1016/j.jhydrol.2008.11.009>
- R: A language and environment for statistical computing. (2019). Vienna, Austria: R Foundation for Statistical Computing.
- Rempe, D. M., & Dietrich, W. E. (2018). Direct observations of rock moisture, a hidden component of the hydrologic cycle. *Proceedings of the National Academy of Sciences*, 115(11), 2664–2669. <https://doi.org/10.1073/pnas.1800141115>
- De Reu, J., Bourgeois, J., Bats, M., Zwertvaegher, A., Gelorini, V., De Smedt, P., et al. (2013). Application of the topographic position index to heterogeneous landscapes. *Geomorphology*, 186, 39–49. <https://doi.org/10.1016/j.geomorph.2012.12.015>
- Rinderer, M., van Meerveld, H. J., & Seibert, J. (2014). Topographic controls on shallow groundwater levels in a steep, prealpine catchment. *Water Resources Research*, 50, 6067–6080. <https://doi.org/10.1002/2013WR015009>. Received
- Sarkar, S., Germer, K., Maity, R., & Durner, W. (2019). Measuring near-saturated hydraulic conductivity of soils by quasi unit-gradient percolation – 2. Application of the methodology. *Journal of Plant Nutrition and Soil Science*, 182, 535–540. <https://doi.org/10.1002/jpln.201800383>
- Scanlon, B. R., Andraski, B. J., & Bilskie, J. (2002). Miscellaneous methods for measuring matric or water potential. In J. H. Dane & G. C. Topp (Eds.), *Methods of Soil Analysis, Part 4: Physical Methods* (pp. 643–670). Madison, WI: SSSA. <https://doi.org/10.2136/sssabookser5.4.c23>
- Schindler, U., Durner, W., von Unold, G., Mueller, L., & Wieland, R. (2010). The evaporation method: Extending the measurement range of soil hydraulic properties using the air-entry pressure of the ceramic cup. *Journal of Plant Nutrition and Soil Science*, 173(4), 563–572. <https://doi.org/10.1002/jpln.200900201>
- Schloerke, B., Cook, D., Larmarange, J., Briatte, F., Marbach, M., Thoen, E., et al. (2020). GGally: Extension to “ggplot2.” Retrieved from <https://cran.r-project.org/package=GGally>
- Seibert, J., & McGlynn, B. L. (2007). A new triangular multiple flow direction algorithm for computing upslope areas from gridded digital elevation models. *Water Resources Research*, 43(4), 1–8. <https://doi.org/10.1029/2006WR005128>
- Shanley, J. B., Hjerdt, K. N., McDonnell, J. J., & Kendall, C. (2003). Shallow water table fluctuations in relation to soil penetration resistance. *Ground Water*, 41(7), 964–972. <https://doi.org/10.1111/j.1745-6584.2003.tb02438.x>

- Spies, T. (2016). LiDAR data (August 2008) for the Andrews Experimental Forest and Willamette National Forest study areas. Long-Term Ecological Research. Forest Science Data Bank, Corvallis, OR: Available:
<http://andlter.forestry.oregonstate.edu/data/abstract.aspx?dbcode=GI010>.
<https://doi.org/10.6073/pasta/c47128d6c63dff39ee48604ecc6fabfc>
- Swetnam, T. L., Brooks, P. D., Barnard, H. R., Harpold, A. A., & Gallo, E. L. (2017). Topographically driven differences in energy and water constrain climatic control on forest carbon sequestration. *Ecosphere*, 8(4). <https://doi.org/10.1002/ecs2.1797>
- Tague, C., Band, L., Kenworthy, S., & Tenebaum, D. (2010). Plot-and watershed-scale soil moisture variability in a humid Piedmont watershed. *Water Resources Research*, 46(12), 1–13. <https://doi.org/10.1029/2009WR008078>
- Takagi, K., & Lin, H. S. (2011). Temporal dynamics of soil moisture spatial variability in the Shale Hills Critical Zone Observatory. *Vadose Zone Journal*, 10(3), 832–842. <https://doi.org/10.2136/vzj2010.0134>
- Topp, G. C., Davis, J. L., & Annan, A. P. (1980). Electromagnetic determination of soil water content: Measurements in coaxial transmission lines. *Water Resources Research*, 16(3), 574–582. <https://doi.org/10.1029/WR016i003p00574>
- Traff, D. C., Niemann, J. D., Middlekauff, S. A., & Lehman, B. M. (2014). Effects of woody vegetation on shallow soil moisture at a semiarid montane catchment. *Ecohydrology*, 947, 935–947. <https://doi.org/10.1002/eco.1542>
- Tromp-van Meerveld, H. J., & McDonnell, J. J. (2006a). On the interrelations between topography, soil depth, soil moisture, transpiration rates and species distribution at the hillslope scale. *Advances in Water Resources*, 29(2), 293–310. <https://doi.org/10.1016/j.advwatres.2005.02.016>
- Tromp-van Meerveld, H. J., & McDonnell, J. J. (2006b). Threshold relations in subsurface stormflow: 2. The fill and spill hypothesis. *Water Resources Research*, 42(W02411), 1–11. <https://doi.org/10.1029/2004WR003800>
- Vanderlinden, K., Vereecken, H., Hardelauf, H., Herbst, M., Martínez, G., Cosh, M. H., & Pachepsky, Y. a. (2012). Temporal stability of soil water contents: A review of data and analyses. *Vadose Zone Journal*, 11(4). <https://doi.org/10.2136/vzj2011.0178>
- De Vries, J., & Chow, T. L. (1978). Hydrologic behavior of a forested mountain soil in coastal British Columbia. *Water Resources Research*, 14(5), 935–942. <https://doi.org/10.1029/WR014i005p00935>
- Weiss, A. (2001). Topographic position and landforms analysis. *Poster Presentation, ESRI User Conference, San Diego, CA, 64*, 227–245. https://doi.org/http://www.jennessent.com/downloads/TPI-poster-TNC_18x22.pdf
- Western, A. W., & Blöschl, G. (1999). On the spatial scaling of soil moisture. *Journal of Hydrology*, 217(3–4), 203–224. [https://doi.org/10.1016/S0022-1694\(98\)00232-7](https://doi.org/10.1016/S0022-1694(98)00232-7)
- Western, A. W., Grayson, R. B., Blöschl, G., Willgoose, G. R., & McMahon, T. A. (1999). Observed spatial organization of soil moisture and its relation to terrain indices. *Water Resources Research*, 35(3), 797–810.

- Western, A. W., Grayson, R. B., & Green, T. R. (1999). The Tarrawarra project: high resolution spatial measurement, modelling and analysis of soil moisture and hydrological response. *Hydrological Processes*, 13(5), 633–652. [https://doi.org/10.1002/\(SICI\)1099-1085\(19990415\)13:5<633::AID-HYP770>3.0.CO;2-8](https://doi.org/10.1002/(SICI)1099-1085(19990415)13:5<633::AID-HYP770>3.0.CO;2-8)
- Wickham, H. (2016). *ggplot2: Elegant graphics for data analysis*. Springer-Verlag New York. Retrieved from <https://ggplot2.tidyverse.org>
- Wickham, H., & Henry, L. (2019). tidyr: Tidy Messy Data. Retrieved from <https://cran.r-project.org/package=tidyr>
- Wickham, H., François, R., Henry, L., & Müller, K. (2019). dplyr: A grammar of data manipulation. Retrieved from <https://cran.r-project.org/package=dplyr>
- Wiekenkamp, I., Huisman, J. A., Bogena, H. R., Lin, H. S., & Vereecken, H. (2016). Spatial and temporal occurrence of preferential flow in a forested headwater catchment. *Journal of Hydrology*, 534, 139–149. <https://doi.org/10.1016/j.jhydrol.2015.12.050>
- Wilke, C. O. (2019). cowplot: Streamlined plot theme and plot annotations for “ggplot2.” Retrieved from <https://cran.r-project.org/package=cowplot>
- Williams, C. J., McNamara, J. P., & Chandler, D. G. (2009). Controls on the temporal and spatial variability of soil moisture in a mountainous landscape: the signature of snow and complex terrain. *Hydrology and Earth System Sciences*, 13(7), 1325–1336. <https://doi.org/10.5194/hess-13-1325-2009>
- Yoshinaga, S., & Ohnuki, Y. (1995). Estimation of soil physical properties from a handy dynamic cone penetrometer test. *Journal of the Japan Society of Erosion Control Engineers*, 48, 22–28.
- Zimmer, M., & Gannon, J. P. (2018). Runoff processes from mountains to foothills: the role of soil stratigraphy and structure in influencing runoff characteristics across high to low relief landscapes. *Hydrological Processes*, (2018), 1–15. <https://doi.org/10.1002/hyp.11488>

2.9 Figures

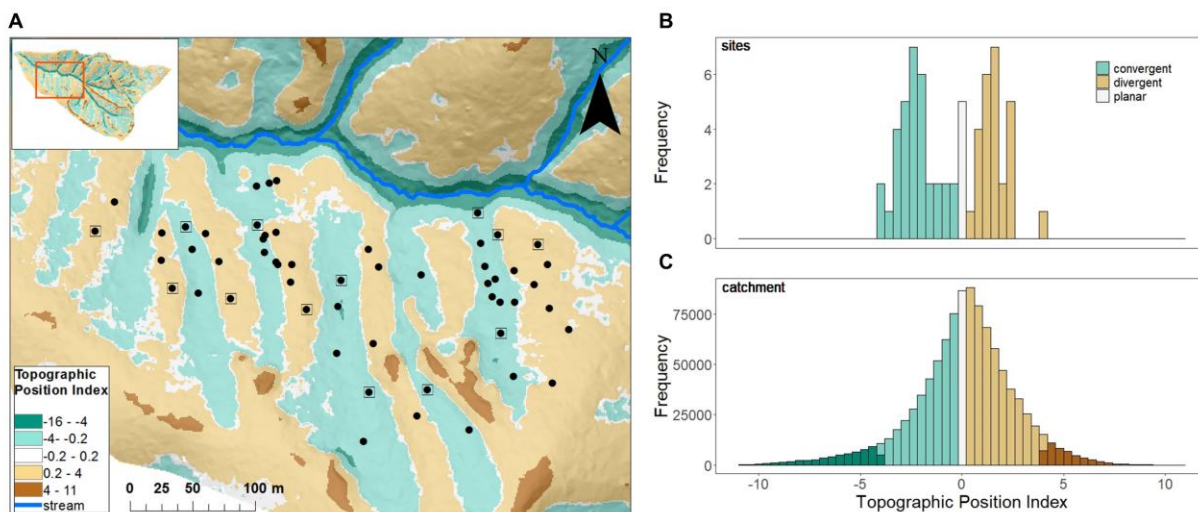


Figure 2.1 Study Area

(A) Soil water content monitoring sites located on divergent (negative values) and convergent (positive values) slopes categorized from TPI at 1 m resolution. We measured soil properties at 13 of the 54 monitoring sites (points with boxes). The distribution of TPI at monitoring sites (B) was representative of the distribution of TPI across the catchment (C). Extreme convergent slopes were perennial and ephemeral streams while extreme divergent locations were bedrock outcrops.

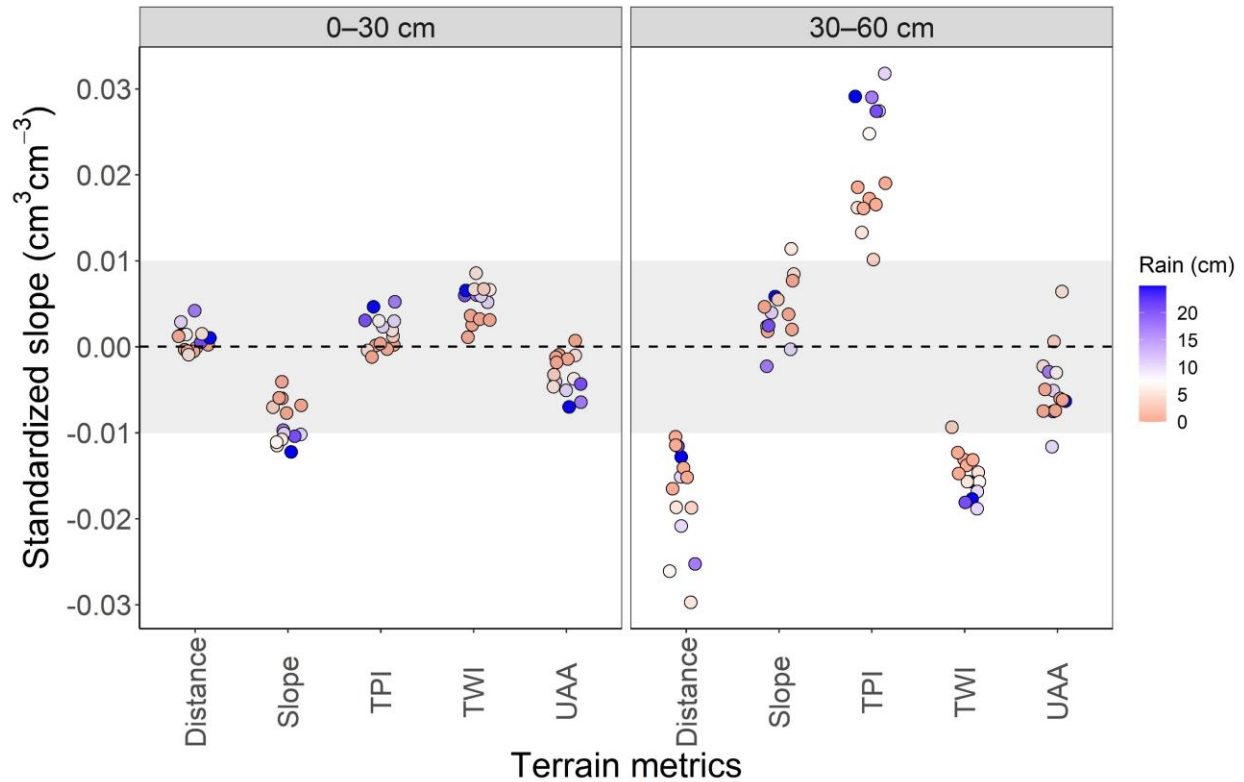


Figure 2.2 Terrain metrics

Standardized slopes represent the change in volumetric water content (VWC) for one standard deviation (SD) change in each of the terrain metrics. SD of distance from stream = 39 m; SD of slope gradient = 6 °; SD of topographic position index (TPI) = 2; SD of topographic wetness index (TWI) = 10; SD of upslope accumulated area (UAA) = 610 m². The gray box indicates no detectable change in VWC (± 0.01 cm³ cm⁻³). TPI had the greatest effect on VWC when two-week antecedent rainfall was > 10 cm, whereas seasonality did not alter the effect of distance from stream on VWC.

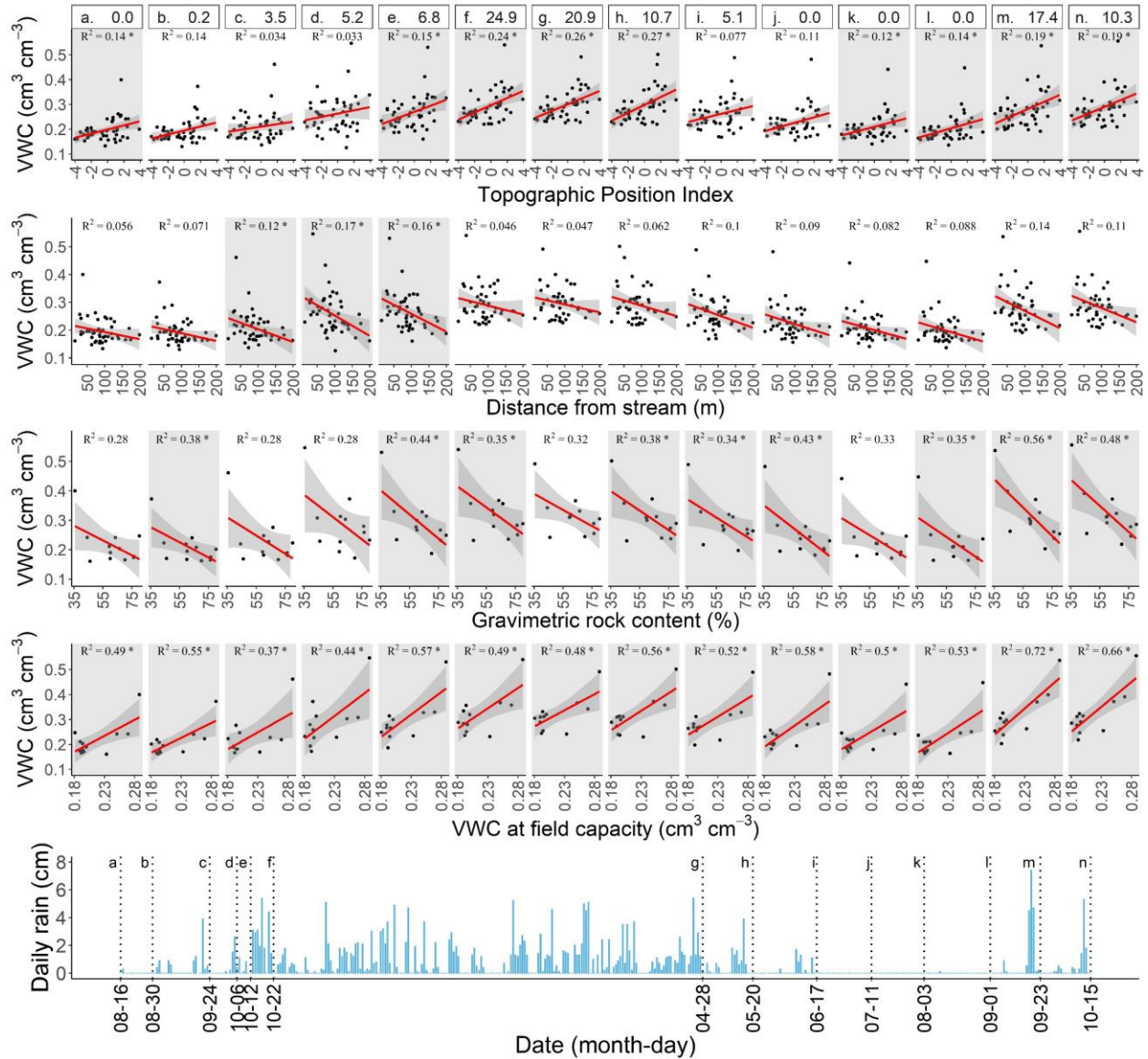


Figure 2.3 Seasonal relationships

There was a significant positive linear relationship between topographic position index (TPI) and volumetric water content (VWC) at 30–60 cm on 9 of 14 sampling dates (a–n) and a significant negative linear relationship between distance from stream and VWC on 3 of 14 sampling dates. If the slope of the linear model was greater than 0 at a level of significance of $\alpha < 0.05$, it is indicated with * and panels are grey. Two-week antecedent rainfall (cm) is indicated above each column of regression plots for each sampling date. A greater amount of variability in VWC was explained by TPI when antecedent rainfall was > 10 cm (panels f, g, h) whereas the most variability was explained by distance from stream during low antecedent rainfall (panels c, d, e). There was a significant negative linear relationship between percent rock content and VWC at 30–60 cm on 9 of 14 sampling dates and a significant positive linear relationship between VWC at field capacity and measured VWC on all sampling dates.

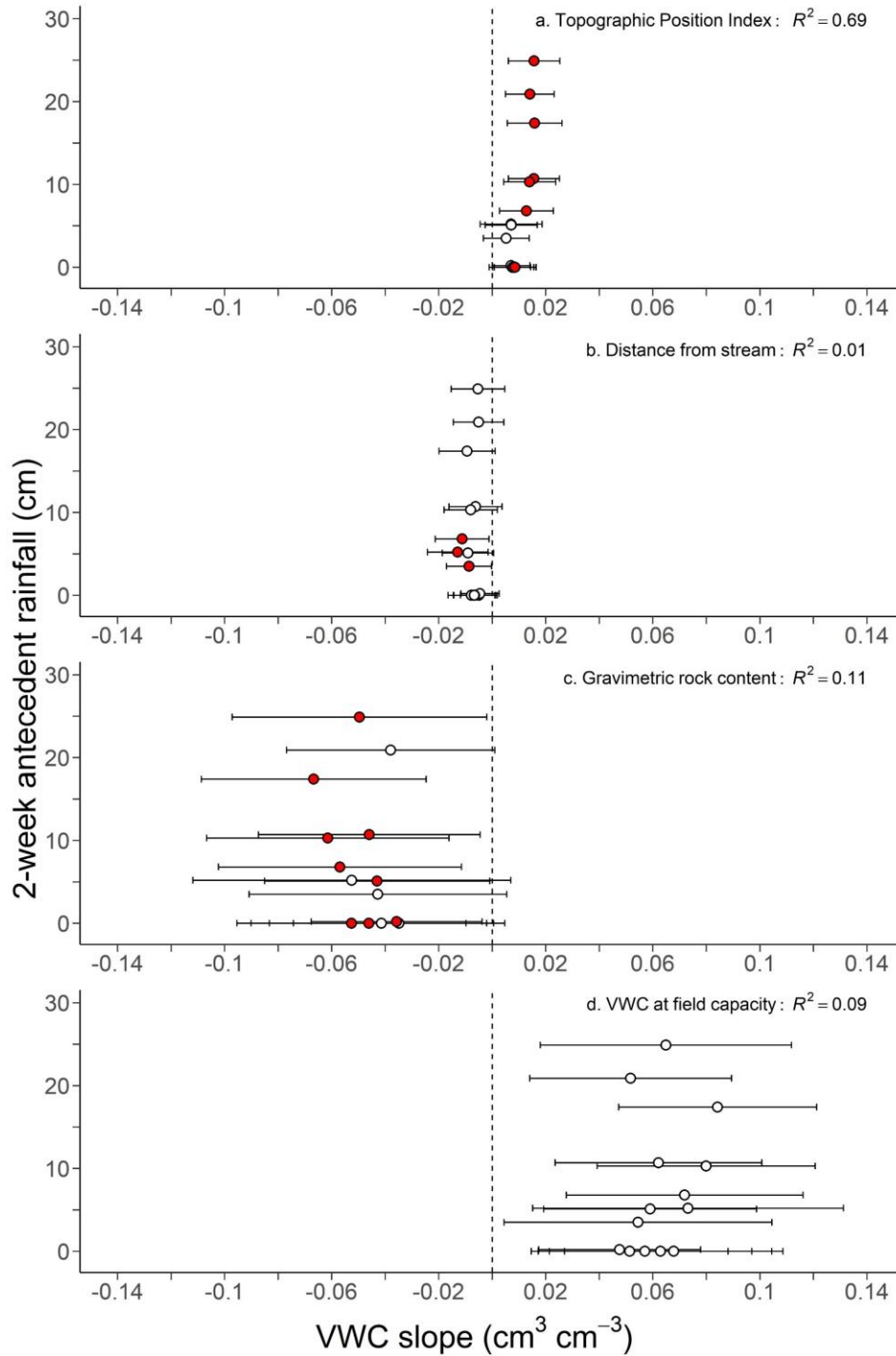


Figure 2.4 Antecedent rainfall

The slope for the change in VWC at 30–60 cm for one standard deviation increase in each variable (Topographic Position Index = 2, distance from stream = 39 m, percent gravimetric rock content = 13.9 %, and VWC at field capacity = $0.04 \text{ cm}^3 \text{ cm}^{-3}$). Red circles indicate the slope $\neq 0$ at the $\alpha = 0.05$ level of statistical significance. Error bars represent the 95% confidence intervals. The R^2 value was derived from the linear relationship between antecedent precipitation (cm) and the slope estimates ($n = 14$).

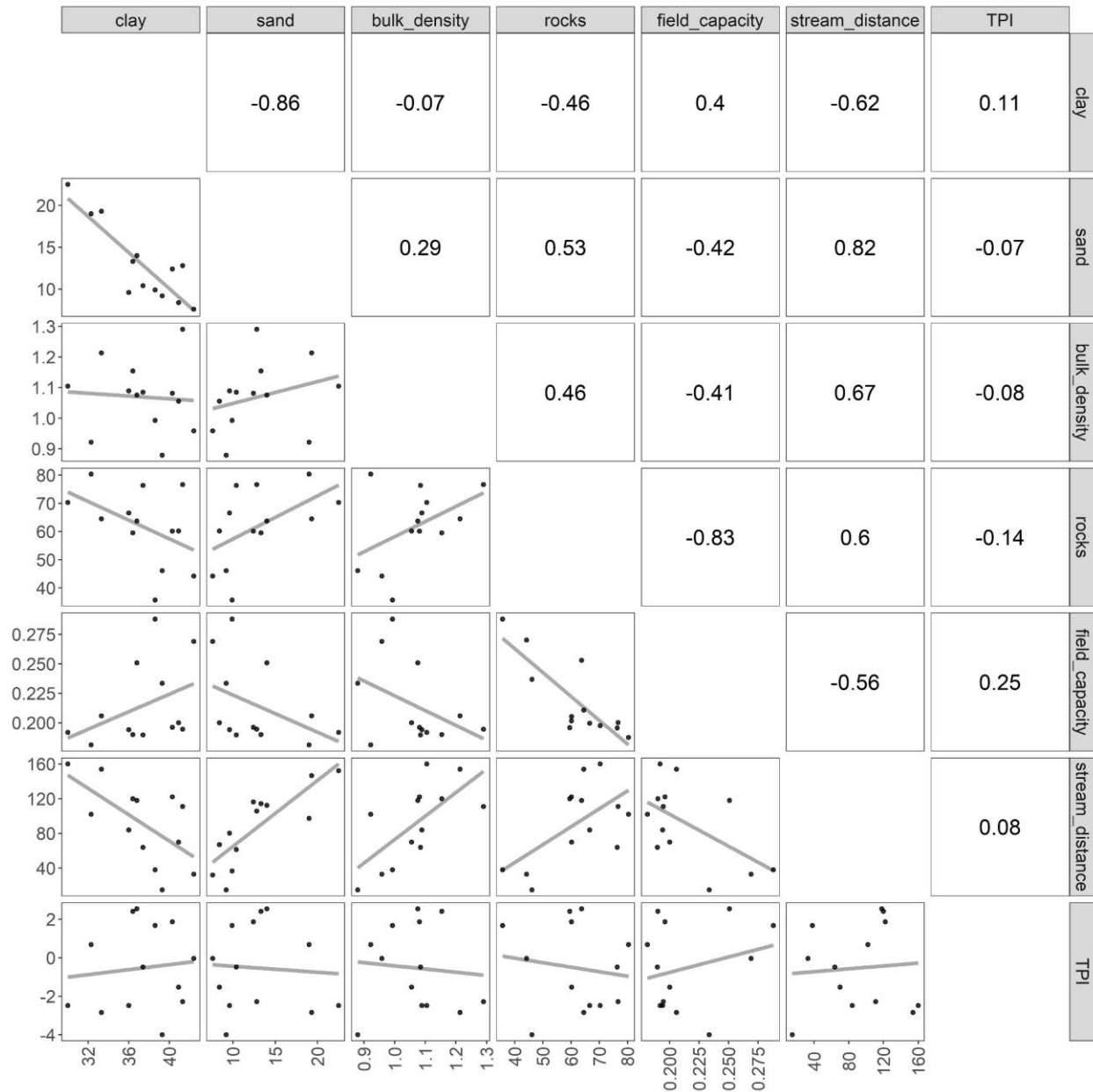


Figure 2.5 Correlations between terrain metrics and soil properties

Linear relationships and the Pearson correlation coefficients among topographic variables—distance to stream (m) and topographic position index—and soil properties at 45 cm depth—clay content (%), sand content (%), bulk density ($\text{cm}^3 \text{cm}^{-3}$), rock content (%), and volumetric water content at field capacity ($\text{cm}^3 \text{cm}^{-3}$).

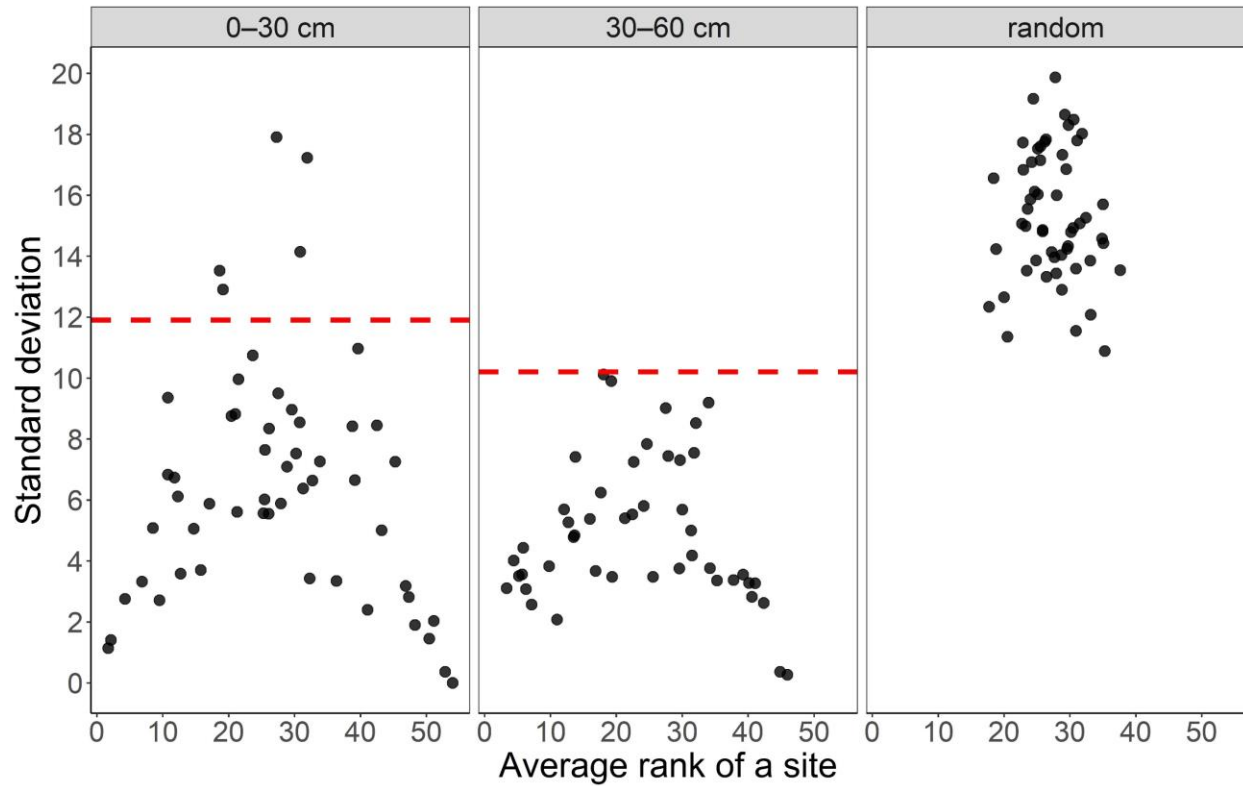


Figure 2.6 Standard deviation of average rank

The distribution of the standard deviations vs. the average rank of a site at both 0–30 and 30–60 cm was different from the distribution of the standard deviations of average rank of site wetness estimated from 1,000 simulations that randomly assigned rank to sites. The right panel is an example of one permutation under the null hypotheses of no spatial pattern or no stability in average rank. The red dashed line is the 5th percentile of the distribution of standard deviations estimated from 1,000 simulations that randomized ranks.

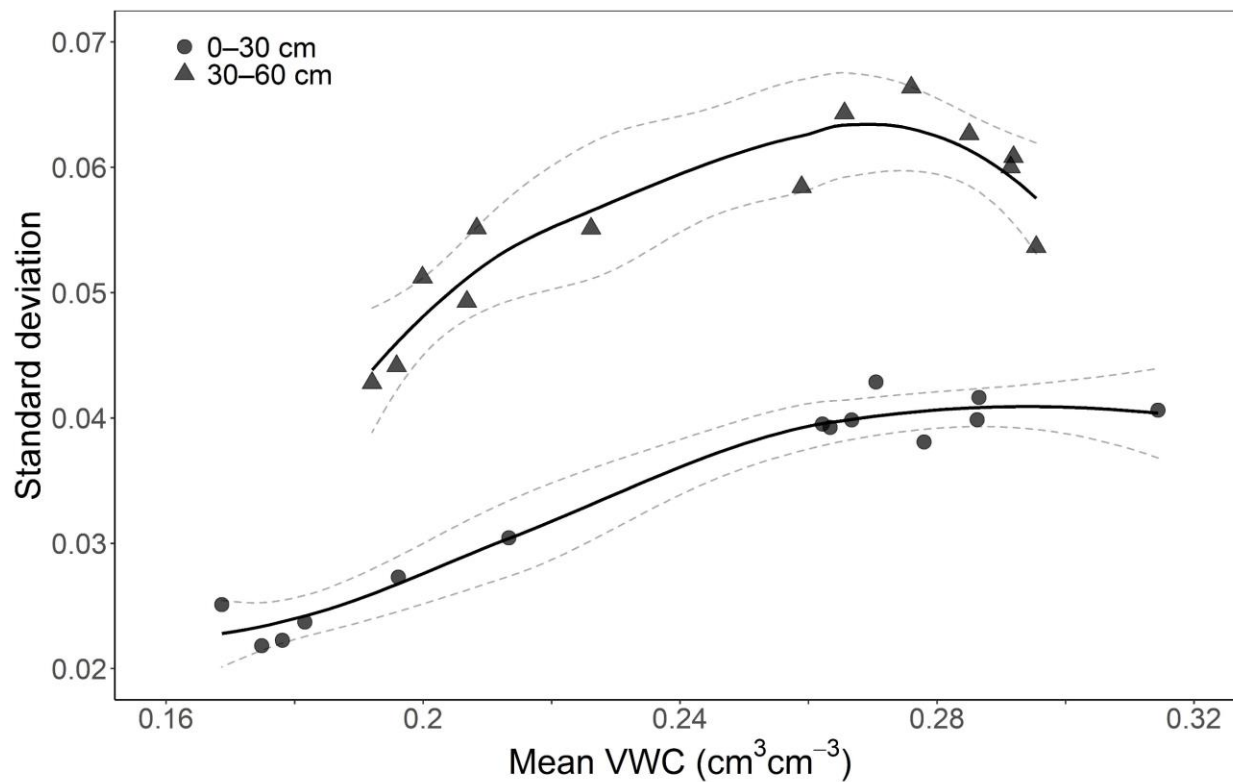


Figure 2.7 Standard deviation across wetness states

The standard deviation of volumetric water content (VWC) generally increased as mean VWC increased. The data was fit using a smooth local regression (solid line) with 95% confidence intervals (dashed line). The relation becomes asymptotic at high mean VWC at 0–30 cm, while the standard deviation peaks with the intermediate range of mean VWC and starts to decrease when overall mean VWC is greatest at 30–60 cm.

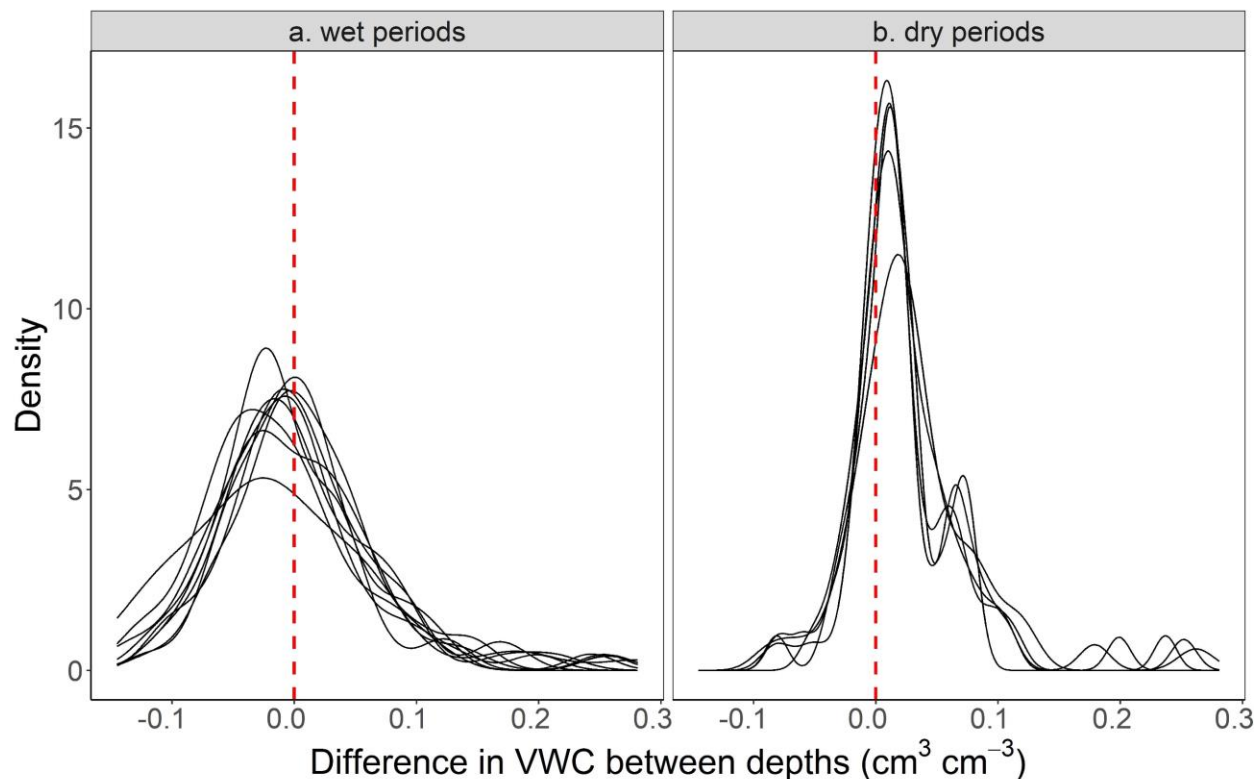


Figure 2.8 Difference in soil water content between depths

Distribution of differences in volumetric water content (VWC) between the two sampling depths (30–60 cm minus 0–30 cm) during wet sampling dates ($n = 9$) when two-week antecedent rainfall > 1 cm and dry sampling dates ($n = 5$) when antecedent rainfall < 1 cm. The distribution of differences was smoothed using a Gaussian kernel density estimate. The mean difference in VWC between the two depths was approximately zero during wet periods ($p = 0.81$, panel a). However, VWC was $0.02 \text{ cm}^3 \text{ cm}^{-3}$ greater at 30–60 cm than at 0–30 cm during the dry periods ($p < 0.01$, panel b).

2.10 Tables

Table 2.1 Statistics for soil and vegetation properties

Mean values for soil properties from soil cores taken at 15 cm and 45 cm depth at a subset of VWC monitoring sites (8 convergent and 5 divergent). Soil depth to bedrock was measured at a subset of sites ($n = 38$) and vegetation properties were measured at all sites ($n = 54$).

		Convergent mean	Divergent mean	Overall mean ± standard deviation
Sand content	15 cm	11.4 %	13.6 %	12.3 ± 6.6 %
	45 cm	12.5 %	13.7 %	13.0 ± 4.7 %
Silt content	15 cm	52.7 %	49.6 %	51.5 ± 3.7 %
	45 cm	49.9 %	49.4 %	49.7 ± 2.3 %
Clay content	15 cm	35.8 %	36.8 %	36.2 ± 5.4 %
	45 cm	37.6 %	36.9 %	37.3 ± 3.7 %
Whole-soil dry bulk density	15 cm	1.0 g cm ⁻³	1.0 g cm ⁻³	1.0 ± 0.1 g cm ⁻³
	45 cm	1.1 g cm ⁻³	1.0 g cm ⁻³	1.1 ± 0.1 g cm ⁻³
Gravimetric rock content (diameters > 2 mm)	15 cm	66.3 %	61.1 %	64.3 ± 11.8 %
	45 cm	63.1 %	59.8 %	61.9 ± 13.3%
Saturated hydraulic conductivity	15 cm	220 cm hr ⁻¹	265 cm hr ⁻¹	238 ± 113 cm hr ⁻¹
	45 cm	207 cm hr ⁻¹	249 cm hr ⁻¹	223 ± 142 cm hr ⁻¹
VWC at -33 kPa (field capacity)	15 cm	0.20 cm ³ cm ⁻³	0.20 cm ³ cm ⁻³	0.20 ± 0.04 cm ³ cm ⁻³
	45 cm	0.21 cm ³ cm ⁻³	0.22 cm ³ cm ⁻³	0.21 ± 0.03 cm ³ cm ⁻³
VWC at -2500 kPa (turgor loss point)	15 cm	0.13 cm ³ cm ⁻³	0.14 cm ³ cm ⁻³	0.13 ± 0.03 cm ³ cm ⁻³
	45 cm	0.14 cm ³ cm ⁻³	0.14 cm ³ cm ⁻³	0.14 ± 0.03 cm ³ cm ⁻³
Depth to bedrock		2.7 m	1.8 m	2.3 ± 1.2 m
Distance to nearest tree		2.0 m	2.0 m	2.0 ± 0.7 m
Total basal area within 5 m		0.33 m ²	0.33 m ²	0.33 ± 0.09 m ²
Total distance-weighted basal area within 5 m		0.16 m ²	0.17 m ²	0.17 ± 0.05 m ²
Basal area per hectare		31.8 m ² ha ⁻¹	33.8 m ² ha ⁻¹	32.7 ± 9.6 m ² ha ⁻¹

Table 2.2 Differences in soil water content between depths

The estimated mean difference in VWC between 0–30 and 30–60 cm using a paired t-test. VWC was greater, on average, at 30–60 cm than 0–30 cm during dry sampling dates (bold) but did not differ between depths during wet sampling dates except on 4/28/2017.

Date	Two-week antecedent rainfall (cm)	Estimated difference in VWC	<i>p</i> -value	Lower, Upper 95% CI
8/16/2016	0.0	0.02	<0.01	0.01, 0.03
8/30/2016	0.2	0.02	<0.01	0.01, 0.04
9/24/2016	3.5	0.00	0.62	-0.02, 0.01
10/6/2016	5.2	-0.01	0.40	-0.04, 0.02
10/12/2016	6.8	0.00	0.89	-0.02, 0.02
10/22/2016	24.9	0.01	0.63	-0.01, 0.02
4/28/2017	20.9	-0.02	0.03	-0.04, 0.00
5/20/2017	10.7	0.01	0.51	-0.01, 0.02
6/17/2017	5.1	-0.01	0.40	-0.03, 0.01
7/11/2017	0.0	0.03	<0.01	0.01, 0.05
8/3/2017	0.0	0.03	<0.01	0.01, 0.04
9/1/2017	0.0	0.02	<0.01	0.01, 0.04
9/23/2017	17.4	0.01	0.18	-0.01, 0.03
10/15/2017	10.3	0.01	0.49	-0.01, 0.03

CHAPTER 3

CLIMATE SENSITIVITY OF LATEWOOD GROWTH OF DOUGLAS-FIR IN THE WESTERN CASCADE MOUNTAINS OF OREGON

Karla M. Jarecke, Forest Ecosystems and Society, Oregon State University

Kevin D. Bladon, Forest Engineering, Resources, and Management, Oregon State University

Steven M. Wondzell, US Forest Service, Pacific Northwest Research Station

Abstract

Tree species worldwide will face exposure to increased drought and warmer temperatures under climate change, resulting in increased water stress. In the Pacific Northwest, increasing temperatures during the dry season are expected to increase the vapor pressure deficit resulting in extreme evaporative demand. Both increased temperature and decreased precipitation are related to growth declines in Douglas-fir (*Pseudotsuga menziesii*), but few studies have examined the impact of vapor pressure deficit. In this study, we tested the effect of vapor pressure deficit, relative humidity, temperature, and precipitation on the latewood growth of ~50-year-old Douglas-fir trees in the western Cascade Mountains in Oregon. Given that mean annual rainfall exceeds 2000 mm in our study area, we expected latewood growth to be more sensitive to vapor pressure deficit than to precipitation. We used a moving window analysis and information-

theoretic approach to determine when climate variables best predicted mean latewood radial growth among all trees ($n = 27$). Latewood growth, measured as the basal area increment, of Douglas-fir was highly sensitive to the average daytime vapor pressure deficit, relative humidity, and temperature from mid-June to mid-July and less sensitive to the timing and amounts of precipitation. We then tested the relationships between the climate window and BAI among trees growing in different positions ($n = 9$) along a steep hillslope gradient using a linear mixed effect model. Climate-growth relationships were not statistically significant among sites ($p = 0.9$) and explained only 34% of the variation in growth in a mixed effect model. The predicted linear trends of latewood growth with VPD at each site were weakly related to soil moisture deficits at 50 ($R^2 = 0.3$) and 100 cm ($R^2 = 0.65$) while linear trends due to precipitation were not correlated with soil moisture deficits ($R^2 = 0.02$ and $R^2 = 0.06$). Our results suggest that although latewood growth may be more sensitive to the timing of increasing VPD than decreasing precipitation, soil moisture limitation may still be important in buffering the negative effects of seasonal aridity on tree water stress. It will be important to disentangle the effect of VPD and soil moisture on tree function to better manage forests for drought resilience.

3.1 Introduction

Rising temperatures are expected to increase evaporative demand in most regions of the continental US in the coming century (Ficklin & Novick, 2017). Higher evaporative demand accompanied by more severe drought is likely to impact tree carbon assimilation and growth (Novick et al., 2016; Sanginés de Cárcer et al., 2018; Sulman et al., 2016; Yuan et al., 2019). The period of year when climate most affects growth varies widely and can be disconnected temporally from the time of year when maximum growth rates are observed (Levesque et al., 2013; Lo et al., 2010). Thus, quantifying both the timing and magnitude of climate effects on tree radial growth can improve predictions of forest productivity and inform forest management decisions aimed to mitigate vegetation water stress (Clark et al., 2016).

Tree ring studies from the northwest U.S.A. and British Columbia suggest that both summer precipitation and temperature are significant predictors of annual growth in Douglas-fir (Chen et al., 2010; Lo et al., 2010). However, the timing of climate sensitivities can depend on region (e.g., interior vs. coastal) and altitude when examined over large geographic scales (Chen et al., 2010; Lo et al., 2010). In general, Douglas-fir growth is positively correlated with wetter summers (Levesque et al., 2013; Littell et al., 2008; Livingston & Spittlehouse, 1996) and increased spring precipitation (Zhang et al., 1999). Annual growth is positively correlated with preceding winter and spring temperatures (Case & Peterson, 2005) but negatively correlated with summer temperatures (Beedlow et al., 2013; Lo et al., 2010). Douglas-fir growth is also more sensitive to precipitation than temperature especially at lower elevations and in coastal forests (Griesbauer & Green, 2010; Little et al., 1995; Zhang & Hebda, 2004). However, it can be difficult to determine the primary source of water stress if only precipitation and temperature are evaluated. For example, precipitation is used as a proxy for soil moisture status, which carries the

implicit assumption that soil water holding capacity and retention are uniform across a given study area. Trees growing in different landscape positions may respond differently to changes in precipitation depending on soil and hydrological process that affect water availability (Adams et al., 2014). In some areas, trees in upper hillslope positions may be more vulnerable to water stress due to greater soil water deficits in high compared to low hillslope positions (Hawthorne & Miniati, 2016; Livingston & Spittlehouse, 1996). These findings suggest that using precipitation as a proxy for available soil moisture may mask important tree-to-tree variation in growth that is caused by differences in soil water availability.

The use of temperature can also be problematic because higher temperatures can impose stress on trees in two distinct ways. First, high temperatures can limit the rate of carbon assimilation in foliage via direct temperature effects on the biochemical reactions involved in photosynthesis. Second, higher temperatures often indicate higher vapor pressure deficit (VPD), which causes higher rates of transpiration from open stoma on foliage. Trees may close their stoma at high atmospheric VPD to conserve water and avoid hydraulic failure. Stomatal closure simultaneously decreases the rate of diffusion of carbon dioxide into the foliage. Thus, when using air temperature data alone, it is not possible to tell whether growth at high temperatures is limited by direct temperature effects or VPD-related effects. Moreover, disentangling the effects of VPD from temperature and other climate drivers of plant function is difficult given they tend to be correlated at seasonal timescales (Grossiord et al., 2020).

Tree ring analysis can provide important insights into which climate variables are limiting growth so that we can begin to unravel the physiological mechanisms driving the growth response. The goal of our study was to explore how the latewood growth of 50-yr old Douglas-fir is affected by VPD, relative humidity, temperature, and precipitation on the west slopes of the

Cascade Mountains of Oregon, USA. A growing body of evidence suggests that increases in atmospheric VPD in warm, dry climates reduce stomatal conductance and gross primary productivity even when soil moisture is plentiful (Jiang et al., 2019; Novick et al., 2016). Elevated VPD also explains declines in annual radial growth (Restaino et al., 2016; Williams et al., 2013) and increasing rates of tree mortality in many regions globally (Allen et al., 2015; Breshears et al., 2013). Yet, few studies have examined the climate signals that affect seasonal latewood formation, which can be different from those that affect earlywood and annual growth (Levesque et al., 2013), and may be distinctly relevant to understanding the vulnerability of Douglas-fir to projected increase in summertime water stress in the Pacific Northwest. We used a moving window analysis to identify the period of the year when climate variables were most strongly related to annual latewood growth. Additionally, we leveraged differences in soil water availability along a steep hillslope gradient to understand how spatial variability soil water stress during the growing season altered climate-growth relationships.

We asked:

1. Over which period of time is latewood growth most highly correlated to VPD, temperature, relative humidity, and precipitation?
2. Do differences in soil moisture deficits along a steep hillslope gradient alter the effect of VPD and precipitation on latewood growth?

3.2 Methods

3.2.1 Study Site

Our study took place at an elevation of ~560 m on two north-facing hillslope transects in Watershed 1, a 96 ha catchment in the HJ Andrews Experimental Forest on the west slopes of the Cascade Mountains in central Oregon (44°12'18.8" N, 122°15'16.2" W). Watershed 1 is characterized by steep (mean slope = 31°), highly dissected ridges and valleys. The watershed was clearcut from 1962–1966 and burned in 1966. There were multiple efforts to re-establish vegetation from 1967–1971 including aerial seeding and planting 2- and 3- year-old trees (Halpern, 1988). At the time of our study (2019) the stand was composed predominantly of second growth Douglas-fir trees (*Pseudotsuga menziesii*, ~40–50 years old), with some bigleaf maple (*Acer macrophyllum*) and Western hemlock (*Tsuga heterophylla*) present.

Mineral soils below the forest floor and organic horizon are gravelly, silty clay loam. Average depth to bedrock measured at each of the nine tree coring sites was 3.2 ± 1.2 m. Soils are underlain predominantly by altered pyroclastic flows of the Little Butte Formation (Swanson & James, 1975). The climate in the region is maritime with cool, wet winters and warm, dry summers. Mean total annual rainfall over 30 water years (1990–2019) was 2210 ± 435 mm (Daly et al., 2019) with over 90% of annual rainfall occurring from October through June. Mean total annual rainfall between July–September in the 1990–2019 water years was 75 ± 39 mm (Daly et al., 2019).

3.2.2 Climate Variables and Field Data Collection

We used meteorological data recorded at the Primary Meteorological Station (hereafter Primet) at the HJ Andrews Experimental Forest. Primet is in a small clearing less than a

kilometer from our study site. Air temperature and relative humidity (HMP45C probe with Vaisala capacitive relative humidity sensor and a Fenwal Electronics UUT51J1 thermistor, Campbell Scientific) were measured at 1.5 and 4.5 m aboveground. Precipitation (PPT) (TE525 tipping bucket rain gauge, Texas Electronics) was measured at 1 m aboveground. We used 15 min rainfall, air temperature, and relative humidity data from 1989 to 2019 (Daly et al., 2019), and calculated the vapor pressure deficit (VPD) from relative humidity and temperature. We aggregated 15 min data to hourly averages and then estimated total daily rainfall, mean daytime air temperature, and mean daytime VPD, where daytime was defined as the intervals of time when solar radiation (Kipp and Zonnen pyranometer with thermopile type sensor, model CM-6B) was greater than 10 W m^{-2} . Missing hourly data occurred for air temperature on 2.6% of dates and for relative humidity on 3.2 % of dates. When an hourly observation was missing, we replaced it with the long-term average daily air temperature and relative humidity for that day/hour.

Annual latewood growth water estimated from one 12 mm tree core to pith at 1.3 m aboveground from 3 dominant trees at 9 sites ($n = 27$ trees) in November 2019. Dominant trees can be more sensitive to climate variation compared to co-dominant and intermediate canopy position trees (Barnard et al., 2012). Thus, the heights of trees at each site were visually inspected, and dominant trees were identified by crowns extending above the average crown height. Additionally, we measured and recorded the diameter of the tree at 1.3 m aboveground. The mean diameter among all trees was 37.5 ± 4.7 cm.

Sites were located approximately 20–40 m apart along two hillslope transects (Figure 3.1). Euclidean distance from the headwater perennial stream in Watershed 1 was estimated at each site using a 1 x 1 m digital elevation model (Spies, 2016) in ArcGIS 10.5.1. We recorded

hourly soil moisture (5TM, METER Environment) at 50 and 100 cm at each site from October 2018 to October 2019 from which we calculated the average daily soil moisture. The 3 dominant sample trees at each site were located within 10 m of the soil moisture sensors.

3.2.3 Lab Processing of Tree Cores

We dried, mounted, and sanded tree cores after which latewood and earlywood boundaries for each year's growth were easily observable. All cores were dated, and cross-dating accuracy was checked using COFECHA software (Holmes, 1983). We measured the width of earlywood and latewood rings along each core with a sliding stage incremental micrometer (Velmex, Inc., Bloomfield, NY, USA, 0.001 mm precision) with Measure J2X software (VoorTech Consulting, Holderness, NH, USA).

Latewood is distinguished from earlywood by a step-change in color and wood density typical of Douglas-fir. Latewood has narrower and thicker-walled conduits, and as a result, appears darker than earlywood. The transition in wood density from the large-diameter, thin-walled earlywood tracheids to the narrow-diameter, thick-walled latewood tracheids occurs during the summer dry season and allows conifer trees to maintain turgor during periods of increased water stress (Arzac et al., 2018). We calculated basal area increment for each year using measurements of earlywood and latewood ring widths and the assumption of a circular stem cross section for our sample trees.

3.2.4 Moving Window Analysis

The annual radial growth of latewood, measured as the basal area increment (BAI), was highly variable among trees between 1990 and 2019 (mean = 1,126 mm² and standard deviation

= 469 mm²). The change in latewood BAI from year-to-year, both in magnitude and direction, was not always the same among the three dominant trees at each site (Figure 3.2a) nor among the nine sites (Figure 3.2b). Despite these site differences in the amount of radial growth in a given year, the average BAI at most of the sites showed a relatively large decrease in latewood growth from 1995–2000 (Figure 3.2b).

We used the average latewood BAI of all trees for each growth year from 1990–2019 (black line, Figure 3.2b) as the response variable in a moving window analysis to determine which climate variables, and during which period of time over the preceding 16 months, were the best predictors of the latewood growth. We used the ‘climwin’ package in R (Bailey & De Pol, 2016) to calculate an average or sum of each climate variable over all possible sizes of moving windows for the 16 months preceding the growth year (e.g., daily from 30 Sept of the current year back to 1 June of the preceding year). This approach allowed us to explore 118,828 time periods or ‘windows’ over which we aggregated each climate variable. We examined each climate variable separately and regressed the yearly average BAI on the moving window average (or sum) of the climate variable using simple linear regression. We tested the linear relationship between average yearly latewood BAI and average daytime VPD, average daytime temperature, average daytime relative humidity, and total daily rainfall for all possible climate windows over the preceding 16 months (total = 118,828 models). Testing climate windows over a 16-month period allowed us to identify the potential lagged effects of climate on latewood formation.

For each climate variable, models were compared using Akaike information criterion corrected for small sample sizes (AIC_c). The difference between AIC_c of each model and the null model with no climate predictor (BAI = average BAI over all years) generated a Δ AIC_c for each model. The Δ AIC_c values were used to evaluate model support for each different climate

window in explaining the variation in our response variable. The single best model for each climate variable was identified from all possible models as the one with the greatest improvement over the null model without a climate predictor variable.

The ‘climwin’ package estimated model weights (posterior model probabilities) that quantified the probability that each model is the best supported model (Burnham et al., 2011). The top models had higher weights or greater probability of being the “best” model. Models were ranked by weight from highest to lowest and the top model weights were summed until a sum of 0.95 was reached. Models included in this sum represented the 95% model confidence set. This 95% confidence set was used to describe the uncertainty in the selection of the single best model. In addition, we examined the range of climate windows (opening and closing dates) within the 95% model confidence set. Small variation in window opening and closing dates in the 95% confidence set indicated that useful models were restricted to a particular period of the year.

Several climate windows may be equally likely to result in a model with similar ΔAIC_c values due to the exploratory nature of the moving window analysis and fine temporal resolution of the climate data (daily). To determine the likelihood of our best model being chosen by random chance, we repeated the moving window analysis after randomly arranging the dates in the original dataset to remove any true climate signal. We repeated this randomization test 100 times to create a distribution of ΔAIC_c values. We used the randomization distribution of ΔAIC_c values to estimate the probability of obtaining the observed or smaller values of ΔAIC_c from our single best model. If the probability was less than 0.05, we concluded that our results were unlikely to have occurred by random chance.

3.2.5 Mixed Effects Model

We tested the effect of VPD and PPT on the yearly latewood BAI for individual trees among sites using a linear mixed effect model (R package ‘lmer’; Pinheiro et al., 2020). Average daytime VPD and total PPT from the moving window analysis were used as fixed effects that interacted with site—a categorical variable. In addition, we included a random effect for individual sample trees within each site. We did not include air temperature and relative humidity in the model because VPD was strongly correlated to both air temperature ($R^2 = 0.78$) and relative humidity ($R^2 = 0.88$). Model residuals were checked for the assumptions of independence, normality, and constant variance. We relaxed the assumption of constant variance for ‘site’ and added an autoregressive lag 1 correlation structure to account for the temporal autocorrelation of BAI over time. Residuals were checked to ensure that the model structure resulted in homogeneity of the residuals.

We estimated the variance components of the model using restricted maximum likelihood and calculated a pseudo- R^2 to determine how well the interaction terms (VPD x site and PPT x site) explained variation in latewood growth. We also used the R package ‘emmeans’ (Lenth, 2021) to estimate and compare the marginal means and confidence intervals of estimated linear slopes associated with each site. Slope estimates from our model described the effect of VPD and PPT on latewood growth at each site ($n = 9$) after accounting for the effect of other variables in the model. Lastly, we explored the relationship between the marginal means/slope estimates to site attributes, including distance from stream and growing season soil moisture deficit at 50 and 100 cm, to understand whether these factors influenced the tree growth-climate relationships in our study area. The soil moisture deficit was determined as the difference between the maximum and minimum daily average volumetric water content between April and September 2019.

3.3 Results

3.3.1 Moving Window Analysis to Detect Climate Signals in Latewood Growth

The climate windows with the single lowest ΔAIC_c value of all the tested windows fell into the period from mid-June to mid-July for each climate variable except PPT (Table 3.1). For linear models of BAI vs. vapor pressure deficit (VPD), 8% of models were included in the 95% confidence set determined from the model weights with the window opening dates for these models showing more variability than the window closing date (Figure 3.3a, Table 3.1). The 95% confidence set for models of BAI vs. relative humidity included 3% of all models, and the 95% confidence set for BAI vs. temperature included 5% of all models (Figure 3.3b, 3.3c, Table 3.1). The window opening and closing dates for the 95% confidence set were narrower for relative humidity and temperature compared to VPD, but the median opening and closing date were similar for all three variables (Figure 3.3a, 3.3b, 3.3c).

The single best model for each climate variable had the lowest ΔAIC_c value, resulting in a strong correlation between each climate variable and latewood BAI (Figure 3.4). We identified a strong negative linear relationship ($R^2 = 0.71$) between BAI and average daytime VPD from June 13 to July 15 (Figure 3.4a) and between BAI and temperature between June 11 and July 12 ($R^2 = 0.51$, Figure 3.4c). The single best model for relative humidity was detected for a similar climate window, between June 17 and July 15, and had a strong positive linear relationship with BAI ($R^2 = 0.72$, Figure 3.4b). The single best models chosen for VPD, temperature, and relative humidity are hereafter referred to as VPD_{optimal} , $Temp_{\text{optimal}}$, and RH_{optimal} . The ΔAIC_c values for VPD_{optimal} (-34.3) and RH_{optimal} (-36.2) were much lower than the ΔAIC_c values generated with the randomized data sets ($p < 0.001$, Figure 3.4a, 3.4b, Table 3.1). In contrast the ΔAIC_c value

for $\text{Temp}_{\text{optimal}}$ (-18.8) overlapped the tail end of the distribution of ΔAIC_c values generated from the randomization tests ($p = 0.02$, Figure 3.4c, Table 3.1).

The single best climate window that emerged for precipitation ($\text{PPT}_{\text{optimal}}$) was from June 13 to June 23 during which we observed a positive linear relationship between BAI and PPT ($R^2 = 0.43$, Figure 3.4d). Although BAI and PPT were reasonably correlated during this period, 77% of models were included in the 95% confidence set creating large variability in the window opening and closing dates among all models considered between September to June of the previous year (Figure 3.3d). $\text{PPT}_{\text{optimal}}$ had a ΔAIC_c value (-14.6) that was not statistically different from the ΔAIC_c values generated from the randomization tests ($p = 0.2$, Figure 3.4d, Table 3.1) suggesting more uncertainty in the model selection.

3.3.2 Differences in Climate-growth Relationship Among Sites

The fixed effects in our model (VPD x site and PPT x site) explained approximately 34% of the variation in our response variable, latewood BAI (pseudo $R^2 = 0.34$). However, the overall interactive effect of VPD x site was not statistically significant ($F = 0.41$, $p = 0.91$) nor was the effect of PPT x site ($F = 0.43$, $p = 0.90$). Although the interaction terms were not significant in our model, we estimated the marginal slopes to understand potential practical differences in linear trends among sites.

The marginal slopes of the linear trends of BAI vs. VPD were statistically different from zero for all sites ($p < 0.05$) except LZ3 ($p = 0.1$) and LZ5 ($p = 0.051$). The range of daytime VPD averaged within the best climate window (June 13 to July 15) was 0.84 kPa ($\text{VPD}_{\text{optimal}}$, Figure 3.4a). The predicted change in latewood BAI for a 0.84 kPa increase in VPD ranged from to -195 to -393 mm^2 across sites, with the 95% confidence intervals among sites ranging from -622 to 41

mm² (Figure 3.5a). In contrast, the linear trends of BAI vs. PPT were not statistically different from zero at any of the sites. The range in total PPT within the best climate window (June 13 to June 23) was 66 mm (PPT_{optimal}, Figure 3.4d). The predicted change in latewood BAI for an increase in PPT by 66 mm ranged from -76 to 155 mm² across sites, with the 95% confidence intervals among sites ranging from -274 to 443 mm² (Figure 3.5b).

We explored whether the marginal slope estimates for each site were correlated to site attributes including the site's distance from the stream and the summer soil moisture deficit measured at each site in 2019. The predicted change in BAI for a 0.84 kPa increase in VPD was not well correlated to sites' distance from the stream ($R^2 = 0.03$). However, the summer soil moisture deficit was weakly related to the predicted change in BAI with increased VPD at 50 cm ($R^2 = 0.3$) and 100 cm ($R^2 = 0.65$). In contrast, the sites' soil moisture deficit at 50 and 100 cm were not correlated to the predicted change in BAI due to PPT ($R^2 = 0.02$ and $R^2 = 0.06$). However, we did find that the effect of PPT on latewood BAI was weakly related to the distance from the stream with sites closer to the stream showing a positive relationship with PPT and sites further from the stream showing a negative relationship with PPT.

3.4 Discussion

3.4.1 Latewood Growth Sensitivity to Climate

We found that climate variability in early summer (June and July) had the greatest impact on latewood growth in Douglas-fir. Air temperature and vapor pressure deficit (VPD) were negatively correlated to annual latewood growth while relative humidity and precipitation (PPT) were positively correlated to yearly latewood growth (Table 3.1). The large number of models

included in the 95% confidence set, when PPT was the sole predictor of growth, indicated that latewood growth was not strongly influenced by a specific period of rainfall accumulation. In contrast, a relatively small number of models were included in the 95% confidence set for VPD, relative humidity, and air temperature, indicating strong relationships between atmospheric variables in early summer and latewood growth.

Summer growth limitation in Douglas-fir growing in a Mediterranean climate is generally attributed to annual summer drought (Beedlow et al., 2013; Livingston & Spittlehouse, 1996) while annual growth can be sensitive to both precipitation and temperature (Little et al. 1995, Zhang et al. 1999, Lo et al. 2010) ranging from a positive influence of previous spring and winter temperatures at higher elevations (Case & Peterson, 2005) and in coastal regions (Little et al., 1995) to a negative influence of decreased summer precipitation and increased temperatures at low- to mid-elevations in regions with more continental climates (Bower et al., 2005; Chen et al., 2010; Griesbauer & Green, 2010; Lo et al., 2010). However, the relative effect of temperature and vapor pressure deficit (VPD) vs. soil moisture on carbon assimilation under hot and dry conditions are not completely understood (Grossiord et al., 2020) and increased VPD has been shown to reduce stomatal conductance independent of precipitation regimes (Grossiord et al., 2018; Jiang et al., 2019) and soil moisture availability (Novick et al., 2016).

Our results are consistent with results reported by Beedlow et al. (2013) who found that summer temperature and VPD were negatively correlated to seasonal growth in Douglas-fir across the western Cascade Mountains of Oregon. Heat-driven increases in VPD during the summer can significantly reduce primary production in Douglas-fir independent of rainfall amounts (Jiang et al., 2019). The optimal temperature for photosynthesis in Douglas-fir in western Oregon is around 20 °C, with photosynthetic rates declining rapidly above 25 °C (Lewis

et al., 2001). In our best models, the average daytime VPD ranged from ~0.6 to 1.5 kPa and temperature ranged from ~16 to 23 °C (Figure 3.4a, 3.4c). We would not expect stomatal conductance and/or photosynthesis to be constrained under these ranges in temperature and VPD. However, these ranges represent the mean daytime temperature and VPD over the time span of ~30 days from mid-June to mid-July. During the period of 1990 to 2019, the maximum daytime temperature during that same 30-day period ranged from 9.6 to 40.3 °C and VPD ranged from 0 to 6.2 kPa. It may be that correlation of latewood growth to monthly mean values served as a proxy for the response of yearly growth to the number of days when high midday temperature and VPD had a negative effect on tree growth. More work is needed to further understand the separate effects of temperature and atmospheric VPD on the physiological mechanisms that influence latewood production during this period.

In contrast with other studies, we did not find a specific time of year in which latewood growth was sensitive to interannual variability in precipitation (PPT). The large uncertainty in the PPT signal in our study could suggest that PPT did not capture the interannual variability in plant-available water since previous research shows latewood growth of Douglas-fir was negatively correlated to the growing season water deficit (Livingston & Spittlehouse, 1996; Robertson et al., 1990). Interestingly, only 6% of models in the 95% confidence set for PPT as a predictor of growth had window opening and closing dates during the summer of the current year's growth. We found that 70% of those models with summer windows described a positive relationship between PPT and latewood growth. This suggests that PPT amounts during the summer had a positive impact on growth despite the lack of evidence that a particular window of time was consequential. The trees sampled for this study were growing on steep, north-facing slopes with relatively deep soils (mean depth = 3.2 m). Brooks et al., (2002) showed that the

hydraulic redistribution of water stored below the 60 cm depth supplied ~40% of the daily transpiration in a Douglas-fir stand over a summer drought season. Thus, greater amounts of rainfall during the summer would contribute to shallow soil moisture and benefit growth processes. However, the timing of rainfall may not be as important in places where trees grow deep roots and have reliable access to stored water, whereas the timing of rainfall might be more important in systems with relatively small subsurface water storage capacities (e.g., shallow soils or shallow rooting zone) that are rapidly depleted during the growing season (Hahm et al., 2019).

3.4.2 Climate-growth Relationships Among Sites

The marginal means of linear trends between latewood BAI and VPD/PPT among sites were not statistically different given the large 95% confidence intervals. We predicted the change in latewood BAI at each site with the maximum increase in early summer VPD observed between 1990 and 2019 (VPD during the driest year on record, 1.46 kPa minus VPD during the wettest year, 0.62 kPa). The predicted decline in latewood BAI for a 0.84 kPa increase in VPD varied from approximately -400 to -200 mm² among sites (Figure 3.5a). A 200 mm² difference in latewood growth from low vs. high VPD conditions was ~30% of the observed range in mean latewood growth (~600 mm²) over 30 years (Figure 3.2b). Thus, these estimated differences are meaningful and suggest that sites along our steep hillslope gradient may respond differently to increases in seasonal VPD.

Factors such as soils, topography, and competition can influence local conditions that mitigate or exacerbate the effect of climate on growth and physiological water stress (Adams et al., 2014; Hawthorne & Miniat, 2016; Oberhuber & Kofler, 2000). Sites in this study were located on two hillslopes and spaced roughly 20–40 m apart along hillslope transects (Figure

3.1). The soil water deficit observed at each site during summer 2019 varied from 0.09 to 0.2 $\text{cm}^3 \text{cm}^{-3}$ at 50 cm and 100 cm below ground. Our previous research on soil moisture patterns in this area suggest that local soil properties were a dominant control on spatial patterns of soil moisture that were persistent across seasons and years (Jarecke et al., 2021). Thus, we'd expect that relative moisture availability among sites would not change from one year to the next given the local soil hydraulic properties.

We found that the slope of the VPD vs. latewood growth relationship at each site was negatively correlated to the site's soil moisture deficit between April 1 and Sept 1, 2019 (Figure 3.6a). The greater decline in latewood growth at sites with higher moisture deficits highlight that variability in local soil properties may alter the degree to which trees experience water stress in this area. We did not find strong evidence that the relationship between VPD and BAI was mitigated by hillslope position/distance from stream. Nor did we find evidence that site attributes modified the relationship between PPT and BAI. Future research aimed at exploring latewood growth response to seasonal temperature and VPD at relatively wet vs. dry sites would help illuminate the influence of soil moisture on seasonal growth and water stress in this environment.

3.4.3 Timing of Radial Growth Phases and Sensitivity to Climate

Latewood formation in Douglas-fir typically begins after shoot elongation is ~90% complete (Beedlow et al., 2013). Some authors have proposed the transition from earlywood to latewood in conifers is triggered by hormones (Uggla et al., 1996), while others have suggested it is triggered by climate constraints on cell water turgor pressure or metabolic activity (Cuny & Rathgeber, 2016). The formation of latewood involves a phase of cell enlargement followed by a separate phase of cell wall thickening. Cell enlargement is a relatively rapid process while cell

wall thickening is a much longer process, involving the complex assembly of materials that contribute to the majority of latewood biomass (Cuny et al., 2015). Latewood growth generally begins when shoot elongation slows and lasts approximately 17 days in the Oregon Cascades and approximately 43 days in the warmer environment of the Coast Range (Emmingham, 1974). More recent research shows that latewood cells in conifers may require as few as six days for enlargement (Cuny & Rathgeber, 2016). In general, cell enlargement stops when the increased thickness of the cell wall inhibits further relaxation, and further thickening of the cell walls occurs without increases in cell size (Carteni et al., 2018; Cosgrove, 2005). This asynchrony between the timing of cell enlargement and cell thickening suggests that these processes are likely to be influenced by different climate conditions (Belmecheri et al., 2018).

We found that the time of year when increased VPD and temperature suppress latewood growth (mid-June to mid-July) corresponds well to the date of latewood initiation which typically occurs between July and August in Douglas-fir populations growing on the west slope of the Oregon Cascades (Emmingham 1974; Beedlow et al. 2013). However, latewood initiation appears to be under some degree of genetic control so that latewood of Coastal Douglas-fir can start forming as early as June and as late as August, with an average transition date of July 6 (Vargas-Hernandez & Adams, 1994). It is possible that that atmospheric water stress—and potentially soil water stress—suppressed cell enlargement during latewood formation in our study. Cell enlargement is often depicted as the process of stem radial growth that is most sensitive to water stress (Gruber et al., 2010). When soil moisture deficits are high, a reduction in turgor pressure can result in the smaller cell dimensions (Cabon et al., 2020). There is evidence that soil water availability can control tracheid enlargement in conifers (Cabon et al., 2020; Gruber et al., 2010) and that latewood growth in Douglas-fir can be suppressed by an increase in

the growing season soil water deficit (Levesque et al., 2013). However, we would not expect soil moisture to be limiting in early summer at our sites, based on the results of our moving window analysis and the fact that June received, on average, 73 mm of rainfall from 1989 to 2019. Our results suggest that elevated VPD, under well-watered conditions in early summer, were more impactful on the process of tracheid enlargement at our site. The loss of water during periods of high VPD can cause a reduction in cell turgor pressure, which may suppress tracheid cell enlargement after latewood initiation; however, more work would be necessary to understand how physiological responses relate to latewood formation during this period. While the physiological mechanisms that suppressed growth during this time require further investigation, we think that the climate window that we identified as the most consequential to growth may be linked to developmental traits that impact the timing of latewood initiation of Douglas-fir at our site.

3.4.4 Study Limitations

We used the mean latewood basal area increment (BAI) to explore the effect of climate variables on latewood growth. Yet, we found considerable variation in latewood BAI from site to site (Figure 3.2b). Differences may be attributed to local abiotic (soil properties, landscape position) and biotic (canopy structure, leaf area, rooting depth, nutrients) factors since trees are similar in age. Differences in local factors that affect growth were not captured in this study, but there is evidence that climate-growth relationships can differ across small spatial extents. The differences in slopes that described the VPD effect on latewood growth among sites is potential evidence that these local conditions, such as the soil water deficit, may exert important controls

on latewood growth, but were not included in our moving window analysis or mixed effect model.

Decadal climate events (e.g., Pacific Decadal Oscillation) have also been shown to affect growth (Griesbauer & Green, 2010) but were not explored in this study. Thus, the correlations observed over our 30-year record may not hold with a shorter, or even longer, climate record due to shifts in regional climate regimes. The sensitivity of Douglas-fir growth to climate has been documented to change over time in the northern Rockies (Hankin et al., 2019). Increasing precipitation variability over time or decreasing variability in summer temperatures are likely to alter tree physiological response to climate, especially if extreme drought conditions become more frequent under climate change. Additionally, local conditions (e.g., microclimate, soil water and nutrient availability) shaped by forest succession and biotic interactions can also affect how Douglas-fir respond to climate over time (Carnwath & Nelson, 2016). These changes complicate our understanding of how future climate will affect tree growth response and indicate that the correlations observed between 1990 and 2019 in this study may not hold if we had explored a shorter or longer record and may not hold in the future due to shifts in local conditions and interannual climate variability.

Climate-growth relationships recorded in tree rings have improved our understanding of species' adaptive capacity to climate variability, lagged effects of drought (Huang et al., 2018), and growth response to forest management such as thinning (Briggs & Kantavichai, 2018; Mitchell, 2000). However, tree ring analysis of carbon stable isotopes—a reflection of the hydrological response to water stress—suggest that isotopes are a more sensitive indicator of carbon uptake than growth because correlations between radial growth and climate can be poor in environments where trees do not cross their physiological thresholds (Meko et al., 1993). We

found that Douglas-fir latewood growth was sensitive to climate from 1990–2019, but another study in the same watershed found that annual radial growth was not sensitive to climate while stable carbon isotopes were (Barnard et al., 2012). Stable carbon isotopes of latewood from 1990–2019 would provide stronger evidence of the Douglas-fir response to inter- and intra-annual climate variability. Analysis of latewood stable carbon isotopes may also reveal a different climate signal that is associated with the process of latewood cell wall thickening, when most of the cellulose is incorporated in latewood formation (Belmecheri et al., 2018).

3.5 Acknowledgments and Data

We thank the HJ Andrews staff for their support with project logistics and use of facilities. Data were provided by the HJ Andrews Experimental Forest research program, funded by the National Science Foundation’s Long-Term Ecological Research Program (LTER7 DEB 1440409), USDA Forest Service Pacific Northwest Research Station, and Oregon State University. We thank David Moy and Haley Weir for their help with field collection of tree cores and lab measurements of rings widths. Tree ring data are publicly available via the Andrews Forest database (<http://andlter.forestry.oregonstate.edu/data/abstract.aspx?dbcode=TV085>) in addition to the LiDAR-based DEM (<http://andlter.forestry.oregonstate.edu/data/abstract.aspx?dbcode=GI010>) and meteorological data (<http://andlter.forestry.oregonstate.edu/data/abstract.aspx?dbcode=MS001>).

3.6 References

- Adams, H. R., Barnard, H. R., & Loomis, A. K. (2014). Topography alters tree growth–climate relationships in a semi-arid forested catchment. *Ecosphere*, *5*(11), art148. <https://doi.org/10.1890/ES14-00296.1>
- Allen, C. D., Breshears, D. D., & McDowell, N. G. (2015). On underestimation of global vulnerability to tree mortality and forest die-off from hotter drought in the Anthropocene. *Ecosphere*, *6*(8), 1–55. <https://doi.org/10.1890/ES15-00203.1>
- Arzac, A., Babushkina, E. A., Fonti, P., Slobodchikova, V., Sviderskaya, I. V., & Vaganov, E. A. (2018). Evidences of wider latewood in *Pinus sylvestris* from a forest-steppe of Southern Siberia. *Dendrochronologia*, *49*(March), 1–8. <https://doi.org/10.1016/j.dendro.2018.02.007>
- Bailey, L. D., & De Pol, M. Van. (2016). Climwin: An R Toolbox for Climate Window Analysis. *PLoS ONE*, *11*(12), 1–27. <https://doi.org/10.1371/journal.pone.0167980>
- Barnard, H. R., Brooks, J. R., & Bond, B. J. (2012). Applying the dual-isotope conceptual model to interpret physiological trends under uncontrolled conditions. *Tree Physiology*, *32*(10), 1183–1198. <https://doi.org/10.1093/treephys/tps078>
- Beedlow, P. A., Lee, E. H., Tingey, D. T., Waschmann, R. S., & Burdick, C. A. (2013). The importance of seasonal temperature and moisture patterns on growth of Douglas-fir in western Oregon, USA. *Agricultural and Forest Meteorology*, *169*, 174–185. <https://doi.org/10.1016/j.agrformet.2012.10.010>
- Belmecheri, S., Wright, W. E., Szejner, P., Morino, K. A., & Monson, R. K. (2018). Carbon and oxygen isotope fractionations in tree rings reveal interactions between cambial phenology and seasonal climate. *Plant Cell and Environment*, *41*(12), 2758–2772. <https://doi.org/10.1111/pce.13401>
- Bower, A. D., Thomas Adams, W., Birkes, D., & Nalle, D. (2005). Response of annual growth ring components to soil moisture deficit in young, plantation-grown Douglas-fir in coastal British Columbia. *Canadian Journal of Forest Research*, *35*(10), 2491–2499. <https://doi.org/10.1139/x05-146>
- Breshears, D. D., Adams, H. D., Eamus, D., McDowell, N. G., Law, D. J., Will, R. E., et al. (2013). The critical amplifying role of increasing atmospheric moisture demand on tree mortality and associated regional die-off. *Frontiers in Plant Science*, *4*(AUG), 2–5. <https://doi.org/10.3389/fpls.2013.00266>
- Briggs, D. G., & Kantavichai, R. (2018). Effects of thinning on ring mass growth along stem of douglas fir in four coastal pacific northwest sites. *Forest Science*, *64*(2), 139–148. <https://doi.org/10.1093/forsci/fxx003>
- Burnham, K. P., Anderson, D. R., & Huyvaert, K. P. (2011). AIC model selection and multimodel inference in behavioral ecology: Some background, observations, and comparisons. *Behavioral Ecology and Sociobiology*, *65*(1), 23–35. <https://doi.org/10.1007/s00265-010-1029-6>
- Cabon, A., Fernández-de-Uña, L., Gea-Izquierdo, G., Meinzer, F. C., Woodruff, D. R., Martínez-Vilalta, J., & De Cáceres, M. (2020). Water potential control of turgor-driven tracheid enlargement in Scots pine at its xeric distribution edge. *New Phytologist*, *225*(1), 209–221.

<https://doi.org/10.1111/nph.16146>

- Carnwath, G. C., & Nelson, C. R. (2016). The effect of competition on responses to drought and interannual climate variability of a dominant conifer tree of western North America. *Journal of Ecology*, *104*(5), 1421–1431. <https://doi.org/10.1111/1365-2745.12604>
- Carteni, F., Deslauriers, A., Rossi, S., Morin, H., De Micco, V., Mazzoleni, S., & Giannino, F. (2018). The physiological mechanisms behind the earlywood-to-latewood transition: A process-based modeling approach. *Frontiers in Plant Science*, *9*(July), 1–12. <https://doi.org/10.3389/fpls.2018.01053>
- Case, M. J., & Peterson, D. L. (2005). Fine-scale variability in growth climate relationships of Douglas-fir, North Cascade Range, Washington. *Canadian Journal of Forest Research*, *35*(11), 2743–2755. <https://doi.org/10.1139/x05-191>
- Chen, P. Y., Welsh, C., & Hamann, A. (2010). Geographic variation in growth response of Douglas-fir to interannual climate variability and projected climate change. *Global Change Biology*, *16*(12), 3374–3385. <https://doi.org/10.1111/j.1365-2486.2010.02166.x>
- Clark, J. S., Iverson, L., Woodall, C. W., Allen, C. D., Bell, D. M., Bragg, D. C., et al. (2016). The impacts of increasing drought on forest dynamics, structure, and biodiversity in the United States. *Global Change Biology*, *22*(7), 2329–2352. <https://doi.org/10.1111/gcb.13160>
- Cosgrove, D. J. (2005). Growth of the plant cell wall. *Nature Reviews Molecular Cell Biology*, *6*(11), 850–861. <https://doi.org/10.1038/nrm1746>
- Cuny, H. E., & Rathgeber, C. B. K. (2016). Xylogenesis: Coniferous trees of temperate forests are listening to the climate tale during the growing season but only remember the last words! *Plant Physiology*, *171*(1), 306–317. <https://doi.org/10.1104/pp.16.00037>
- Cuny, H. E., Rathgeber, C. B. K., Frank, D., Fonti, P., Makinen, H., Prislan, P., et al. (2015). Woody biomass production lags stem-girth increase by over one month in coniferous forests. *Nature Plants*, *1*(October), 1–6. <https://doi.org/10.1038/nplants.2015.160>
- Daly, C., Schulze, M., & McKee, W. (2019). Meteorological data from benchmark stations at the HJ Andrews Experimental Forest, 1957 to present. Long-Term Ecological Research. Forest Science Data Bank, Corvallis, OR: Available: <http://andlter.forestry.oregonstate.edu/data/abstract.aspx?dbcode=MS001>. <https://doi.org/10.6073/pasta/c021a2ebf1f91adf0ba3b5e53189c84f>
- Emmingham, W. H. (1974). *Physiological responses of four Douglas-fir populations in three contrasting field environments*. Oregon State University.
- Ficklin, D. L., & Novick, K. A. (2017). Historic and projected changes in vapor pressure deficit suggest a continental-scale drying of the United States atmosphere. *Journal of Geophysical Research-Atmospheres*, *122*, 2061–2079. <https://doi.org/10.1002/2016JD025855>
- Griesbauer, H. P., & Green, D. S. (2010). Assessing the climatic sensitivity of Douglas-fir at its northern range margins in British Columbia, Canada. *Trees - Structure and Function*, *24*(2), 375–389. <https://doi.org/10.1007/s00468-009-0407-z>
- Grossiord, C., Gessler, A., Reed, S. C., Borrego, I., Collins, A. D., Dickman, L. T., et al. (2018). Reductions in tree performance during hotter droughts are mitigated by shifts in nitrogen

- cycling. *Plant Cell and Environment*, 41(11), 2627–2637. <https://doi.org/10.1111/pce.13389>
- Grossiord, C., Buckley, T. N., Cernusak, L. A., Novick, K. A., Poulter, B., Siegwolf, R. T. W., et al. (2020). Plant responses to rising vapor pressure deficit. *New Phytologist*, nph.16485. <https://doi.org/10.1111/nph.16485>
- Gruber, A., Strobl, S., Veit, B., & Oberhuber, W. (2010). Impact of drought on the temporal dynamics of wood formation in *Pinus sylvestris*. *Tree Physiology*, 30(4), 490–501. <https://doi.org/10.1093/treephys/tpq003>
- Hahm, W. J., Dralle, D. N., Rempe, D. M., Bryk, A. B., Thompson, S. E., Dawson, T. E., & Dietrich, W. E. (2019). Low subsurface water storage capacity relative to annual rainfall decouples Mediterranean plant productivity and water use from rainfall variability. *Geophysical Research Letters*, 6544–6553. <https://doi.org/10.1029/2019GL083294>
- Halpern, C. B. (1988). Early successional pathways and the resistance and resilience of forest communities. *Ecological Society of America*, 69(6), 1703–1715.
- Hankin, L. E., Higuera, P. E., Davis, K. T., & Dobrowski, S. Z. (2019). Impacts of growing-season climate on tree growth and post-fire regeneration in ponderosa pine and Douglas-fir forests. *Ecosphere*, 10(4). <https://doi.org/10.1002/ecs2.2679>
- Hawthorne, S., & Miniati, C. F. (2016). Topography may mitigate drought effects on vegetation along a hillslope gradient. *Ecohydrology*, 11(1). <https://doi.org/10.1002/eco.1825>
- Holmes, R. (1983). Computer-assisted quality control in tree-ring dating and measurement. *Tree-Ring Bulletin*.
- Huang, M., Wang, X., Keenan, T. F., & Piao, S. (2018). Drought timing influences the legacy of tree growth recovery. *Global Change Biology*, 24(8), 3546–3559. <https://doi.org/10.1111/gcb.14294>
- Jarecke, K. M., Bladon, K. D., & Wondzell, S. M. (2021). The influence of local and nonlocal factors on soil water content in a steep forested catchment. *Water Resources Research*, 57(5), 1–21. <https://doi.org/10.1029/2020wr028343>
- Jiang, Y., Kim, J. B., Trugman, A. T., Kim, Y., & Still, C. J. (2019). Linking tree physiological constraints with predictions of carbon and water fluxes at an old-growth coniferous forest. *Ecosphere*, 10(4). <https://doi.org/10.1002/ecs2.2692>
- Lenth, R. V. (2021). emmeans: Estimated marginal means, aka least-squares means. Retrieved from <https://cran.r-project.org/package=emmeans>
- Levesque, M., Saurer, M., Siegwolf, R., Eilmann, B., Brang, P., Bugmann, H., & Rigling, A. (2013). Drought response of five conifer species under contrasting water availability suggests high vulnerability of Norway spruce and European larch. *Global Change Biology*, 19, 3184–3199. <https://doi.org/10.1111/gcb.12268>
- Lewis, J. D., Lucash, M., Olszyk, D., & Tingey, D. T. (2001). Seasonal patterns of photosynthesis in douglas fir seedlings during the third and fourth year of exposure to elevated CO₂ and temperature. *Plant, Cell and Environment*, 24(5), 539–548. <https://doi.org/10.1046/j.1365-3040.2001.00700.x>
- Littell, J. S., Peterson, D. L., & Tjoelker, M. (2008). Douglas-fir growth in mountain ecosystems:

- Water limits tree growth from stand to region. *Ecological Monographs*, 78(3), 349–368.
<https://doi.org/10.1890/07-0712.1>
- Little, R. L., Peterson, D. L., Silsbee, D. G., L.J., S., & Bednar, L. F. (1995). Radial growth patterns and the effects of climate on second-growth Douglas-fir (*Pseudotsuga menziesii*) in the Siskiyou Mountains, Oregon. *Canadian Journal of Fisheries and Aquatic Sciences*, 25, 724–735.
- Livingston, N. J., & Spittlehouse, D. L. (1996). Carbon isotope fractionation in tree ring early and late wood in relation to intra-growing season water balance. *Plant, Cell and Environment*, 19(6), 768–774. <https://doi.org/10.1111/j.1365-3040.1996.tb00413.x>
- Lo, Y. H., Blanco, J. A., Seely, B., Welham, C., & Kimmins, J. P. (Hamish). (2010). Relationships between climate and tree radial growth in interior British Columbia, Canada. *Forest Ecology and Management*, 259(5), 932–942.
<https://doi.org/10.1016/j.foreco.2009.11.033>
- Meko, D. M., Cook, E. R., Stahle, D. W., Stockton, C. W., & Hughes, M. K. (1993). Spatial patterns of tree-growth anomalies in the United States and Southeastern Canada. *Journal of Climate*, 1773–1785.
- Mitchell, S. J. (2000). Stem growth responses in Douglas-fir and sitka spruce following thinning: Implications for assessing wind-firmness. *Forest Ecology and Management*, 135(1–3), 105–114. [https://doi.org/10.1016/S0378-1127\(00\)00302-9](https://doi.org/10.1016/S0378-1127(00)00302-9)
- Novick, K. A., Ficklin, D. L., Stoy, P. C., Williams, C. A., Bohrer, G., Oishi, A. C., et al. (2016). The increasing importance of atmospheric demand for ecosystem water and carbon fluxes. *Nature Climate Change*, 6(11), 1023–1027. <https://doi.org/10.1038/nclimate3114>
- Oberhuber, W., & Kofler, W. (2000). Topographic influences on radial growth of Scots pine (*Pinus sylvestris* L.) at small spatial scales. *Plant Ecology*, 146(2), 231–240.
<https://doi.org/10.1023/A:1009827628125>
- Pinheiro, J., Bates, D., DebRoy, S., & Sarkar, D. (2020). Linear and nonlinear mixed effects models. Retrieved from <https://cran.r-project.org/package=nlme>
- Restaino, C. M., Peterson, D. L., & Littell, J. (2016). Increased water deficit decreases Douglas fir growth throughout western US forests. *Proceedings of the National Academy of Sciences of the United States of America*, 113(34), 9557–9562.
<https://doi.org/10.1073/pnas.1602384113>
- Robertson, E. O., Jozsa, L. A., & Spittlehouse, D. L. (1990). Estimating Douglas-fir wood production from soil and climate data. *Canadian Journal of Forest Research*, 20, 357–364.
- Sanginés de Cárcer, P., Vitasse, Y., Peñuelas, J., Jasey, V. E. J., Buttler, A., & Signarbieux, C. (2018). Vapor–pressure deficit and extreme climatic variables limit tree growth. *Global Change Biology*, 24(3), 1108–1122. <https://doi.org/10.1111/gcb.13973>
- Spies, T. (2016). LiDAR data (August 2008) for the Andrews Experimental Forest and Willamette National Forest study areas. Long-Term Ecological Research. Forest Science Data Bank, Corvallis, OR: Available:
<http://andlter.forestry.oregonstate.edu/data/abstract.aspx?dbcode=GI010>.
<https://doi.org/10.6073/pasta/c47128d6c63dff39ee48604ecc6fabfc>

- Sulman, B. N., Roman, D. T., Yi, K., Wang, L., Phillips, R. P., & Novick, K. A. (2016). High atmospheric demand for water can limit forest carbon uptake and transpiration as severely as dry soil. *Geophysical Research Letters*, 9686–9695. <https://doi.org/10.1002/2016GL069416>. Received
- Swanson, F. J., & James, M. E. (1975). *Geology and geomorphology of the H.J. Andrews Experimental Forest, Western Cascades, Oregon*. Pac. Northwest Forrest and Range Experiment Station, Forest Service, U.S. Dept. of Agriculture. Portland, OR.
- Ugla, C., Moritz, T., Sandberg, G., & Sundberg, B. (1996). Auxin as a positional signal in pattern formation in plants. *Proceedings of the National Academy of Sciences of the United States of America*, 93(17), 9282–9286. <https://doi.org/10.1073/pnas.93.17.9282>
- Vargas-Hernandez, J., & Adams, W. T. (1994). Genetic relationship between wood density component and cambial growth rhythm in young coastal Douglas-fir. *Canadian Journal of Forest Research*, 24, 1871–1876.
- Williams, P. A., Allen, C. D., Macalady, A. K., Griffin, D., Woodhouse, C. A., Meko, D. M., et al. (2013). Temperature as a potent driver of regional forest drought stress and tree mortality. *Nature Climate Change*, 3(3), 292–297. <https://doi.org/10.1038/nclimate1693>
- Yuan, W., Zheng, Y., Piao, S., Ciais, P., & Lombardozzi, D. (2019). Increased atmospheric vapor pressure deficit reduces global vegetation growth. *Science Advances*, 1–13.
- Zhang, Q., & Hebda, R. J. (2004). Variation in radial growth patterns of *Pseudotsuga menziesii* on the central coast of British Columbia, Canada. *Canadian Journal of Forest Research*, 34(9), 1946–1954. <https://doi.org/10.1139/X04-078>
- Zhang, Q., Alfaro, R. I., & Hebda, R. J. (1999). Dendroecological studies of tree growth, climate and spruce beetle outbreaks in Central British Columbia, Canada. *Forest Ecology and Management*, 121(3), 215–225. [https://doi.org/10.1016/S0378-1127\(98\)00552-0](https://doi.org/10.1016/S0378-1127(98)00552-0)

3.7 Figures

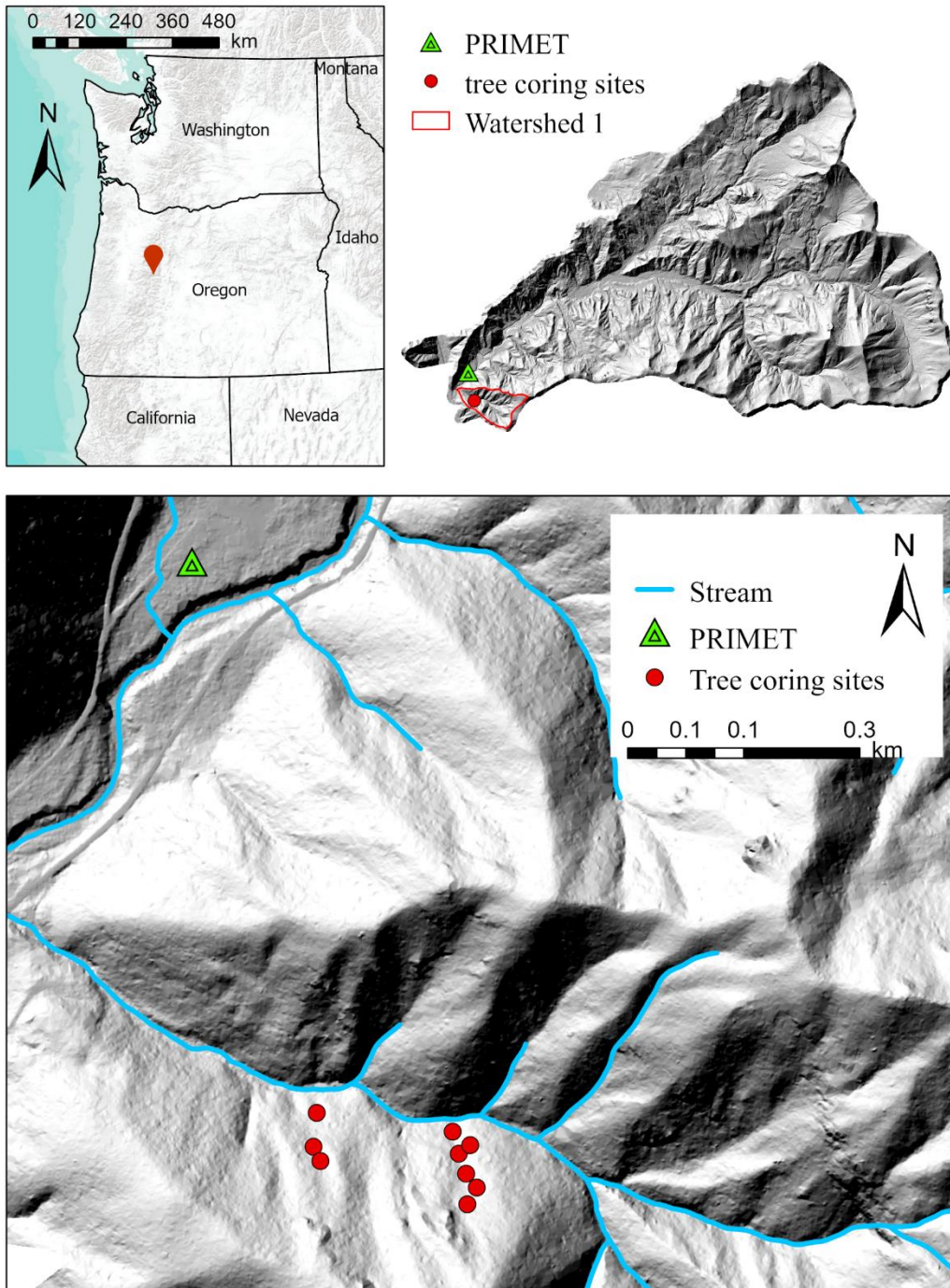


Figure 3.1 Site map

Location Watershed 1 at the HJ Andrews Experimental Forest near Blue River, Oregon. Tree cores were collected along two hillslopes at nine sites (red dots). Meteorological data was collected at PRIMET station (green triangle) approximately 1 km from tree coring sites.

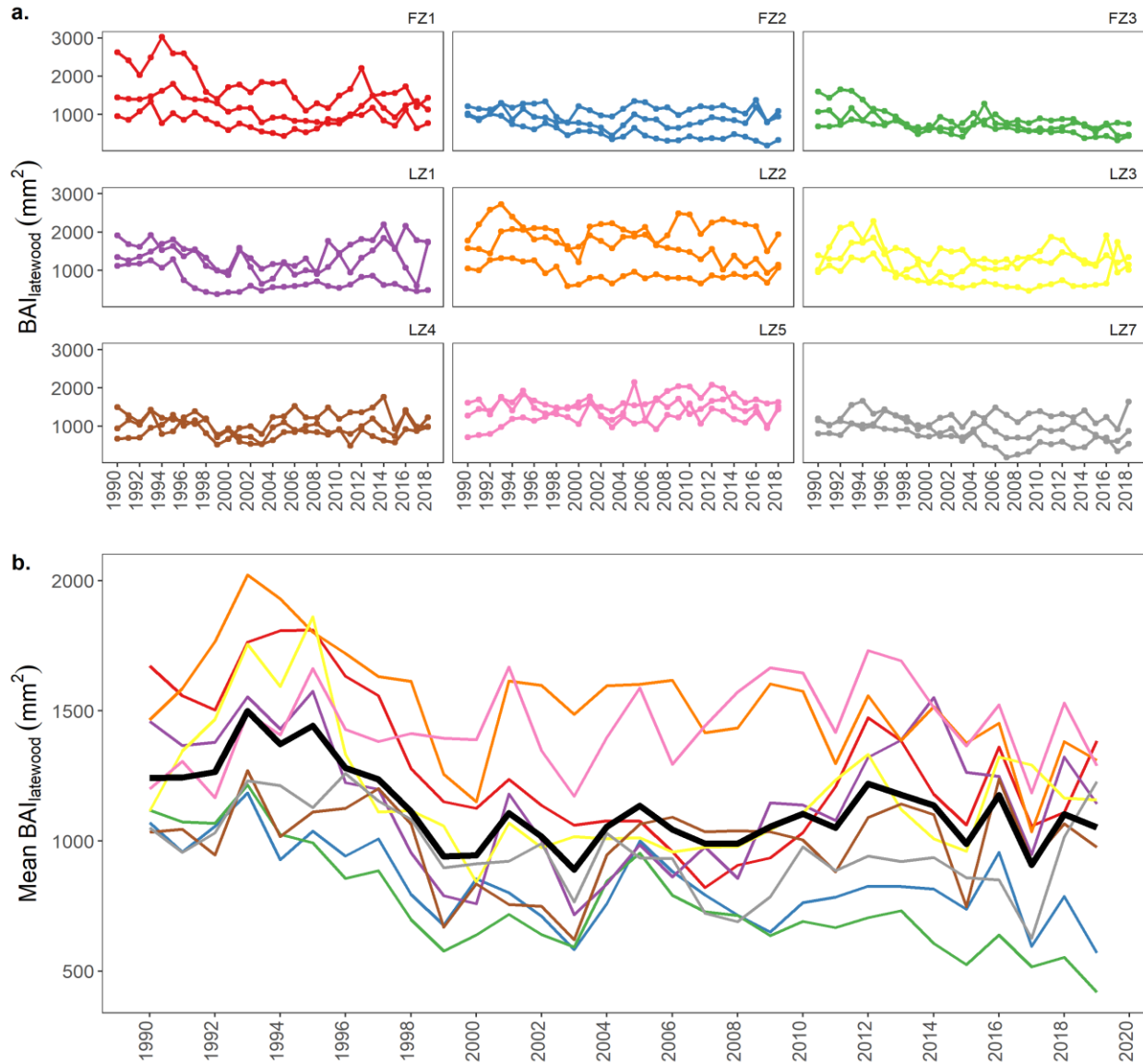


Figure 3.2 Chronology of basal area increment

(a) The latewood basal area increment (BAI) for individual trees at each site and (b) the mean BAI at each site and the overall mean BAI (black) from 1990–2019.

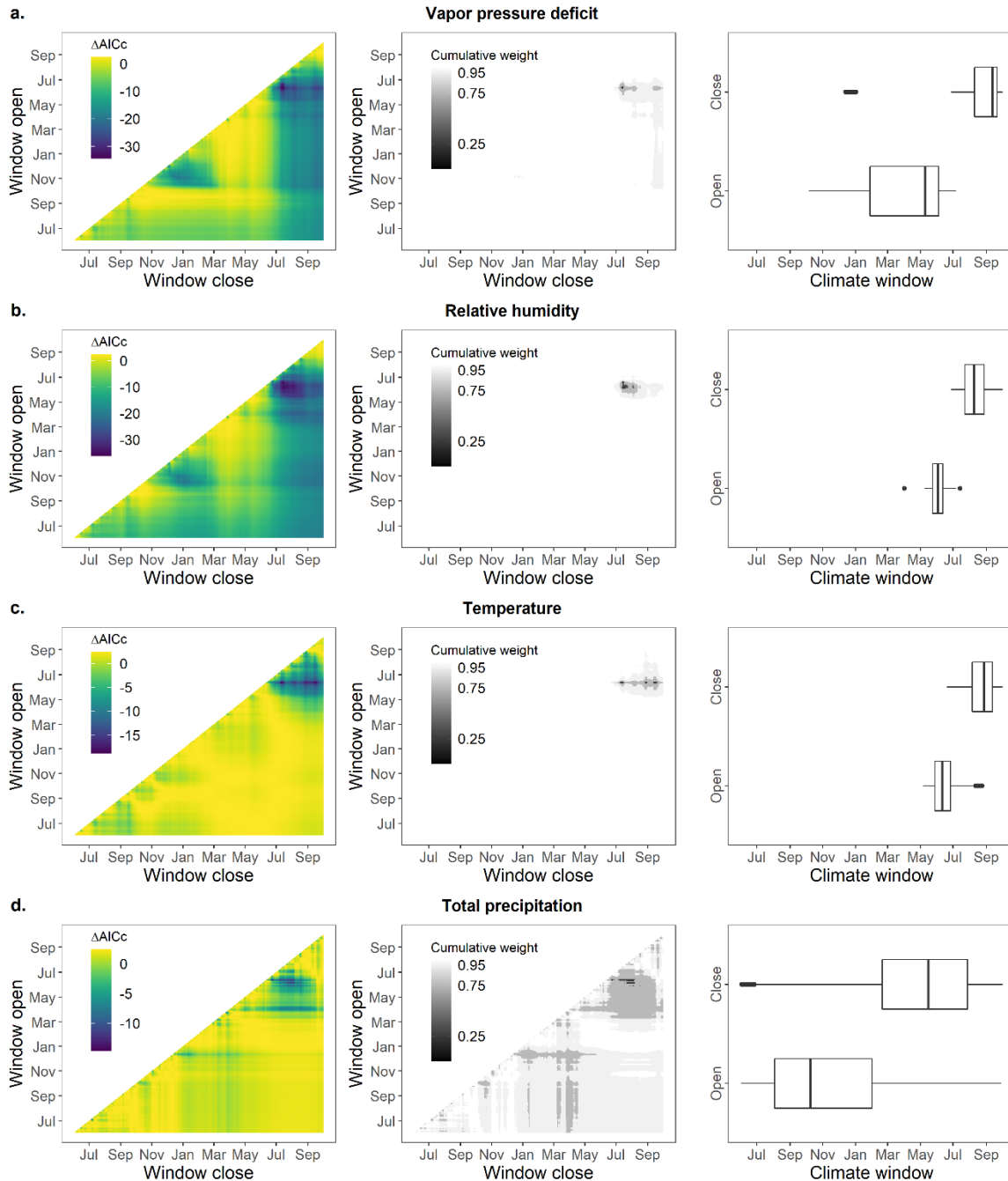


Figure 3.3 Moving window analysis

Visualization of model selection criteria used for defining the climate window with the best linear relationship between radial growth versus average daytime vapor pressure deficit (a), average daytime temperature (b), average daytime relative humidity (c), and total precipitation (d). The first column shows the model support ($\Delta AICc$) for each combination of window opening and window closing between October 1 and June 1 of the previous year ($n = 118,828$). The second column shows the 95% model confidence set, shaded in gray. The third column shows the range in climate window opening and closing dates within the 95% model confidence set.

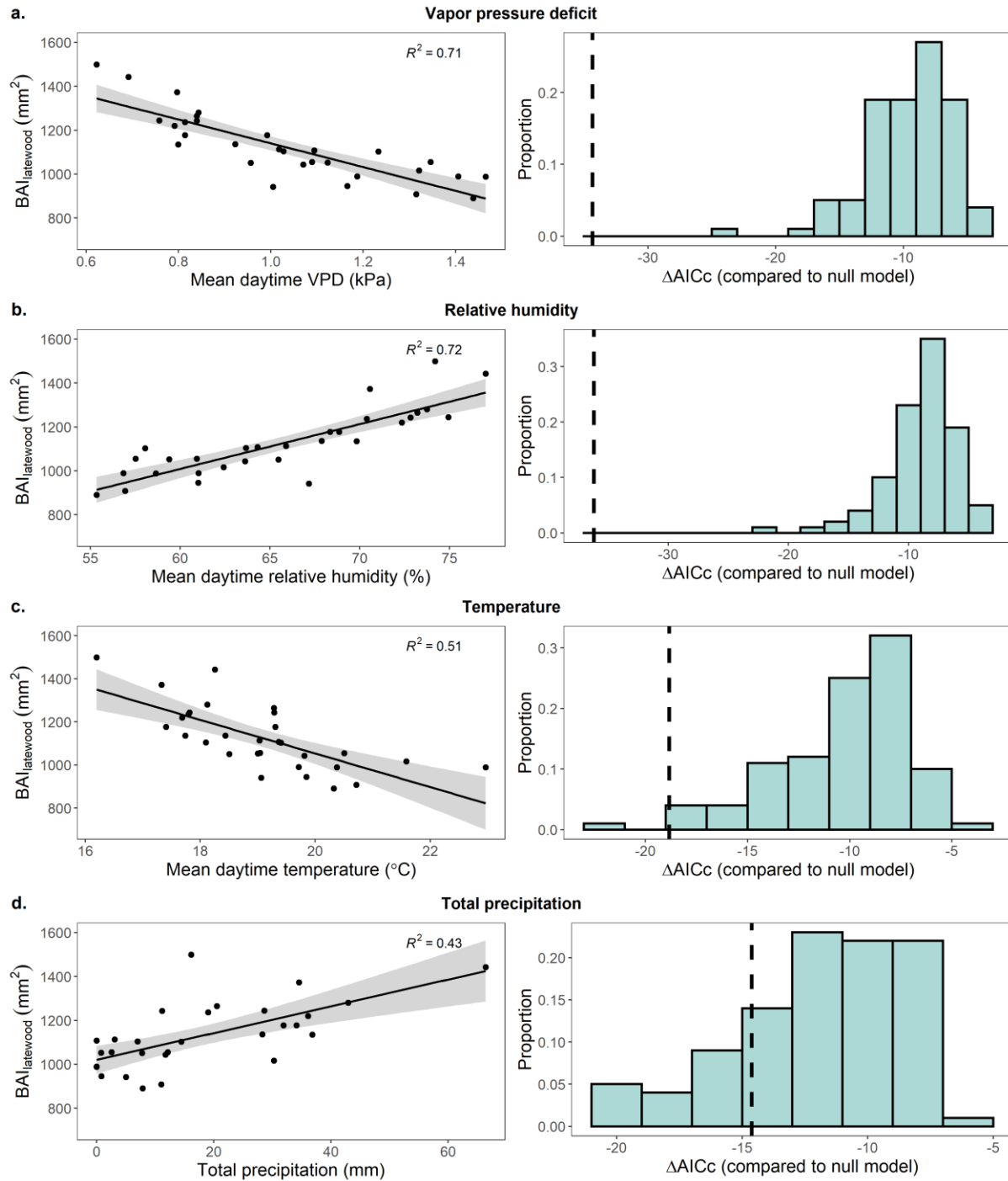


Figure 3.4 Climate-growth relationships

The relationship between mean latewood basal area increment (BAI) and average daytime vapor pressure deficit (a), average daytime temperature (b), average daytime relative humidity (c), and total precipitation (d) represents the model that was chosen as the single best model for each variable. We tested whether the ΔAIC_c value for the single best model (dashed line) differed from the distribution of ΔAIC_c values from the moving window analysis that removed any true climate signal by randomly rearranging the date in the original dataset.

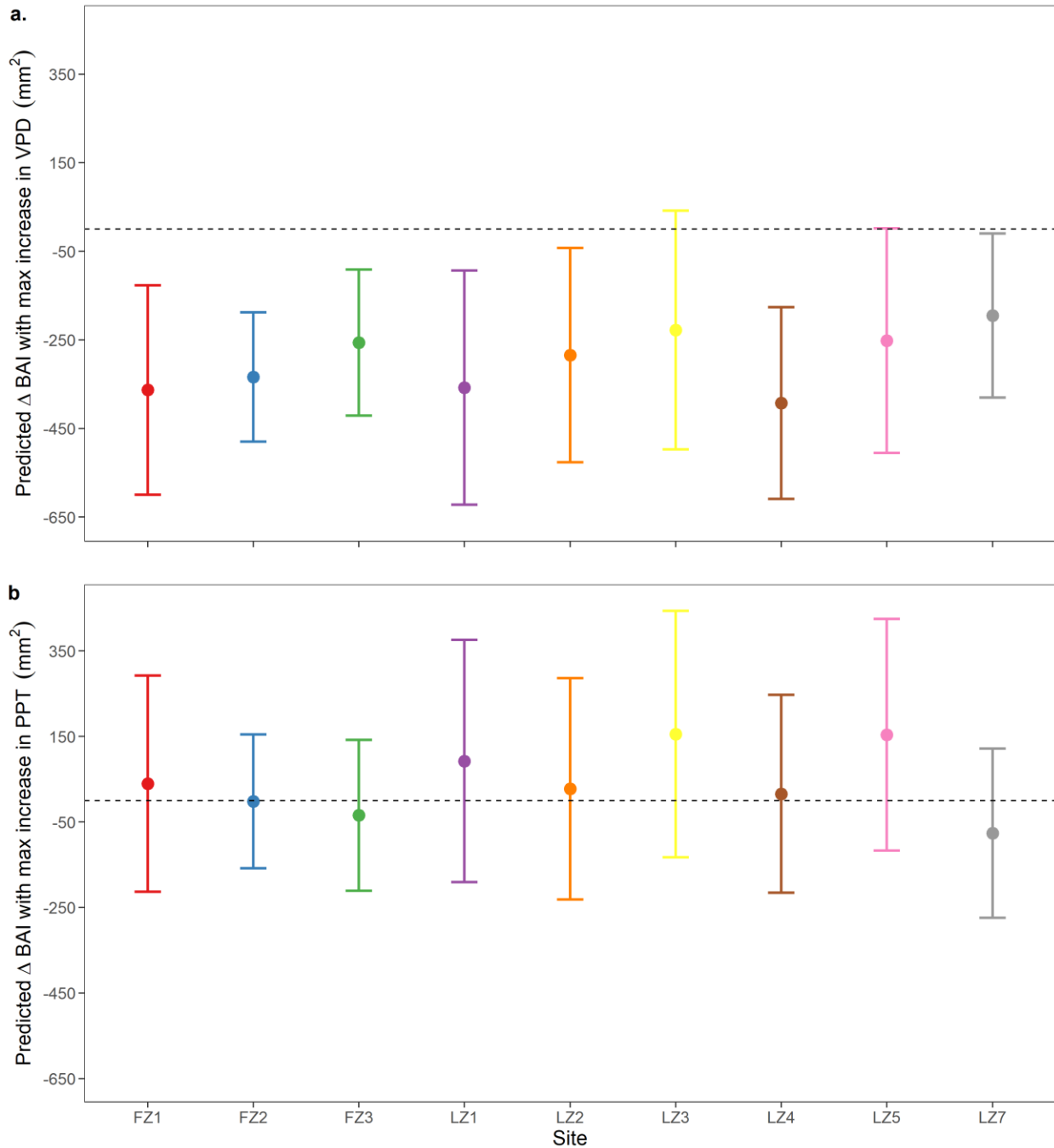


Figure 3.5 Model estimates

The predicted change in latewood basal area increment (BAI) and 95% confidence intervals at each site for the maximum observed increase in **a.**) vapor pressure deficit (VPD) (0.84 kPa) and **b.**) precipitation (PPT) (66 mm). Estimates and confidence intervals were derived from the marginal effects of VPD x site and PPT x site in our mixed effect model.

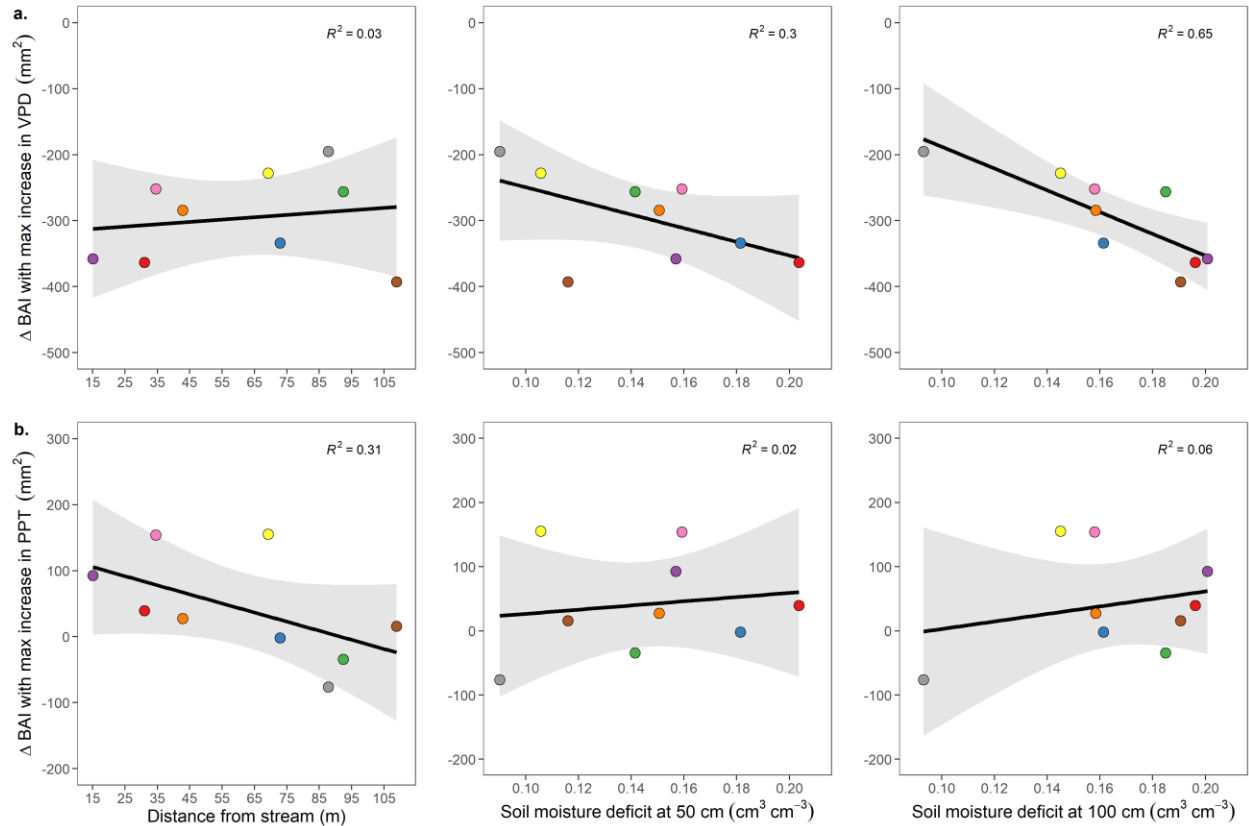


Figure 3.6 Relationship between slopes estimates and site attributes

The relationship between distance from the stream and summer soil moisture deficit at 50 cm and 100 cm at each site and the predicted change in latewood basal area increment (BAI) for the maximum observed increase in **a.)** vapor pressure deficit (VPD), 0.84 kPa, and **b.)** precipitation (PPT), 66 mm.

3.8 Tables

Table 3.1 Results from moving window analysis

Summary of results from the moving window analysis performed for each of the climate variables—vapor pressure deficit, relative humidity, temperature, and precipitation. Mean values for the climate variables were estimated over all possible window opening and closing dates from September 30 of each growth year to June of the previous year. Linear regression relationships between climate means and latewood basal area increment were evaluated with Akaike information criterion (AICc).

Variable	Statistic	Climate Window	Δ AICc	Linear Model				Percent of models in 95% confidence set	<i>p</i> of the randomization test
				intercept	slope estimate	R^2	<i>p</i>		
Daytime average vapor pressure deficit	mean	June 13 – July 15	-34.34	1681.9	-541.4	0.71	< 0.001	8	< 0.001
Daytime average relative humidity	mean	June 17 – July 15	-36.18	-215.98	20.42	0.72	< 0.001	3	0.02
Daytime average temperature	mean	June 11 – July 12	-18.83	2612.4	-77.94	0.51	< 0.001	5	< 0.001
Daytime average precipitation	total	June 13 – June 23	-14.62	1020.5	6.1	0.43	< 0.001	77	0.2

CHAPTER 4

MODELLING THE EFFECTS OF DECREASED RAINFALL AND INCREASED VAPOR PRESSURE DEFICIT ON DOUGLAS-FIR CARBON AND WATER FLUXES IN A MEDITERRANEAN CLIMATE

Karla M. Jarecke, Forest Ecosystems and Society, Oregon State University

Kevin D. Bladon, Forest Engineering, Resources, and Management, Oregon State University

Steven M. Wondzell, US Forest Service, Pacific Northwest Research Station

Linnia R. Hawkins, Forest Ecosystems and Society, Oregon State University

Abstract

Improved understanding of how trees respond to drought is critical to quantify forest sensitivity to global climate variability and is needed to inform forest management decisions. Mechanisms governing forest carbon and water fluxes in response to increased temperatures and water limitation in Mediterranean regions with wet winters and dry summers remain only partially understood. We test how increasing vapor pressure deficit and decreasing rainfall affect tree physiological water stress in Douglas-fir trees using the Soil-Plant-Atmosphere model (SPA). Our model represents a typical 50-year-old Douglas-fir stand on the western slopes of the Cascade Mountains in Oregon, USA. An increase in the daily maximum vapor pressure deficit

(VPD) by 0.25–2.5 kPa during the summer resulted in a 1–2 % increase in cumulative transpiration and a 2–13 % decrease in cumulative gross primary production. In contrast, a 10–100% decrease in rainfall during spring and summer resulted in a 1–11 % decrease in cumulative transpiration and a 0.3–2 % decrease in cumulative gross primary production. Climate scenarios showed that transpiration was highly sensitive to decreases in rainfall especially in late spring and early summer (April–June), whereas transpiration was less sensitive to increases in maximum daily VPD during the summer. In contrast, increasing the VPD during summer reduced gross primary productivity much more than did decreasing rainfall amount. The effect of VPD on gross primary production was similar throughout the summer causing cumulative gross primary production to decrease linearly over time.

4.1 Introduction

Warmer temperatures projected due to climate change are expected to increase the severity of vegetation water stress in most regions of the continental U.S. (Ficklin and Novick, 2017) and in many areas around the world (Yuan et al., 2019). As air temperatures rise, saturation vapor pressure increases, creating an increase in the vapor pressure deficit (VPD) for a given actual vapor pressure (Lawrence, 2005). Rising VPD has already been observed across a range of climate and site conditions and can increase the risk of xylem embolism, and in severe cases, lead to tree mortality (Allen et al., 2010; Breshears et al., 2013; Goulden and Bales, 2019; Grossiord et al., 2017).

Climate change is likely to drive unprecedented increases in daytime VPD and decreases in spring and summer rainfall in the Pacific Northwest (Dalton et al., 2013; Rupp et al., 2017). Together, these changes may induce atmospheric and soil drought that intensifies water stress in tree species without the physiological and structural strategies to cope with extreme environmental conditions. The greatest increases in daily maximum VPD are expected to occur during the summer (June–August) and these dry atmospheric conditions may be superimposed on soil drought because of a decrease in seasonal rainfall (Dalton et al., 2013). Furthermore, decreased rainfall may have differential effects on transpiration and gross primary productivity (GPP) depending on the time of year. For example, less than 10 % of the annual rainfall occurs in the summer in the Pacific Northwest (Daly et al., 2019); however early summer rainfall appears to have the greatest impact on annual tree growth (Littell et al., 2008; Restaino et al., 2016) and forest canopy decline (Bell et al., 2018) due to its impact on the summer water balance.

Tree physiological responses to large increases in temperature and VPD (e.g., heat waves) and decreased rainfall involve many interacting processes that encompass a wide range of species-specific strategies to deal with heat and soil water stress (Venturas et al., 2017). When exposed to sunlight, it is advantageous for vascular plants to keep their stomata open so that carbon dioxide can diffuse into the leaf for photosynthesis. As temperature and VPD rise during the day, increased water loss via transpiration induces more tension on the water in the xylem causing leaf water potential to drop. As a result, some species will partially close stomata to limit xylem tensions that cause cavitation or leaf water potentials that drop below a critical minimum (Brodribb et al., 2020). In addition, low soil moisture may also trigger plants to close their stomata earlier in the day in efforts to avoid dangerously low xylem water potentials (Zweifel et al., 2007). Although other studies have documented the combined effects of soil drought (low plant-available soil water) and atmospheric drought (high VPD) on tree function, the independent physiological effect of high VPD without soil drought has been less explored (Grossiord et al., 2020).

The direct impact of increasing VPD under climate warming has been shown to reduce carbon uptake regardless of soil water status (Novick et al., 2016; Sulman et al., 2016). However, disentangling the role of soil water availability and VPD on ecosystem water and carbon fluxes is difficult because they tend to be strongly correlated at monthly and seasonal time scales (Novick et al., 2016). For example, high VPD can increase rates of water loss from moist soils and set the stage for more severe soil drought (Eamus et al., 2013). However, other studies conclude that vegetation sensitivity to seasonal drought stress may depend on subsurface water storage capacity/depth relative to annual rainfall (Hahm et al., 2019). For instance, plant-available soil water increases with depth under seasonally dry periods due to depth-dependent

changes in soil physical characteristics that promote greater soil-water retention in deeper vs. shallower soils (Warren et al., 2005). This deep subsurface water storage (e.g., > 1 m) can be a critical water source for trees late in the growing season in seasonally dry Mediterranean climates (Bales et al., 2018; Hahm et al., 2020). Moreover, the redistribution of water from deep to shallow soils in forests has been shown to slow the drying of near-surface soils and prevent embolism in shallow roots (Brooks et al., 2002; Domec et al., 2010; Tromp-van Meerveld and McDonnell, 2006; Warren et al., 2005). Thus, in locations where trees have access to deep subsurface water during seasonally dry periods, the effect of increased temperature and VPD on tree water stress could be increasingly decoupled from soil water stress (e.g., large daily increase in VPD with relatively small daily decreases in soil water). Still, our understanding of climate-driven impacts on forest ecosystems remain limited, in part, due to the uncertainty in how trees respond to increased temperature/VPD and decreased precipitation (Grossiord et al., 2020).

We used the Soil-Plant-Atmosphere (SPA) model to disentangle the relative effects of atmospheric demand vs. precipitation on carbon and water fluxes from 50-yr Douglas-fir trees growing on the west slope of the Cascade Mountains in Oregon, USA. Other studies have linked climate drivers and tree physiological traits to understand the degree to which carbon and water fluxes from forest ecosystems will change under future climate projections (Anderegg and Venturas, 2020; Jiang et al., 2019). However, fewer studies have isolated the effects of atmospheric aridity (e.g., increasing VPD) and soil drought (decreasing precipitation) on tree physiological response (Eamus et al., 2013). Our specific objectives were to:

1. Determine how soil water availability, gross primary productivity, and transpiration respond to increased temperature and VPD (with no change in rainfall) during the

summer and decreased rainfall (with no change in temperature and VPD) during spring and summer.

2. Examine the interactive effects of increased VPD and decreased rainfall on gross primary productivity and transpiration.

4.2 Methods

4.2.1 Site Description

We simulated gross primary production (GPP) and transpiration for a 50-yr-old Douglas fir tree growing in Watershed 1, a 96-ha catchment at the HJ Andrews Experimental Forest on the west slope of the central Cascade Mountains of Oregon, USA. The region experiences strong seasonality with cool, wet winters and warm, dry summers. Average elevation of the soil monitoring sites is 576 m, while average slope is 37 degrees. The overstory canopy is dominated by ~50-year-old Douglas-fir (*Pseudotsuga menziesii*) trees with younger Western hemlock (*Tsuga heterophylla*) and Western red cedar (*Thuja plicata*) trees in the understory. Oregon grape (*Mahonia aquifolium*) and sword fern (*Polystichem munitum*) are the predominant understory shrub species. More information on the land management history can be found in Jarecke et al. (2021).

Soils in the study area are gravelly, silty clay loams. The organic horizon is approximately 5 cm thick and average depth to bedrock is 2.3 m (Jarecke et al., 2021). Hillslope soils are underlain by unconsolidated, highly weathered saprolite and fractured bedrock that allow for deep drainage so that saturation seldom occurs within the top 2 m of soil (Jarecke et al.,

2021). Tuffs and breccias are the most common parent materials, but basalts and andesites are also present (Halpern, 1988).

4.2.2 Model Description

The Soil-Plant-Atmosphere model (SPA) was originally developed for a mixed deciduous forest to link stomatal behavior to plant hydraulic traits, canopy structure, soil properties, and atmospheric conditions (Williams et al., 1996). SPA simulates carbon and water fluxes at hourly time steps across a multi-layer tree canopy and soil profile. The model simulates leaf-level transpiration using the Penman-Monteith equation (Monteith and Unsworth, 2008) and leaf-level photosynthesis using the Farquhar model (Farquhar and von Caemmerer, 1982). Stomatal conductance is optimized to maximum carbon gain while avoiding hydraulic damage given species-specific hydraulic traits including root-to-stem conductance (determined by the path length) and minimum leaf water potential. The plant hydraulic resistance of each canopy layer was assumed to increase with path length and was calculated from three parameters: stem hydraulic conductivity ($\text{mmol m}^{-1} \text{s}^{-1} \text{MPa}^{-1}$), canopy height (m), and leaf area of the canopy layer ($\text{m}^2 \text{m}^{-2}$) (Table 4.1). Photosynthetically active radiation, leaf temperature, leaf boundary layer conductance, and soil water supply were determined for each canopy layer. The change in leaf water potential was determined iteratively at each time step using the simulated leaf-to-air vapor pressure deficit, transpiration rate, soil water potential, gravitational potential, and hydraulic resistance along the soil-to-leaf pathway. Higher leaf specific VPD, which is based on leaf temperature and the water deficit of the air, results in higher evapotranspiration rates for a given stomatal aperture. Thus, plants lose more water per unit carbon gain under higher

atmospheric VPD (all else held equal). Additional details describing the SPA model can be found in Williams et al. (2001).

We used SPA 3.0.0 with a modification used in Ruehr et al. (2014) to improve estimates of soil water retention. A sigmoid relationship between soil water content and soil water potential was defined in place of the empirical relationships with soil texture from Saxton et al., (1986) (Appendix 4.1). We assigned values to model parameters that describe tree attributes and physiology based on a typical 50-yr old Douglas-fir tree in our study area (Table 4.1). We included four canopy layers at 21, 24, 27, and 30 m with equal leaf area in each layer. The vertical distribution and leaf area index of canopy layers affect the absorption of photosynthetically active radiation and other wavelengths of light. We used a 2 m soil profile divided into 20 layers, each 10 cm thick. The model estimates root biomass from the surface to the maximum rooting depth with an exponential decay function. The maximum rooting depth is, on average, ~2 m for Douglas-fir (Fan et al., 2017). Soil properties including soil porosity and soil water retention were held constant throughout the soil profile. We used model outputs of leaf water potential for the top canopy layer and weighted soil water potential ($SWP_{weighted}$) to evaluate tree water stress. Weighted soil water potential adjusts to the maximum potential water uptake in each soil layer (E_i) defined as the difference between soil water potential for each soil layer (SWP_i) and the minimum leaf water potential (LWP_{min}), divided by the hydraulic resistance of soil and roots in each soil layer (R_i):

$$E_i = \frac{SWP_i - LWP_{min}}{R_i}$$

The estimate of E_i is then used to determine the $SWP_{weighted}$ for the rooting zone:

$$SWP_{weighted} = \frac{\sum_{i=1}^l (SWP_i E_i)}{\sum_{i=1}^l (E_i)}$$

4.2.3 Model Parameterization and Meteorological Drivers

The SPA model parameters for Douglas-fir were determined from the literature wherever possible. We used a spin-up period of 15 months—from January 2018 to March 2019—to establish initial conditions before the period of model calibration from April to September 2019. Meteorological data used for model spin-up and calibration were measured at the HJ Andrews Experimental Forest (Figure 4.1). Rainfall, temperature, relative humidity, wind speed, and shortwave radiation were recorded every 15 minutes at the Primary Meteorological Station (PRIMET) and aggregated to hourly data using the mean for all variables except rainfall, which was summed. We calculated atmospheric VPD from air temperature and relative humidity. Photosynthetically active radiation was calculated as 50% of hemispherical shortwave radiation, which was measured 1 m above the ground in a clearing at PRIMET. CO₂ concentration was obtained from the US-Me6 AmeriFlux tower (Law, 2021) located in central Oregon, approximately 55 km northeast of PRIMET. PRIMET received 1,948 mm of rainfall during the 2019 water year. The average annual rainfall for water years 1989–2019 was $2,212 \pm 427$ mm. Thus, annual rainfall for the 2019 water year was 263 mm below the long-term average, but this difference was well within the standard deviation. The maximum annual rainfall from 1980–2019 was 3,244 mm, and the minimum was 1,276 mm.

Calibration data for SPA were collected at nine sites along two north-facing hillslopes (Figure 4.1) where we monitored soil water content (SWC) and soil water potential. The hillslopes have similar slope and tree density (Jarecke et al., 2021). Soil sensors (5TM and TEROS 21, METER Environment) were installed horizontally into undisturbed soil at 50-cm depth in October 2018 and SWC and soil water potential were recorded every 30 min. We calculated SWC from the dielectric permittivity using the manufacturer's equation, which

follows Topp et al. (1980). We calculated the mean daily SWC at each site and calibrated our model using data from the single site that best represented the median daily SWC across all sites from April to October 2019 (Figure 4.2a).

Parameters were adjusted iteratively to produce the best agreement between simulated and observed SWC at 50 cm depth (Figure 4.2a). This process was performed with nine parameters—stem conductivity, water use efficiency, minimum leaf water potential, total root biomass, root biomass to 50% of rooting depth, and four constants that define the shape of the soil water retention curve (Table 4.1). We used a Latin hypercube sampling scheme (McKay et al., 2000) to generate combinations of parameter values within a predefined range for each parameter with a sample size of $n = 100$ parameter sets. The range for soil water retention parameters were based on our estimate of soil water retention from field observations of SWC and soil water potential at 50 cm during a period without rainfall from July 1–August 10, 2019 (Appendix 4.1). All other ranges were based on literature values reported in studies of conifer forests or estimated when no literature values were found (Table 4.1). Model simulations were evaluated for agreement with observed daily SWC at 50 cm from April to September 2019 (Figure 4.2a), and the model parameterization with the minimum RMSE and highest R^2 between simulated and observed values was selected (Appendix 4.2).

4.2.4 Climate Scenarios

Climate scenarios were defined relative to baseline meteorological input from March to August 2019, hereafter referred to as the “baseline model”. First, we tested the effect of increased VPD between June and August 2019 (hereafter referred to as “summer”) on GPP and transpiration fluxes from Douglas-fir. Second, we tested the effect of decreased rainfall between

March and August 2019 (hereafter referred to as “spring and summer”) to simulate soil drought conditions during the growing season. We compared our model output under the climate scenarios to our baseline model to evaluate the effects of decreased rainfall and increased VPD on GPP and transpiration. We changed VPD and temperature while keeping precipitation at baseline conditions and vice versa. Lastly, we examined the interactive effects of increased VPD and decreased rainfall on GPP and transpiration by increasing VPD across the different levels of decreased rainfall and vice versa.

We established climate scenarios to test the independent effect of each factor, increased VPD and decreased rainfall, with the objective to model a range of conditions from mild to severe atmospheric and soil drought. We used the long-term climate record from PRIMET (Daly et al., 2019) to determine average conditions of maximum daily VPD and temperature during the summer. The daily maximum VPD during the summer from 1989 to 2019 averaged 2.4 ± 1.3 kPa and the daily maximum temperature averaged 26.7 ± 6.1 °C. To simulate an extreme warming scenario, we increased the daily max VPD up to 2.5 kPa or approximately two standard deviations above the long-term average.

We developed 10 VPD scenarios, using the hourly 2019 climate from the baseline model, in which we increased the VPD in increments of 0.25 kPa from +0.25 to +2.5 kPa. We refer to these scenarios as ‘vpd0.25’, ‘vpd0.5’, and so on. We increased the hourly VPD in 2019 ($VPD_{baseline}$) as a proportion of the daily max VPD ($VPD_{baseline \text{ daily max}}$).

$$VPD_{new} = VPD_{baseline} + \text{increase in daily max VPD} \left(\frac{VPD_{baseline}}{VPD_{baseline \text{ daily max}}} \right)$$

This allowed for a minimal increase in VPD during nighttime hours and maximum increase in VPD as it approached the daily maximum (Figure 4.3a). After determining the VPD time series, we calculated the increase in air temperature necessary to achieve the desired hourly VPD

without changing the actual vapor pressure. The result was an increase in hourly air temperature with the maximum increase in temperature occurring mid-day when VPD was greatest (Figure 4.3b). Similarly, we developed 10 rainfall scenarios by decreasing the 2019 hourly rainfall by 10% increments from 100% (no change in precipitation) to 0% (no precipitation) between March and August. The baseline model, referred to as ‘rain100’, received 726 mm of rain between March and August. Removal of all rainfall between March and August was called ‘rain0’. For comparison, the total rainfall between March and August from 1989 to 2019 averaged 762 ± 184 mm.

We evaluated the independent effect of increased VPD and decreased rainfall by calculating the difference in cumulative GPP and transpiration between the baseline model and each of the climate scenarios. Negative values for change in cumulative GPP and transpiration indicate a reduction with respect to the baseline condition. All data processing and analyses were done using R Studio 1.4.17.17.

4.3 Results

4.3.1 Model Agreement with Observations

The simulated baseline transpiration from the calibrated SPA model agreed with field measurements reported by Moore et al. (2004) in the same watershed. Their estimates of sap flow during July and August of 2000 ranged from 1 to 3.5 mm day⁻¹ whereas the simulated baseline transpiration during July and August 2019 ranged from 2 to 5 mm day⁻¹. The peak transpiration in late June in our baseline model was ~6 mm day⁻¹, which was nearly double that reported by Moore et al. (2004). The discrepancy between the maximum simulated transpiration

and the observed maximum could have resulted from either overestimating shallow root density in the model or errors associated with sap flow measurements that can be as large as $\pm 40\text{--}60\%$ (Ruehr et al., 2014). While simulated and observed transpiration values did not always agree in magnitude, transpiration in our baseline model did adequately reflect seasonal trends—cool spring temperatures limited transpiration when water was plentiful (i.e. atmospheric demand was less than potential rates of supply) while increasing evaporative demand in late spring and summer resulted in increased transpiration rates that declined by late summer when plant-available soil water decreased.

Our simulations of gross primary productivity (GPP) between June and August ($6\text{ to }12\text{ g m}^{-2}\text{ C day}^{-1}$) were also in good agreement with values reported for a similar forest type and climate at Wind River Experimental Forest in Washington, U.S.A (Jiang et al., 2019). GPP was estimated at Wind River with eddy covariance and ranged from $5\text{ to }7\text{ g C day}^{-1}$ between June and August with peak GPP occurring in late June (Jiang et al., 2019), which corresponded with the timing of peak GPP observed in our baseline model (Figure 4.6). The prediction error for GPP due to parameter uncertainty is estimated to be $\pm 10\%$ (Williams et al., 2001). While peak observations were slightly greater than those reported for Wind River, the seasonal dynamics of GPP in our baseline simulation also agreed with the seasonal dynamics observed at Wind River by Jiang et al. (2019)—GPP increased from March to June as temperatures and PAR increased and declined during July and August with increased evaporative demand and soil water stress.

4.3.2 Effects of Increased VPD and Decreased Rainfall on Soil Water

Under the Pacific Northwest's winter wet climate, soil moisture reservoirs are typically completely recharged by mid-winter and remain so until the beginning of the growing season.

We found that reducing rainfall during the winter (from January to March) had no effect on simulated water storage due to the lack of evaporation and transpiration during this time. Thus, the simulated soil water content (SWC) was at saturation or $0.3 \text{ m}^3 \text{ m}^{-3}$ at the beginning of our scenarios in March. Total rainfall in March and April of 2019 was 121 and 374 mm in the baseline model, respectively. This was lower than the long-term average rainfall of 254 mm in March and greater than the long-term average of 207 mm in April (Figure 4.4a., Table 4.2). Decreasing rainfall during March and April had very little effect on the average SWC and soil water potential (SWP) except for the scenario that removed all rainfall (rain0), which caused SWC in late April to decline from the baseline model by $0.04 \text{ m}^3 \text{ m}^{-3}$ at 20 cm and $0.02 \text{ m}^3 \text{ m}^{-3}$ at 50 cm (Figure 4.5a).

Shallow soil moisture was sensitive to total rainfall in May (56 mm) and June (29 mm). In all scenarios receiving 60% to 100% of the baseline rainfall during May and June, simulated SWC at 20 cm returned to saturation in late May whereas neither SWC nor SWP at 20 cm increased substantially in any scenarios with less than 60% rainfall (Figure 4.5a, 4.5c). The relatively low water content of the shallow soil layers in July triggered greater rates of soil water uptake at 100 cm for low rainfall scenarios—SWC at 100 cm was $0.04 \text{ m}^3 \text{ m}^{-3}$ lower in rain0 than in rain100 by the end of August (Figure 4.5a, 4.5c). The greater decline in SWC at 100 cm with decreased antecedent rainfall was related to a more rapid depletion of soil water in shallow layers early in the summer.

The increases in mean daily max vapor pressure deficit (VPD) in our climate scenarios ranged from 0.25 to 2.5 kPa and corresponded to an increase in mean daily max temperature by 1.2 to 9.5 °C. Increased VPD during summer did not affect SWC and SWP as much as decreased rainfall during May and June. In the baseline model, mean daily maximum temperature and VPD

were greater in July and August than June (Figure 4.4b). The mean daily max VPD and temperature for our scenarios typically exceeded the long-term median and mean in June, July, and August (Figure 4.4b, 4.4c, Table 4.3). Further, scenarios in which the daily max VPD increased by more than 0.75 kPa, the simulated mean daily max VPD exceeded the 75th percentile of the long-term mean daily max VPD throughout the summer. Increased VPD led to decreased SWC and SWP with a greater reduction at 20 cm than at 50 cm (Figure 4.5b, 4.5d). The greatest reduction in SWC and SWP with increased VPD occurred at 100 cm during August (Figure 4.5b, 4.5d) when shallow soil water became unavailable and root water uptake in deeper soil layers increased.

4.3.3 Temporal Dynamics of Water Stress with Decreased Rainfall

The daily maximum leaf water potential (LWP) and weighted soil water potential (SWP_{weighted}) were relatively unaltered by decreased rainfall in March and April even in our most extreme scenario without any rainfall. Maximum daily LWP, which typically occurred early in the morning, followed the same pattern as daily SWP_{weighted} between May and August (Figure 4.6a.). The rainy period in May created large differences in SWP_{weighted} among rainfall scenarios. These differences persisted through mid-June. Reduced rainfall led to lower LWP and transpiration relative to the baseline model (rain100). The differences in SWP_{weighted} among rainfall scenarios diminished from mid to late June without additional rainfall (Figure 4.6a, arrow 1).

In scenarios receiving 50% or more of the rainfall in the baseline scenario, the rain events in late June led to an increase in transpiration. However, the higher rates of transpiration depleted the additional soil water and ultimately reduced the SWP by late July. In the rain0–rain50 scenarios the rain events in late June did not sufficiently increase soil water availability which caused

transpiration to decline consistently, reducing soil water losses. The feedbacks between transpiration and soil water manifested by late July and the rain100 scenario had lower SWP than the rain0 scenario (Figure 4.6a, arrow 2). A small rain event in late August created a temporary increase in SWP_{weighted} , LWP, and transpiration for scenarios with > 70% rainfall.

Changes in gross primary production (GPP) from the baseline model (rain100) due to decreased rainfall were similar to patterns observed for transpiration. However, the percent change in transpiration from the baseline model was typically much greater than the percent change in GPP from the baseline model (Figure 4.6a). Given the negligible effect of decreased rainfall on LWP and SWP_{weighted} during March and April, it is not surprising that we observed no difference in GPP or transpiration among rainfall scenarios during this time. The lower LWP and SWP_{weighted} , resulting from reduced rainfall in May had a lagged effect on GPP and transpiration starting in June. From June to early July, GPP decreased due to lower LWP and SWP_{weighted} for low rainfall scenarios. However, for scenarios with greater rainfall (rain50-100) we observed a feedback between GPP and SWP in July when GPP, like transpiration, spiked following June precipitation events. The increase in GPP and transpiration used up soil water and reduced the SWP which resulted in reduced GPP by late-July. By early August, GPP was similar across the rainfall scenarios and increased for rain70–rain100 in late August following a rain event.

4.3.4 Temporal Dynamics of Water Stress with Increased VPD

In general, increasing the maximum daily VPD by 0.5–2.5 kPa (vpd0.25–2.5) during the summer increased transpiration, which reduced SWP_{weighted} relative to the baseline model (vpd0) (Figure 4.6b). Given the feedback between transpiration, LWP, SWP, we also saw transpiration decrease during periods when LWP and SWP_{weighted} fell below -1.0 MPa. Periods of relatively low

LWP and SWP_{weighted} occurred from mid-June to mid-July. The greatest decrease in transpiration relative to the baseline model occurred when LWP and SWP_{weighted} were lowest in July (Figure 4.6b, arrow 3). Conversely, we found that increased transpiration under periods of relatively lower water stress prompted a lagged effect on LWP and SWP_{weighted} by late July such that LWP and SWP_{weighted} were similar across all VPD scenarios (e.g., Figure 4.6b, arrow 4). The convergence of LWP among scenarios led to an increase in transpiration with increased VPD.

The effect of increased VPD on GPP persisted throughout the summer. We observed a decrease in GPP as the daily max VPD increased from 0.25 to 2.5 kPa (Figure 4.6b). The greatest decreases in GPP from vpd0 to vpd2.5 occurred in late June and mid-July when the decrease in LWP and SWP_{weighted} was also greatest. The smallest difference in GPP among VPD scenarios occurred when LWP and SWP_{weighted} were similar across scenarios (e.g., Figure 4.6b, arrow 4).

4.3.5 Effect of VPD and Rainfall Scenarios on Cumulative GPP and Transpiration

Scenarios that reduced rainfall from 10 to 100% with no change in VPD had a greater effect on cumulative transpiration than those that increased max daily VPD by 0.25–2.5 kPa with no change in rainfall. Cumulative transpiration decreased from the baseline scenario by 7–70 mm or ~1–11% due to reduced rainfall (Figure 4.7a). In contrast, cumulative transpiration increased by 6–11 mm or ~1–2% due to increased VPD (Figure 4.7b).

Increased VPD had a greater effect on cumulative GPP than decreased rainfall. Scenarios with increased max daily VPD by 0.25–2.5 kPa decreased cumulative GPP by 23–200 g C or 1.5–13% (Figure 4.7b). In contrast, scenarios with reduced rainfall from 10 to 100% decreased GPP by 4–30 g C or 0.3–2% (Figure 4.7a). An increase in daily max VPD by 0.25 kPa resulted in a similar decrease in cumulative GPP as did a reduction in daily rainfall by 50%. In fact,

completely eliminating rainfall from March through June only decreased cumulative GPP by 30 g C whereas it only required a 0.5 kPa increase in daily max VPD to decrease cumulative GPP by 44 g C (Figure 4.7).

The difference between cumulative transpiration and GPP for climate scenarios and cumulative transpiration and GPP for the baseline model changed over time (Figure 4.7). The decrease in cumulative GPP and transpiration from the baseline model under scenarios of high to low rainfall increased from June to mid-July, but these differences decreased by mid-August (Figure 4.7a). In contrast, the differences in cumulative GPP from the baseline increased monotonically over time for scenarios of increased VPD while differences in cumulative transpiration from the baseline model were greater from June to mid-July, decreased in mid-July, and increased again from mid-July to mid-August. (Figure 4.7b).

We also explored interactive scenarios where we modified both VPD and rainfall. We observed a similar effect of decreased rainfall on cumulative GPP across all levels of increased VPD (Figure 4.8a). Likewise, the effects of increased VPD on GPP were similar across all levels of decreased rainfall (Figure 4.8b). We did observe an interactive effect of decreased rainfall and increased VPD on cumulative transpiration (Figure 4.8c, 4.8d). For example, the range in cumulative transpiration from the baseline scenario (vpd0) to the most extreme VPD scenario (vpd2.5) depended on the amount of rainfall and was greatest for models with 30 and 40% of total daily rainfall (Figure 4.8d). Similarly, the range and ranking of cumulative transpiration from rain10 to rain60 differed across the levels of increased VPD (Figure 4.8c).

4.4 Discussion

4.4.1 Effects of Increased VPD vs. Decreased Rainfall on GPP and Transpiration

The decline in cumulative GPP from the baseline model was much greater for scenarios of increased VPD than scenarios of reduced rainfall. This suggests that the effects of atmospheric drought on carbon assimilation may outweigh the effect of soil drought in this region.

Temperatures in the northwest U.S. are projected to warm by 1.2 to 4.7 °C from 2014–2070 under the Representative Concentration Pathway 4.5 (Mote et al., 2013). Our climate scenario that simulated an average increase in max daily temperature by 1.2 °C between June and August was associated with an increase in max daily VPD by 0.25 kPa. This scenario (vpd0.25) caused cumulative GPP to decline by -22.8 g C m^{-2} or 1.5% of total GPP during the summer. An increase in max daily temperature by 5 °C during the summer was associated with an increase in maximum daily VPD by 1.0 kPa. This scenario (vpd1.0) caused cumulative GPP to decline by -87.1 g C m^{-2} or 6% of total GPP during the summer.

Projected changes in temperature and precipitation during the summer are strongly correlated (Rupp et al., 2017), and the greatest decrease in precipitation is expected during the summer when rainfall is projected to decline by as much as 34% (Mote et al., 2013). A decline in cumulative GPP by 1.5% (resulting from a 1.2 °C warming) could also occur with a 40% reduction in spring and summer rainfall (Figure 4.7a). However, a decline in cumulative GPP by 6% (resulting from a 5 °C warming) was much greater than the decline in GPP after removing all spring and summer rainfall, which caused a 2% decline in seasonal GPP. Under a conservative estimate for decreased spring and summer rainfall in the Pacific Northwest (30%), our model predicts that GPP will decline by -17.8 g C m^{-2} or 1%. Thus, in light of expected changes in temperature and precipitation that are projected for the region, we believe that climate-driven

reductions in forest productivity are more likely to be attributed to increases in VPD than from decreases in rainfall.

Ruehr et al. (2014), who calibrated SPA for a semi-arid pine forest in eastern Oregon, also found a decline in GPP when simulating warmer temperatures and decreased rainfall using climate projections for 2080. By disentangling the climate controls on carbon fluxes, they found that the decline in GPP due to hotter summers was nearly double the effect of reduced precipitation. Douglas-fir, like ponderosa pine have isohydric stomatal behavior, which allows them to conserve water while maintaining a relatively constant midday leaf water potential even if soil water is not limiting (Bond and Kavanagh, 1999; Martnez-Vilalta et al., 2004). Thus, when VPD is high during the summer, Douglas-fir tend to reduce their stomatal opening earlier in the day to prevent xylem cavitation (Bond and Kavanagh, 1999). The decrease in stomatal aperture to prevent hydraulic failure explains the strong decline in carbon assimilation with increased temperature and VPD observed in this study. Decline in carbon assimilation with increasing VPD is also supported by other studies that find a direct impact of VPD on leaf water stress without soil water limitation (Eamus et al., 2013; Grossiord et al., 2017; Jiang et al., 2019; Novick et al., 2016; Ruehr et al., 2014).

Unlike GPP, cumulative transpiration increased in response to elevated VPD. This may be explained by the relatively high evaporation rates from stomata when conditions were favorable for gas exchange. For example, daily transpiration rates increased as VPD increased during periods when LWP provided evidence of low water stress among all VPD scenarios. In contrast, we observed that transpiration rates decreased as VPD increased during periods when LWP was low enough to restrict gas exchange. Jiang et al. (2019) found that stomatal conductance in Douglas-fir was primarily regulated by soil water status under conditions of low

VPD. However, as VPD increased, the role of soil water diminished and extreme VPD conditions greatly reduced stomatal conductance regardless of soil moisture status. Thus, without soil water limitation, we would expect seasonal periods of relatively low VPD (i.e., early summer or after rain events) would cause greater transpiration rates with increased VPD. However, during periods of high baseline VPD, any increases in VPD can cause the leaf water potential to decline, and potentially reach the minimum sustainable leaf water potential, which would trigger a significant reduction in stomatal conductance.

Other studies described a net decline in cumulative transpiration as a result of increased VPD during seasonally dry periods (Eamus et al., 2013; Fang et al., 2021; Ruehr et al., 2014). While transpiration might increase with VPD up to a point, the exacerbation of soil water stress leads to its eventual decline (Breshears et al., 2013). Ruehr et al. (2014) found that cumulative transpiration decreased by ~10% in response to an increase in temperature by 4.5 °C and associated 40% increase in VPD. In contrast, a 40% increase in the average max daily VPD during the summer (approximately +1.0 kPa) led to 12 mm or 2% increase in cumulative transpiration in our study. Although we did observe periodic declines in daily transpiration rates in response to elevated VPD that were associated with periods of very low LWP. Thus, it is likely that the negative response in cumulative transpiration observed in other studies is likely due to the exhaustion of soil water resources due to the relatively lower soil water availability and shallower rooting depth at their site compared to ours. Given the decrease in simulated LWP and SWP_{weighted} by late August, an extension of the dry season beyond August and further exhaustion of soil water resources would likely trigger a rapid decline in transpiration under all rainfall scenarios in our study.

Soil drought has been shown to negatively impact tree growth and water stress in other studies (Powell et al., 2013). However, our results suggested that soil water was not limiting even in the model scenario that removed all spring and summer rainfall. While shallow soil water was depleted earlier in the season for low rainfall scenarios, deep roots compensated for lack of water in shallow layers, and without atmospheric water stress, we found relatively small declines in GPP with decreasing rainfall. Because most of the roots are concentrated in the upper meter of soil, reducing rainfall by 10 to 100% caused cumulative transpiration to decrease by 7 to 70 mm or 1 to 11% of total transpiration. Although plant-available water decreased significantly at 100 cm for the most extreme scenarios of decreased rainfall (Figure 4.5a), we found SWP_{weighted} was greater than -1.5 MPa throughout the summer (Figure 4.6a). This suggests that soil water from 100–200 cm was accessible by deep roots. Thus, even after removing all spring and summer rainfall, values of LWP were above the minimum sustainable leaf water potential (-2.8 MPa) for most of the summer. However, by the end of August, LWP was approximately -2.5 MPa in all rainfall scenarios, which suggested that deep soil water resources were limiting by the end of summer regardless of antecedent rainfall amounts. The convergence of SWP_{weighted} by the end of summer is explained by the feedbacks between SWC and transpiration—while SWC decreased earlier in the growing season for scenarios with low rainfall inputs, all scenarios converged on a common minimum SWC ($\sim 0.12 \text{ cm}^3 \text{ cm}^{-3}$) at 20 and 50 cm by late summer (Figure 4.5a).

4.4.2 Interactive Effects of Increased VPD and Decreased Rainfall on GPP and Transpiration

Atmospheric conditions of high VPD often accompany soil drought. We saw that increasing VPD from the baseline model led to increased transpiration from moist soils (Figure

4.6b), which created only modest decreases in SWC at 20, 50, and 100 cm (Figure 4.5b).

Research from Wind River provides evidence that warmer temperatures in the spring could lead to greater soil water loss early in the growing season, setting the stage for more extreme drought effects in the summer (Jiang et al., 2019). We did not simulate increased temperature and VPD in the spring, but we hypothesize that elevated temperature and VPD during April and May would increase photosynthesis rates and lead to the depletion of shallow soil water earlier in the growing season. In the low rainfall scenarios, this may have led to significantly more water stress by late summer.

Other studies using the SPA model calibrated for *Angophora bakeri* and *Eucalyptus sclerophylla* in a temperate climate and *Pinus ponderosa* in a Mediterranean climate have found that hotter summers when combined with soil drought has a much larger negative impact on carbon assimilation and transpiration than warming without drought (Eamus et al., 2013; Ruehr et al., 2014). Unlike these studies, we found decreased rainfall during spring and summer did not interact with increased VPD to create greater reduction in GPP. Cumulative GPP decreased by 200 g C from the baseline scenario to +2.5 kPa. The rainfall reduction scenarios only affected the cumulative GPP in the baseline model. In any scenario where we increased VPD, GPP always decreased monotonically, it varied little with changes in rainfall, and in the most extreme VPD scenario it always decreased by ~200 g C relative to the baseline model. We hypothesize the effect of decreased rainfall on GPP was relatively minor because trees had access to deep soil water during the extremely dry summer which allowed SWP_{weighted} to remain above -1.5 MPa throughout the summer. This deep water served to support transpiration during the summer regardless of when shallow soil water was depleted—e.g., earlier in the summer for low rainfall scenarios or later in the summer for high rainfall scenarios (Figure 4.5a). Because rainfall totals

during late summer are relatively low to begin with (e.g., 13 mm between July and August in our baseline model), decreasing rainfall by up to 100% during this time was not a large reduction in the amount of water that entered the soil (Figure 4.5a). However decreasing rainfall during May and June, which together received ~15 times more rainfall than July and August, (Figure 4.4a) is likely to change year-to-year variability in the soil moisture availability heading into these drier months. However, the impact of decreased rainfall/soil moisture in May and June on the vegetation water stress during July and August depends on subsurface water storage and rooting depth.

4.5 Conclusion

The west slope of the Cascades Mountains is projected to experience warmer temperatures during the summer and greater declines in spring and summer rainfall due to climate change. By disentangling the climatic controls on GPP and transpiration, we were able to show that precipitation-based drought is likely to have a minor effect on forest productivity relative to increasing VPD. Additionally, we show that decreased rainfall has a significant impact on cumulative transpiration and soil water resources above 1 m. However, the access to deep (>1 m) soil water late in the summer mitigated soil water stress. This lack of soil water limitation led to relatively modest changes in LWP and SWP_{weighted} with decreasing rainfall. This suggests that the consequences of reduced precipitation during the growing seasons may be minimal in this region but will depend on subsurface water storage capacity/soil properties, rooting depth, and timing of precipitation.

We found climate change projections of elevated VPD are likely to reduce forest productivity regardless of soil moisture availability at our site. Despite the co-occurrence of soil and atmospheric drought in many cases, increased in VPD/temperature can lead to tree physiological water stress without soil water limitation and, if prolonged, create large-scale forest die-off. Substantial, knowledge gaps remain, however, especially regarding the effect of large temperature/VPD anomalies on physiological function. In the future, combined field and modeling studies of Douglas-fir response to a warmer climate under varying conditions of subsurface water availability would provide useful insights into the mechanisms of forest response to climate change.

4.6 Acknowledgements

The authors thank the H.J. Andrews staff for their support with project logistics and Zach Hoylman and Rob Livesay for assisting with field campaigns to install sensors and data loggers. Meteorological data was provided by the HJ Andrews Experimental Forest's Long-Term Ecological Research Program (Daly et al., 2019), and our research was funded by the National Science Foundation (LTER7 DEB 1440409), USDA Forest Service Pacific Northwest Research Station, and Oregon State University.

4.7 References

Allen, C.D., Macalady, A.K., Chenchouni, H., Bachelet, D., McDowell, N., Vennetier, M., Kitzberger, T., Rigling, A., Breshears, D.D., Hogg, E.H. (Ted), Gonzalez, P., Fensham, R., Zhang, Z., Castro, J., Demidova, N., Lim, J.H., Allard, G., Running, S.W., Semerci, A., Cobb, N., 2010. A global overview of drought and heat-induced tree mortality reveals

- emerging climate change risks for forests. *For. Ecol. Manage.* 259, 660–684.
<https://doi.org/10.1016/j.foreco.2009.09.001>
- Anderegg, W.R.L., Venturas, M.D., 2020. Plant hydraulics play a critical role in Earth system fluxes. *New Phytol.* 226, 1535–1538. <https://doi.org/10.1111/nph.16548>
- Bales, R.C., Goulden, M.L., Hunsaker, C.T., Conklin, M.H., Hartsough, P.C., O’Geen, A.T., Hopmans, J.W., Safeeq, M., 2018. Mechanisms controlling the impact of multi-year drought on mountain hydrology. *Sci. Rep.* 8, 1–8. <https://doi.org/10.1038/s41598-017-19007-0>
- Barnard, H.R., 2009. Inter-relationships of Vegetation, Hydrology and Micro-climate in a Young Douglas-fir forest. Dissertation.
- Bell, D.M., Cohen, W.B., Reilly, M., Zhiqiang, Y., 2018. Visual interpretation and time series modeling of Landsat imagery highlight drought’s role in forest canopy declines. *Ecosphere* 9. <https://doi.org/10.1002/ecs2.2195>
- Berner, L.T., Law, B.E., 2016. Plant traits, productivity, biomass and soil properties from forest sites in the Pacific Northwest, 1999-2014. *Sci. Data* 3, 1–14.
<https://doi.org/10.1038/sdata.2016.2>
- Bonan, G.B., Williams, M., Fisher, R.A., Oleson, K.W., 2014. Modeling stomatal conductance in the earth system: Linking leaf water-use efficiency and water transport along the soil-plant-atmosphere continuum. *Geosci. Model Dev.* 7, 2193–2222. <https://doi.org/10.5194/gmd-7-2193-2014>
- Bond, B.J., Kavanagh, K.L., 1999. Stomatal behavior of four woody species in relation to leaf-specific hydraulic conductance and threshold water potential. *Tree Physiol.* 19, 503–510.
<https://doi.org/10.1093/treephys/19.8.503>
- Breshears, D.D., Adams, H.D., Eamus, D., McDowell, N.G., Law, D.J., Will, R.E., Williams, A.P., Zou, C.B., 2013. The critical amplifying role of increasing atmospheric moisture demand on tree mortality and associated regional die-off. *Front. Plant Sci.* 4, 2–5.
<https://doi.org/10.3389/fpls.2013.00266>
- Brodribb, T.J., Powers, J., Choat, B., 2020. Hanging by a thread? Forests and drought. *Science* (80-.). 266, 261–266.
- Brooks, J.R., Meinzer, F.C., Coulombe, R., Gregg, J., 2002. Hydraulic redistribution of soil water during summer drought in two contrasting Pacific Northwest coniferous forests. *Tree Physiol.* 22, 1107–1117. <https://doi.org/10.1093/treephys/22.15-16.1107>
- Dalton, M.M., Mote, P.W., Snover, A.K., 2013. Climate Change in the Northwest. Oregon Climate Change Research Institute 230.
- Daly, C., Schulze, M., McKee, W., 2019. Meteorological data from benchmark stations at the HJ Andrews Experimental Forest, 1957 to present. Long-Term Ecological Research.
<https://doi.org/10.6073/pasta/c021a2ebf1f91adf0ba3b5e53189c84f>
- Domec, J.C., King, J.S., Noormets, A., Treasure, E., Gavazzi, M.J., Sun, G., McNulty, S.G., 2010. Hydraulic redistribution of soil water by roots affects whole-stand evapotranspiration and net ecosystem carbon exchange. *New Phytol.* 187, 171–183.
<https://doi.org/10.1111/j.1469-8137.2010.03245.x>

- Eamus, D., Boulain, N., Cleverly, J., Breshears, D.D., 2013. Global change-type drought-induced tree mortality: Vapor pressure deficit is more important than temperature per se in causing decline in tree health. *Ecol. Evol.* 3, 2711–2729. <https://doi.org/10.1002/ece3.664>
- Fan, Y., Miguez-Macho, G., Jobbágy, E.G., Jackson, R.B., Otero-Casal, C., 2017. Hydrologic regulation of plant rooting depth. *Proc. Natl. Acad. Sci.* 201712381. <https://doi.org/10.1073/pnas.1712381114>
- Fang, Y., Leung, L.R., Wolfe, B.T., Detto, M., Knox, R.G., McDowell, N.G., Grossiord, C., Xu, C., Christoffersen, B.O., Gentine, P., Koven, C.D., Chambers, J.Q., 2021. Disentangling the effects of vapor pressure deficit and soil water availability on canopy conductance in a seasonal tropical forest during the 2015 El Niño drought. *J. Geophys. Res. Atmos.* 126, 1–20. <https://doi.org/10.1029/2021JD035004>
- Farquhar, G.D., von Caemmerer, S., 1982. Modelling of photosynthetic response to the environment, in: Lange, O.L., Nobel, P.S., Osmond, C.B., Ziegler, H. (Eds.), *Physiological Plant Ecology II. Encyclopedia of Plant Physiology, New Series.* Springer-Verlag, Berlin, pp. 549–587.
- Ficklin, D.L., Novick, K.A., 2017. Historic and projected changes in vapor pressure deficit suggest a continental-scale drying of the United States atmosphere. *J. Geophys. Res.* 122, 2061–2079. <https://doi.org/10.1002/2016JD025855>
- Gabrielli, C.P., McDonnell, J.J., Jarvis, W.T., 2012. The role of bedrock groundwater in rainfall–runoff response at hillslope and catchment scales. *J. Hydrol.* 450–451, 117–133. <https://doi.org/10.1016/j.jhydrol.2012.05.023>
- Goulden, M.L., Bales, R.C., 2019. California forest die-off linked to multi-year deep soil drying in 2012–2015 drought. *Nat. Geosci.* <https://doi.org/10.1038/s41561-019-0388-5>
- Grossiord, C., Buckley, T.N., Cernusak, L.A., Novick, K.A., Poulter, B., Siegwolf, R.T.W., Sperry, J.S., McDowell, N.G., 2020. Plant responses to rising vapor pressure deficit. *New Phytol.* <https://doi.org/10.1111/nph.16485>
- Grossiord, C., Sevanto, S., Borrego, I., Chan, A.M., Collins, A.D., Dickman, L.T., Hudson, P.J., McBranch, N., Michaletz, S.T., Pockman, W.T., Ryan, M., Vilagrosa, A., McDowell, N.G., 2017. Tree water dynamics in a drying and warming world. *Plant Cell Environ.* 40, 1861–1873. <https://doi.org/10.1111/pce.12991>
- Hahm, W.J., Dralle, D.N., Rempe, D.M., Bryk, A.B., Thompson, S.E., Dawson, T.E., Dietrich, W.E., 2019. Low subsurface water storage capacity relative to annual rainfall decouples Mediterranean plant productivity and water use from rainfall variability. *Geophys. Res. Lett.* 46, 6544–6553. <https://doi.org/10.1029/2019GL083294>
- Hahm, W.J., Rempe, D.M., Dralle, D.N., Dawson, T.E., Dietrich, W.E., 2020. Oak transpiration drawn from the weathered bedrock vadose zone in the summer dry season. *Water Resour. Res.* 56, 1–24. <https://doi.org/10.1029/2020WR027419>
- Halpern, C.B., 1988. Early successional pathways and the resistance and resilience of forest communities. *Ecol. Soc. Am.* 69, 1703–1715.
- Jarecke, K.M., Bladon, K.D., Wondzell, S.M., 2021. The influence of local and nonlocal factors on soil water content in a steep forested catchment. *Water Resour. Res.* 57, 1–21.

<https://doi.org/10.1029/2020wr028343>

- Jiang, Y., Kim, J.B., Trugman, A.T., Kim, Y., Still, C.J., 2019. Linking tree physiological constraints with predictions of carbon and water fluxes at an old-growth coniferous forest. *Ecosphere* 10. <https://doi.org/10.1002/ecs2.2692>
- Law, B.E., 2021. AmeriFlux BASE US-Me6 Metolius Young Pine Burn, Ver. 15-5, AmeriFlux AMP, (Dataset).
- Lawrence, M.G., 2005. The relationship between relative humidity and the dewpoint temperature in moist air: A simple conversion and applications. *Bull. Am. Meteorol. Soc.* 86, 225–233. <https://doi.org/10.1175/BAMS-86-2-225>
- Lee, E.H., Tingey, D.T., Beedlow, P.A., Johnson, M.G., Burdick, C.A., 2007. Relating fine root biomass to soil and climate conditions in the Pacific Northwest. *For. Ecol. Manage.* 242, 195–208. <https://doi.org/10.1016/j.foreco.2007.01.033>
- Licata, J.A., 2003. Structural and physiological changes with stand age: Use of a process-based model to compare carbon and water fluxes in young and old-growth Douglas - fir / western hemlock forest stands. Thesis. Oregon State University.
- Littell, J.S., Peterson, D.L., Tjoelker, M., 2008. Douglas-fir growth in mountain ecosystems: Water limits tree growth from stand to region. *Ecol. Monogr.* 78, 349–368. <https://doi.org/10.1890/07-0712.1>
- Martnez-Vilalta, J., Sala, A., Piol, J., 2004. The hydraulic architecture of Pinaceae - A review. *Plant Ecol.* 171, 3–13. <https://doi.org/10.1023/B:VEGE.0000029378.87169.b1>
- McKay, M.D., Beckman, R.J., Conover, W.J., 2000. A comparison of three methods for selecting values of input variables in the analysis of output from a computer code. *Technometrics* 42, 55–61. <https://doi.org/10.1080/00401706.2000.10485979>
- Monteith, J.L., Unsworth, M.H., 2008. *Principles of Environmental Physics*, 3rd ed. ed. Elsevier, Amsterdam; Boston.
- Moore, G.W., Bond, B.J., Jones, J.A., Phillips, N., Meinzer, F.C., 2004. Structural and compositional controls on transpiration in 40- and 450-year-old riparian forests in western Oregon, USA. *Tree Physiol.* 24, 481–491. <https://doi.org/10.1093/treephys/24.5.481>
- Mote, P.W., Bethel, J., Capalbo, S.M., Dalton, M.M., Eigenbrode, S.E., Glick, P., Houston, L., Littell, J.S., Lynn, K., Raymond, R.R., Reeder, W.S., Snover, A.K., 2013. Climate Change in the Northwest, Brief Summary. <https://doi.org/10.5822/978-1-61091-512-0>
- Novick, K.A., Ficklin, D.L., Stoy, P.C., Williams, C.A., Bohrer, G., Oishi, A.C., Papuga, S.A., Blanken, P.D., Noormets, A., Sulman, B.N., Scott, R.L., Wang, L., Phillips, R.P., 2016. The increasing importance of atmospheric demand for ecosystem water and carbon fluxes. *Nat. Clim. Chang.* 6, 1023–1027. <https://doi.org/10.1038/nclimate3114>
- Powell, T.L., Galbraith, D.R., Christoffersen, B.O., Harper, A., Imbuzeiro, H.M.A., Rowland, L., Almeida, S., Brando, P.M., da Costa, A.C.L., Costa, M.H., Levine, N.M., Malhi, Y., Saleska, S.R., Sotta, E., Williams, M., Meir, P., Moorcroft, P.R., 2013. Confronting model predictions of carbon fluxes with measurements of Amazon forests subjected to experimental drought. *New Phytol.* 200, 350–365. <https://doi.org/10.1111/nph.12390>

- Restaino, C.M., Peterson, D.L., Littell, J., 2016. Increased water deficit decreases Douglas fir growth throughout western US forests. *Proc. Natl. Acad. Sci. U. S. A.* 113, 9557–9562. <https://doi.org/10.1073/pnas.1602384113>
- Ruehr, N.K., Law, B.E., Quandt, D., Williams, M., 2014. Effects of heat and drought on carbon and water dynamics in a regenerating semi-arid pine forest: A combined experimental and modeling approach. *Biogeosciences* 11, 4139–4156. <https://doi.org/10.5194/bg-11-4139-2014>
- Rupp, D.E., Li, S., Mote, P.W., Shell, K.M., Massey, N., Sparrow, S.N., Wallom, D.C.H., Allen, M.R., 2017. Seasonal spatial patterns of projected anthropogenic warming in complex terrain : a modeling study of the western US. *Clim. Dyn.* 48, 2191–2213. <https://doi.org/10.1007/s00382-016-3200-x>
- Sulman, B.N., Roman, D.T., Yi, K., Wang, L., Phillips, R.P., Novick, K.A., 2016. High atmospheric demand for water can limit forest carbon uptake and transpiration as severely as dry soil. *Geophys. Res. Lett.* 43, 9686–9695. <https://doi.org/10.1002/2016GL069416>
- Topp, G.C., Davis, J.L., Annan, A.P., 1980. Electromagnetic determination of soil water content: Measurements in coaxial transmission lines. *Water Resour. Res.* 16, 574–582. <https://doi.org/10.1029/WR016i003p00574>
- Tromp-van Meerveld, H.J., McDonnell, J.J., 2006. On the interrelations between topography, soil depth, soil moisture, transpiration rates and species distribution at the hillslope scale. *Adv. Water Resour.* 29, 293–310. <https://doi.org/10.1016/j.advwatres.2005.02.016>
- Venturas, M.D., Sperry, J.S., Hacke, U.G., 2017. Plant xylem hydraulics: What we understand, current research, and future challenges. *J. Integr. Plant Biol.* 59, 356–389. <https://doi.org/10.1111/jipb.12534>
- Warren, J.M., Meinzer, F.C., Brooks, J.R., Domec, J.C., 2005. Vertical stratification of soil water storage and release dynamics in Pacific Northwest coniferous forests. *Agric. For. Meteorol.* 130, 39–58. <https://doi.org/10.1016/j.agrformet.2005.01.004>
- Williams, M., Law, B.E., Anthoni, P.M., Unsworth, M.H., 2001. Use of a simulation model and ecosystem flux data to examine carbon-water interactions in ponderosa pine. *Tree Physiol.* 21, 287–298. <https://doi.org/10.1093/treephys/21.5.287>
- Williams, M., Rastetter, E.B., Fernandes, D.N., Goulden, M.L., Wofsy, S.C., Shaver, G.R., Melillo, J.M., Munger, J.W., Fan, S.M., Nadelhoffer, K.J., 1996. Modelling the soil-plant-atmosphere continuum in a *Quercus-acer* stand at Harvard forest: The regulation of stomatal conductance by light, nitrogen and soil/plant hydraulic properties. *Plant, Cell Environ.* 19, 911–927. <https://doi.org/10.1111/j.1365-3040.1996.tb00456.x>
- Yuan, W., Zheng, Y., Piao, S., Ciais, P., Lombardozzi, D., 2019. Increased atmospheric vapor pressure deficit reduces global vegetation growth. *Sci. Adv.* 1–13.
- Zweifel, R., Steppe, K., Sterck, F.J., 2007. Stomatal regulation by microclimate and tree water relations: Interpreting ecophysiological field data with a hydraulic plant model. *J. Exp. Bot.* 58, 2113–2131. <https://doi.org/10.1093/jxb/erm050>

4.8 Figures

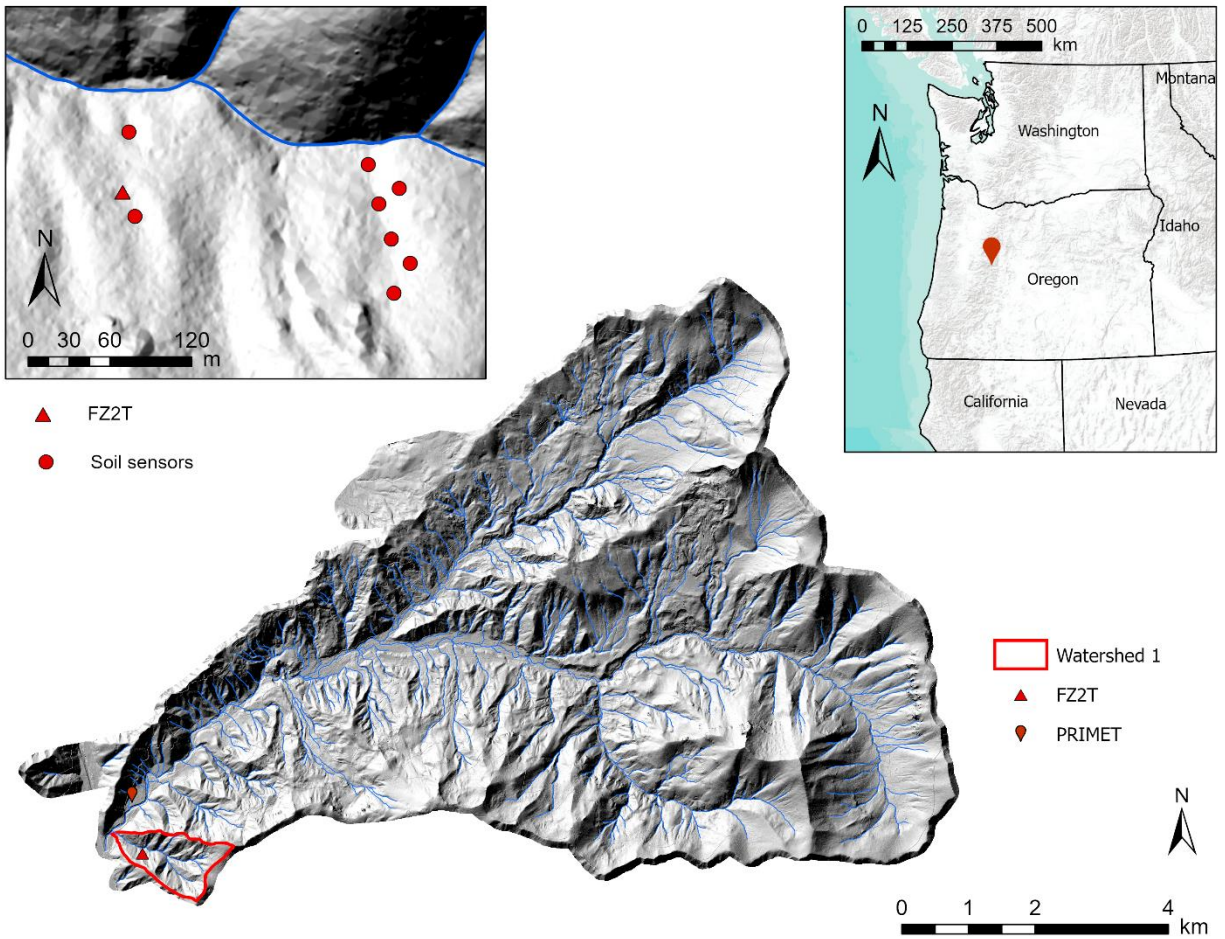


Figure 4.1 Site map

Location Watershed 1 at the HJ Andrews Experimental Forest near Blue River, Oregon. Soil water content at 50 cm was collected along two hillslopes at nine sites, and site FZ2T was used to calibrate the SPA model.

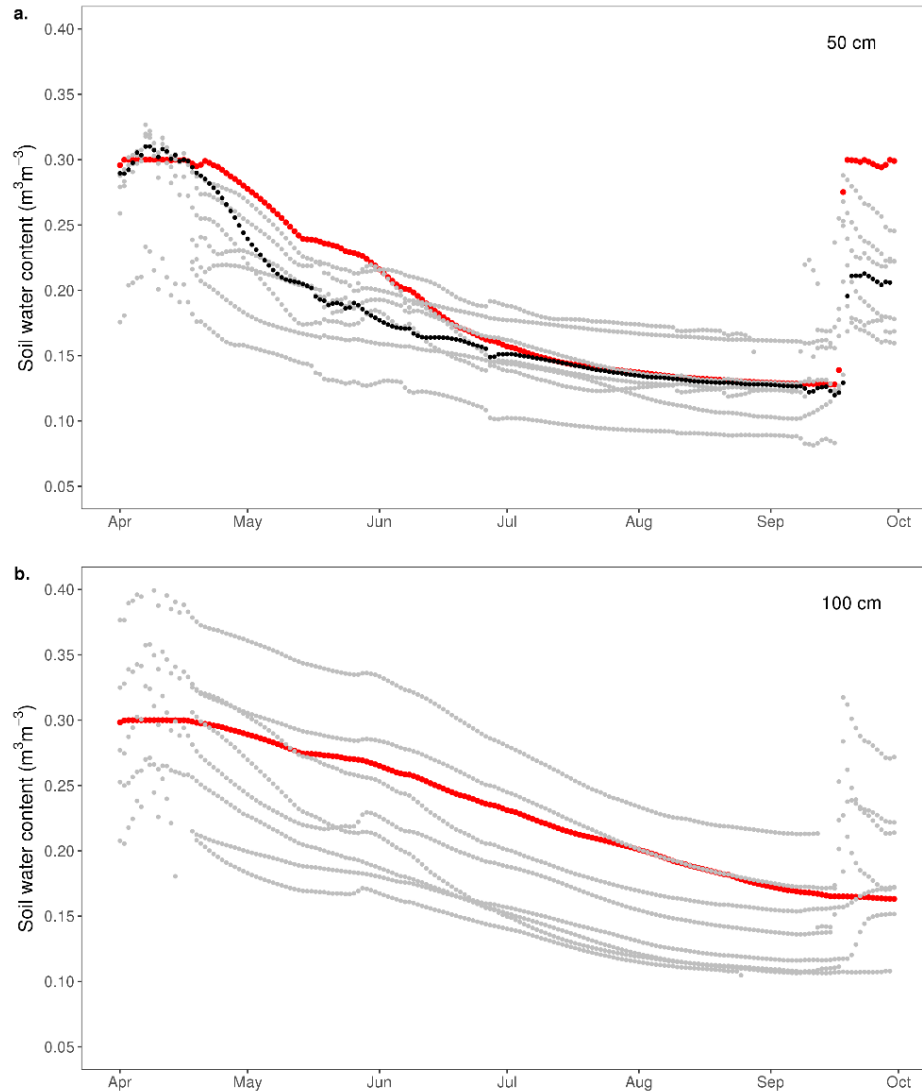


Figure 4.2 Soil water content for calibration

Time series of measured mean daily soil water content (black and grey points) and modelled mean daily soil water content (red points) at 50 cm (a) and 100 cm (b) from April 1–September 30, 2019. Daily measurements of soil water content at site FZ2T at 50 cm (black points) were used to calibrate the model.

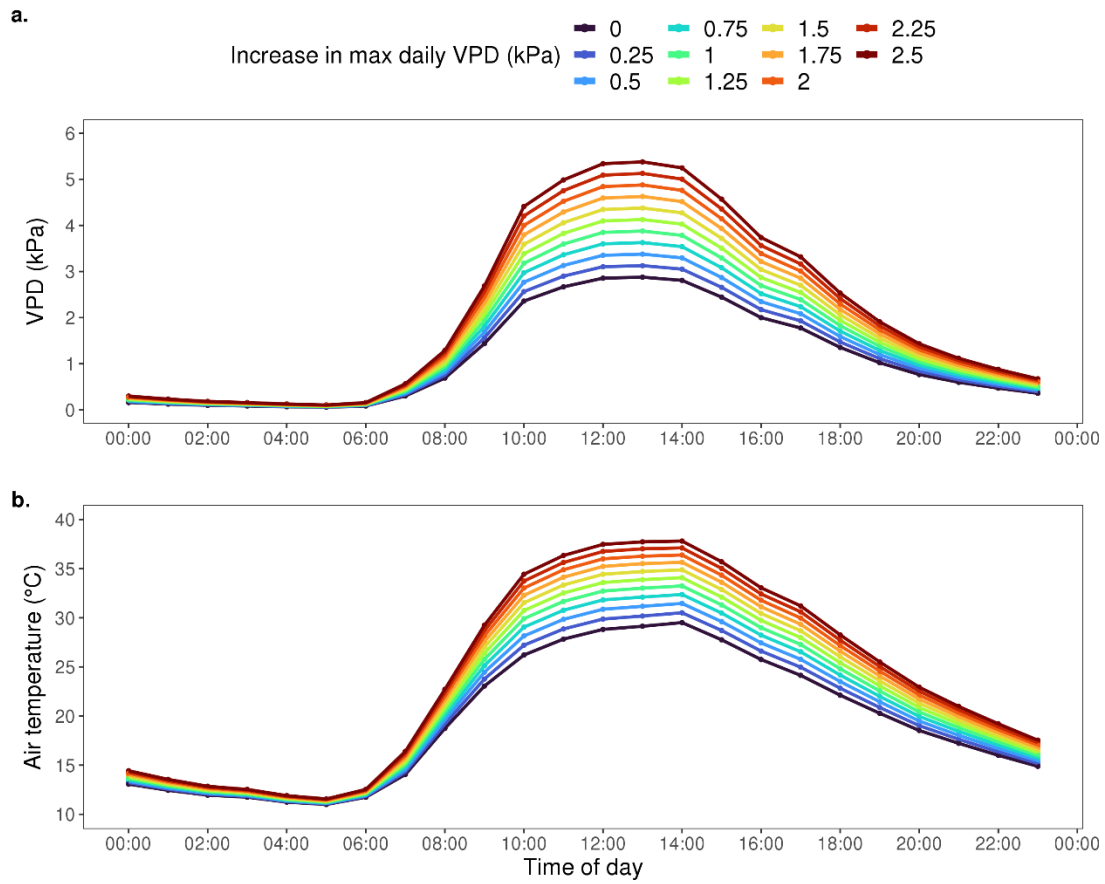


Figure 4.3 Climate scenarios

Hourly vapor pressure deficit (VPD, **a.**) and hourly air temperature (**b.**) on July 14th under the ten climate scenarios that increased the daily maximum VPD, relative to 2019 conditions.

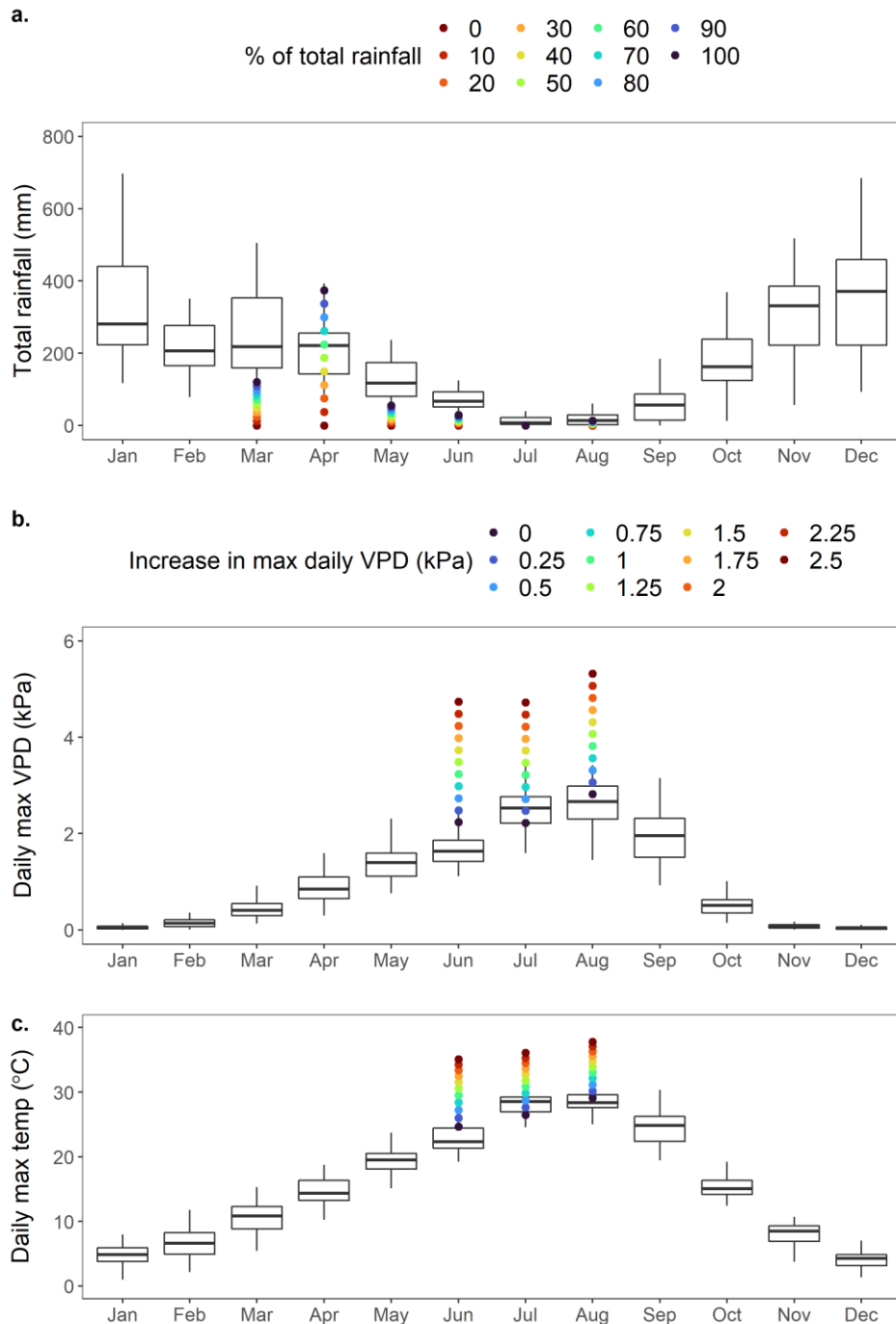


Figure 4.4 Monthly climate

Distribution of monthly total rainfall (**a**), monthly mean daily maximum VPD (**b**), and monthly mean daily maximum air temperature (**c**) from 1989–2019 and monthly means for experimental climate scenarios that increase daily max VPD during June, July, and August and decrease rainfall from March to August. The boxplot shows the interquartile range which included the median, 25th, and 75th percentiles with whiskers representing the smallest and largest values no further than 1.5 times the interquartile range. Extreme outliers beyond the whiskers were omitted from the graphic to improve visualization of data.

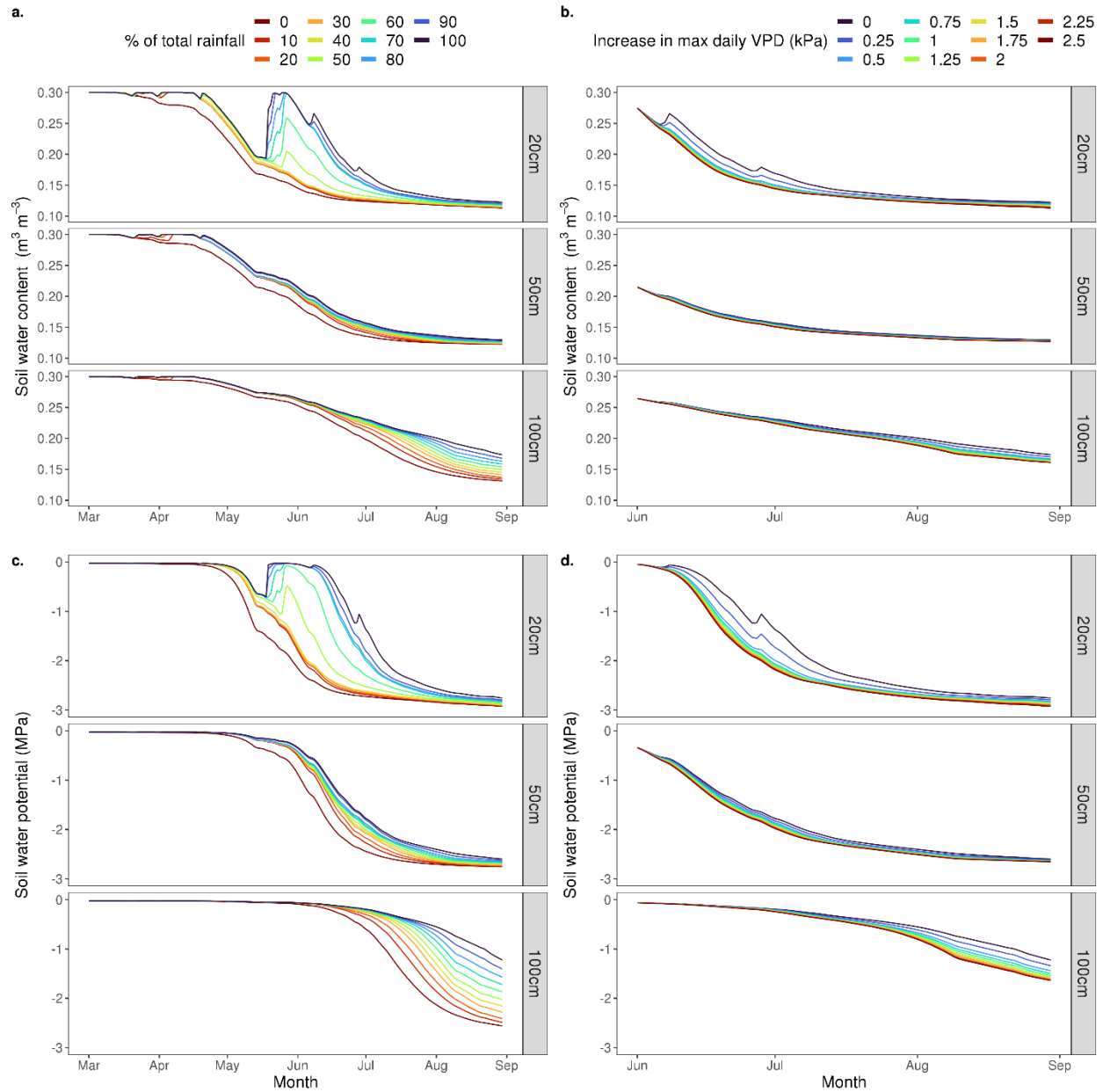


Figure 4.5 Soil water content and water potential

Modelled soil water content and soil water potential at 20, 50, and 100 cm for decreased rainfall from March to August (**a, c**) and increased VPD from June to August (**b, d**).

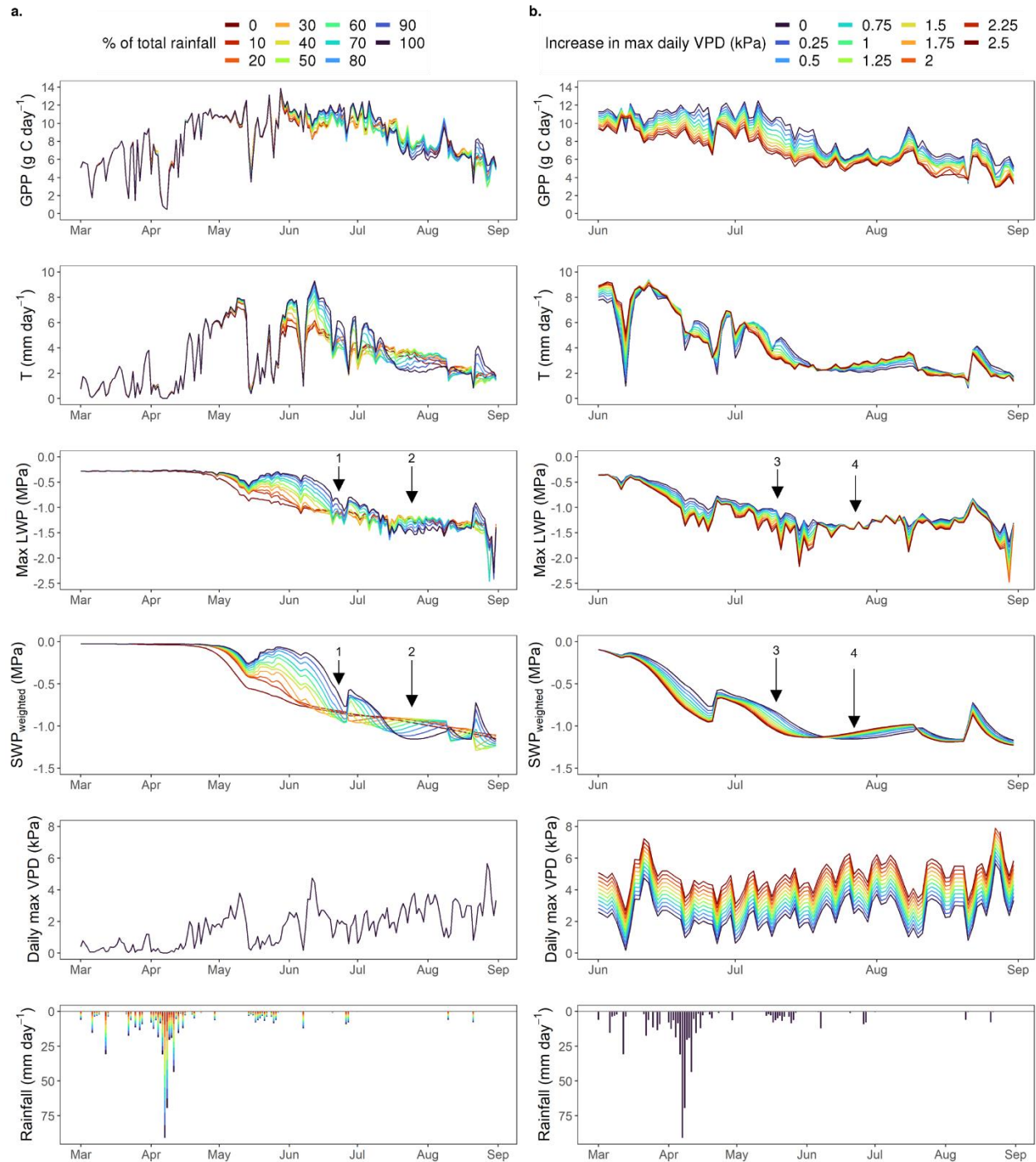


Figure 4.6 Temporal dynamics of gross primary production and transpiration

Model results for daily total transpiration (T), daily total gross primary production (GPP), and daily max leaf water potential (LWP), and weight soil water potential (SWP) under various scenario for rainfall (**a**) and daily max VPD (**b**). The control model experimental is shown in panel a. with precipitation and VPD for 2019. Experimental changes to rainfall occurred from March 1–August 31 and experimental changes to VPD and air temperature occurred during the climatological summer, June 1–August 31.

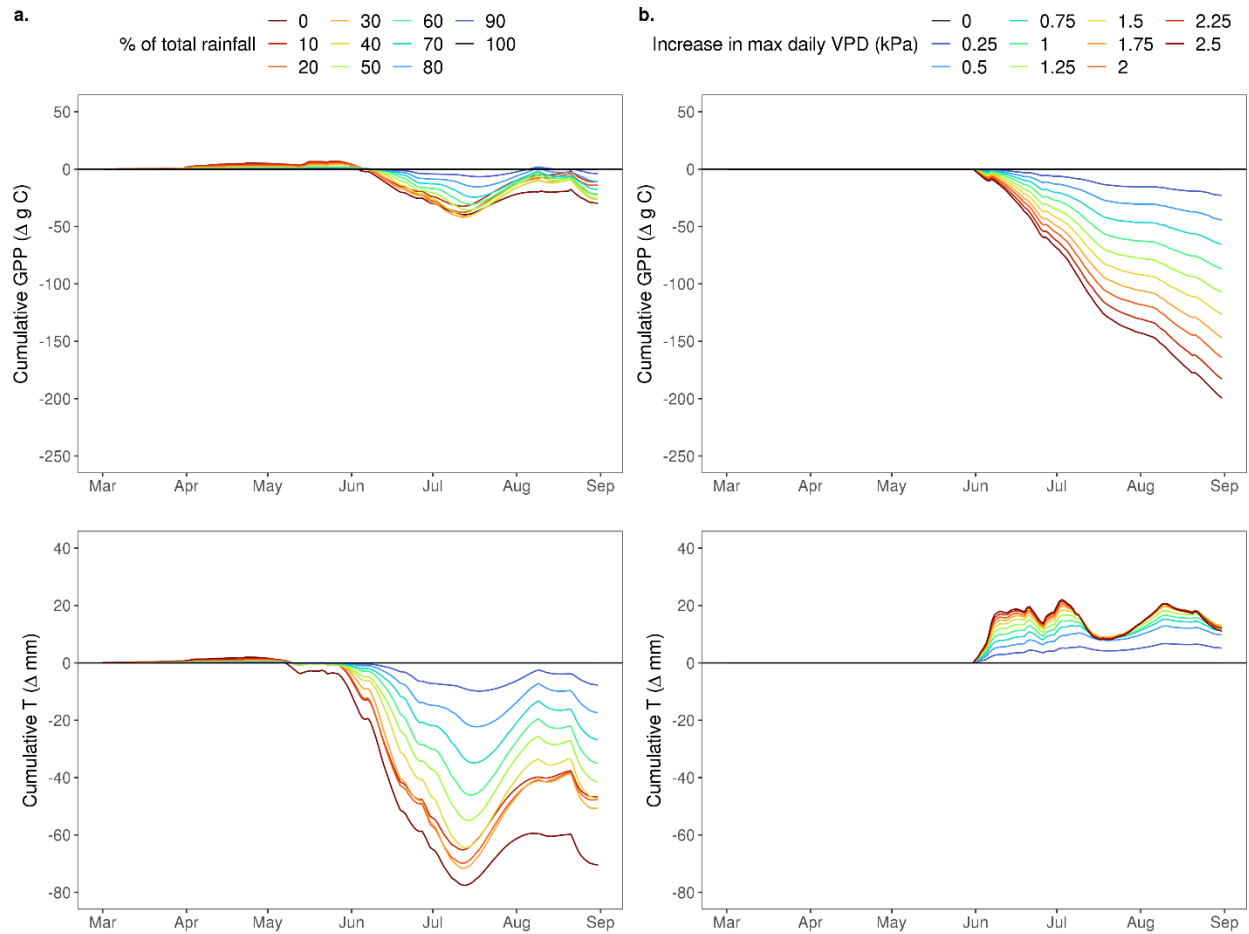


Figure 4.7 Change in cumulative gross primary production and transpiration

The difference in cumulative gross primary productivity (GPP) and transpiration (T) from the 2019 baseline model ($\Delta = 0$) in response to decreased rainfall scenarios from March to August (a) and increased VPD scenarios from June to August (b).

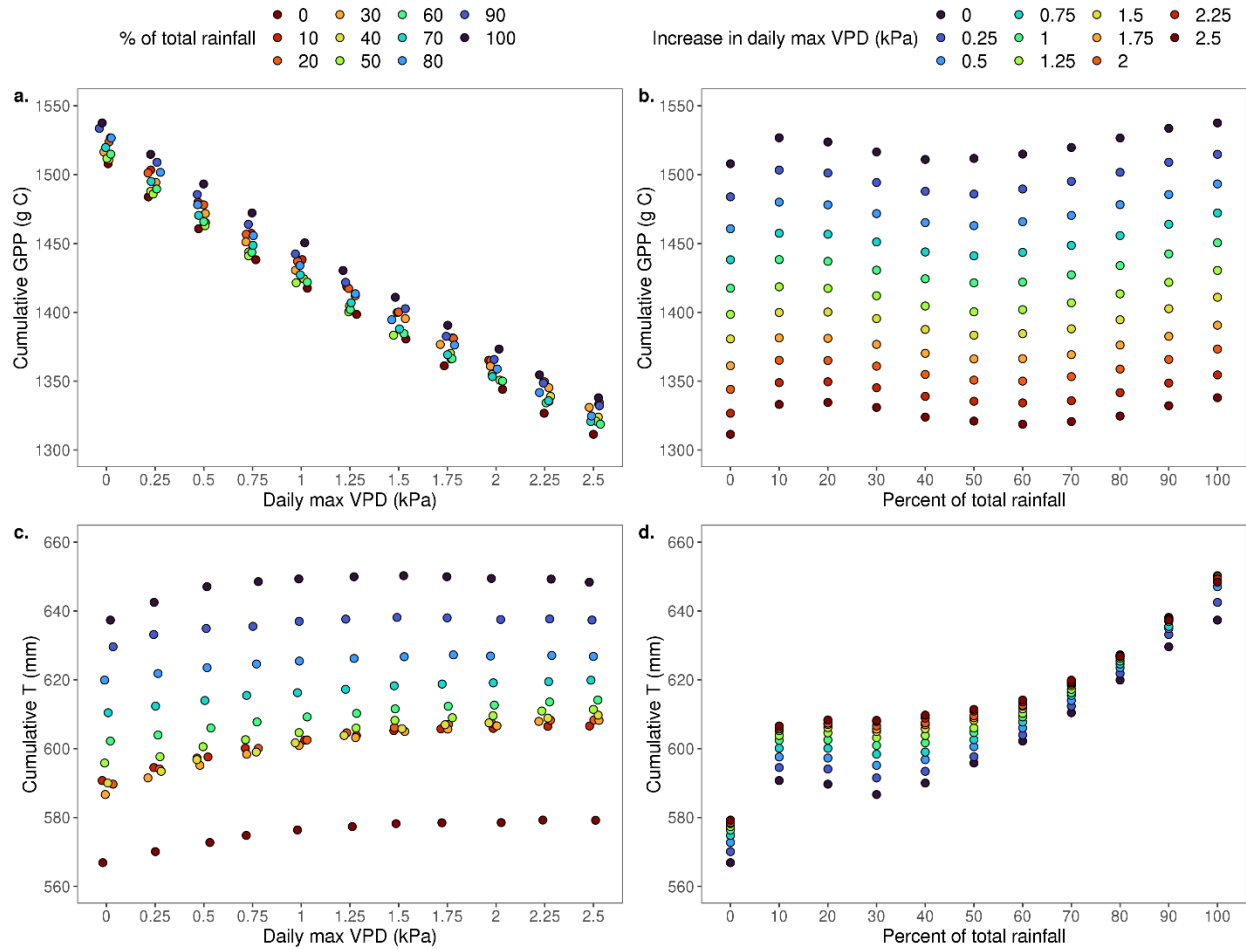


Figure 4.8 Interactive effects of climate modifications

The interactive effect of decreased rainfall and increased VPD on cumulative gross primary production (GPP) and cumulative transpiration (T) from March–August with colors representing percent of total rainfall (a, c) and increase in daily max VPD (b, d).

4.9 Tables

Table 4.1 Model parameters

Parameters used in the Soil-Plant-Atmosphere model, which were derived from literature values or estimated using a Latin hypercube (LH) sampling scheme.

Parameters	Units	Source	Value
Foliar nitrogen concentration	g N m ⁻² leaf area	Berner & Law, 2016	1.08
Foliar carbon concentration	g C m ⁻² leaf area	Berner & Law, 2016	51.4
Leaf area index (LAI)	unitless	Barnard, 2009	7.5
Leaf capacitance	mmol m ⁻² MPa ⁻¹	Licata, 2003	625
RuBP carboxylation catalytic rate coefficient at 30 °C (V _{cmax})	μmol g ⁻¹ N s ⁻¹	Licata, 2003	26.3
Electron transport rate coefficient at 30 °C (J _{max})	μmol g ⁻¹ N s ⁻¹	Licata, 2003	74.73
Maximum rooting depth	m	Fan et al., 2017	2
Root resistivity	MPa s g mmol ⁻¹	Bonan et al., 2014	25
Tree height	m	estimate	30
Soil porosity	m ³ m ⁻³	estimate	0.3
Whole plant (stem) hydraulic conductivity*	mmol m ⁻¹ s ⁻¹ MPa ⁻¹	estimated with LH Ruehr et al., 2014	12
Water use efficiency*	unitless	estimated with LH	537
Minimum leaf water potential*	MPa	estimated with LH Bond & Kavanagh, 1999	-2.8
Total root biomass per volume*	g m ⁻³	estimated with LH Lee et al., 2007	1330
Root biomass to 50% of rooting depth*	g m ⁻³	estimated with LH	150
Soil water retention constant a*	unitless	estimated with LH	-0.015
Soil water retention constant b*	unitless	estimated with LH	3.38
Soil water retention constant c*	unitless	estimated with LH	0.159
Soil water retention constant d*	unitless	estimated with LH	0.025

*Adjusted during model parameterization using a Latin hypercube (LH) sampling scheme

Table 4.2 Monthly rainfall

Minimum, maximum, and mean monthly rainfall from 1989–2019 compared to 2019 conditions (rain100).

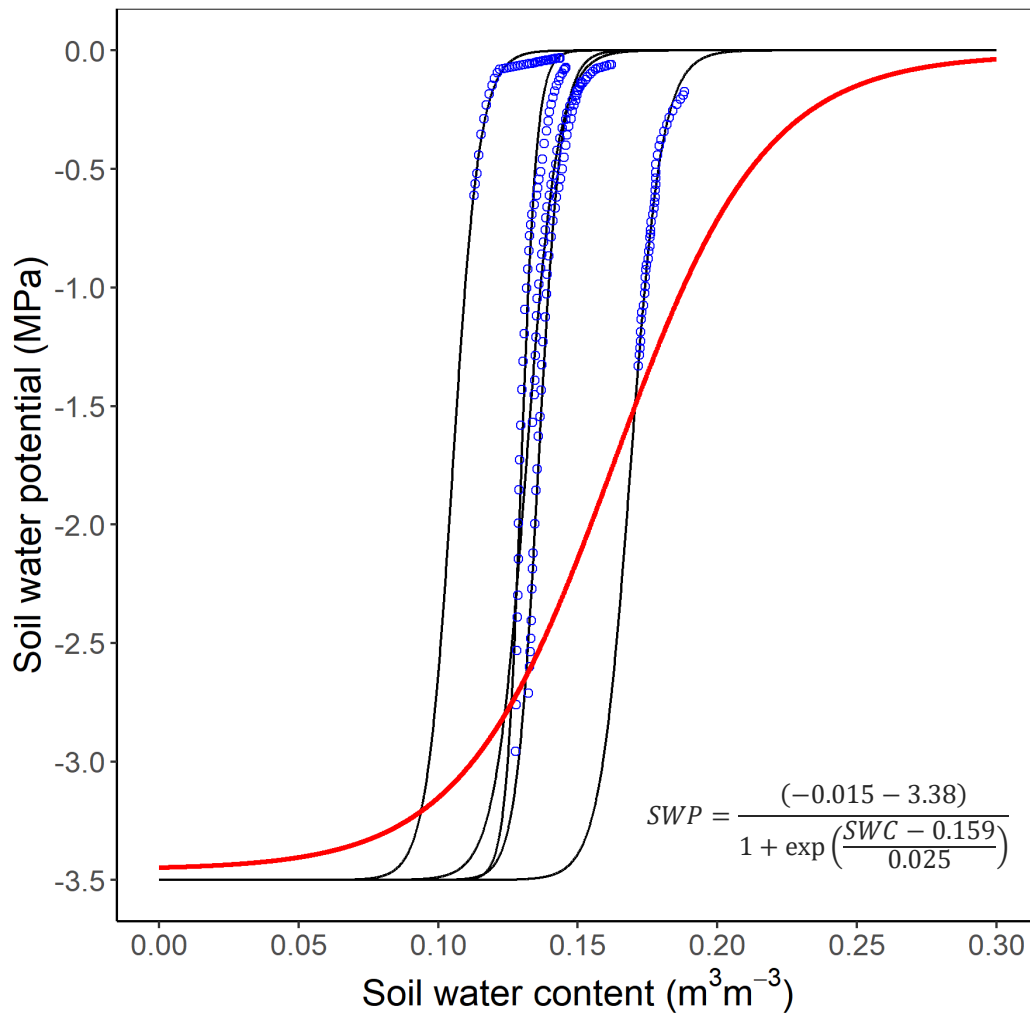
	mean	min	max	rain100 (2019)
March	254	41	505	121 mm
April	207	87	239	374 mm
May	127	9	236	56 mm
June	73	8	184	29 mm
July	13	0	40	0.3 mm
August	23	0.3	121	13 mm

Table 4.3 Monthly vapor pressure deficit and temperature

Minimum, maximum, and mean daily max VPD and air temperature from 1989–2019 compared to mean daily max VPD and mean daily max temperature in 2019 (vpd0).

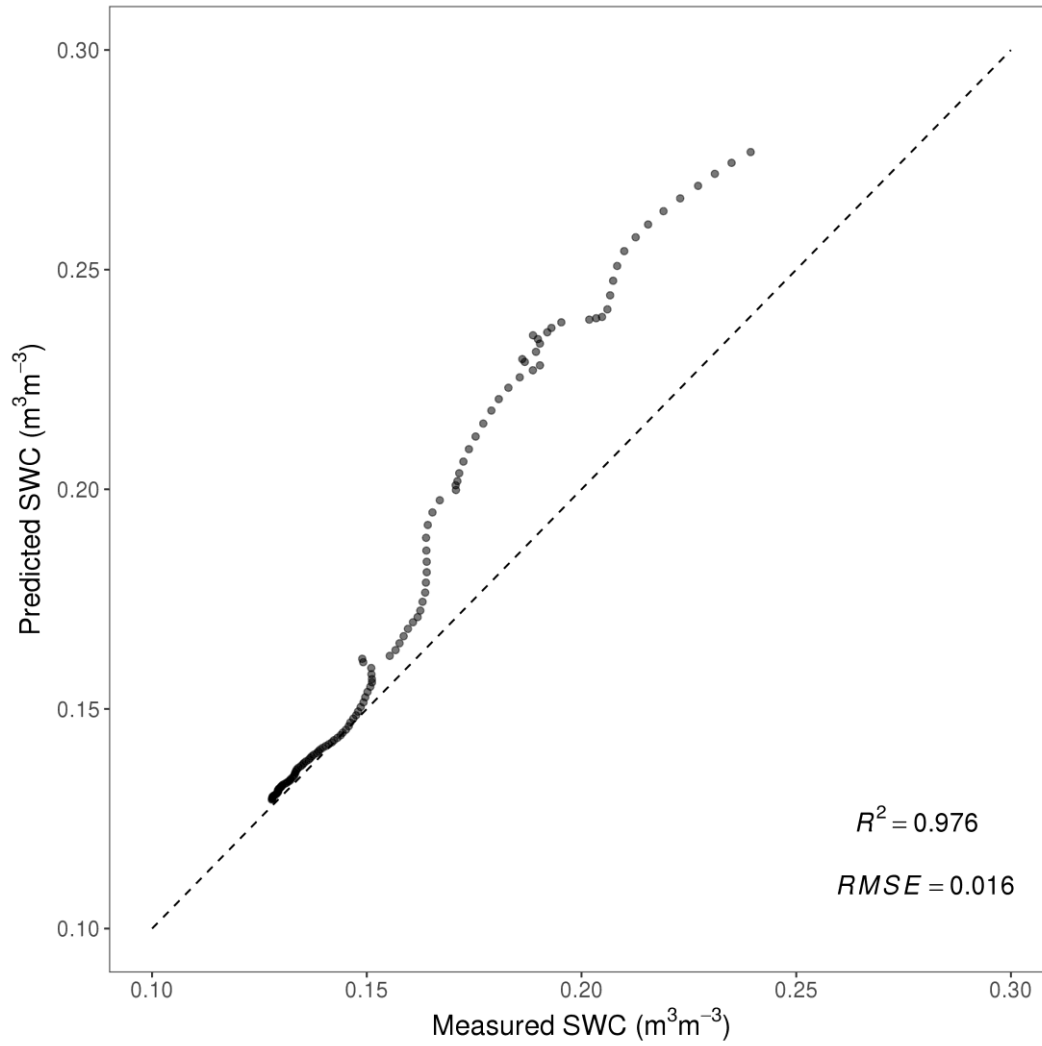
	mean	min	max	vpd0 (2019) mean	vpd2.5 mean
June	1.82 kPa 23.2 °C	1.11 kPa 19.2 °C	4.33 kPa 34.1 °C	2.2 kPa 24.7 °C	4.7 kPa 35.1 °C
July	2.55 kPa 28.3 °C	1.07 kPa 20.1 °C	4.96 kPa 36.7 °C	2.2 kPa 26.5 °C	4.7 kPa 36.1 °C
August	2.69 kPa 28.5 °C	1.46 kPa 23.9 °C	5.29 kPa 37.3 °C	2.8 kPa 29.1 °C	5.3 kPa 37.8 °C

4.10 Appendices



Appendix 4.1 Soil water retention curve

The sigmoid relationship of soil water potential (SWP) and soil water content (SWC) determined through parameterization of the model (red line) as compared to the sigmoid relationship (black line) fit to field observations of SWC and SWP at 50 cm (blue dots) during a period without rain, July 1–August 10, 2019. Parameters for the sigmoid relationship were adjusted using a Latin hypercube sampling scheme to find the best agreement between measured and predicted soil water content at 50 cm.



Appendix 4.2 Measured versus predicted soil water content

Measured versus modeled daily mean soil water content ($\text{m}^3 \text{m}^3$) from May 1–August 31, 2019.

CHAPTER 5

5.1 Summary of Conclusions

The impact of climate change on forest ecosystems in the 21st century include climate-related increases in tree mortality (Allen et al., 2015; Anderegg et al., 2015), more frequent and severe wildfire events (Higuera and Abatzoglou, 2021), and reductions in vegetation growth (Yuan et al., 2019). Extreme drought and heat in recent years has raised concerns about the resilience of forests to a changing climate. Scientists and land managers have suggested forest management practices like thinning in order to increase soil moisture availability and increase forest resilience, particularly during seasonally dry periods (Grant et al., 2013). Yet, studies have reported a wide range of eco-hydrologic responses to thinning across a range of geo-climatic conditions (Tague et al., 2019). The mixed results of forest thinning demonstrate how an incorrect understanding of the inter-relationships between climate, soils, vegetation, and hydrology could lead to ineffective or counterproductive management prescriptions.

This research aimed to improve our understanding of the relationships between climate, vegetation, and soil hydrology in steep, mountainous landscapes of the Pacific Northwest, U.S.A. This work contributes to ongoing efforts to refine our process-based understanding of tree water stress in even-aged stands of Douglas-fir (*Pseudotsuga menziesii*), the most prevalent forest type in the Pacific Northwest. Douglas-fir forests in this region are subject to a Mediterranean climate with hot and dry summers where water stress conditions will be exacerbated by a changing climate (Jiang et al., 2019). The studies in this dissertation combined field, lab, and modelling approaches to address: (a) factors that control soil moisture patterns in steep, variable terrain, (b) tree growth respond to interannual climate variability, and (c) the relative role of atmospheric and soil water stress on gross primary productivity and transpiration.

Findings from this research are important for informing forest management aimed at reducing ecosystem water stress. Below I outline key findings and important next steps for understanding the future of forest ecosystems in a warmer, drier climate.

In Chapter 2, I examined the soil, vegetation, and topographic factors that controlled spatial patterns of soil moisture in steep, complex terrain in the western Cascade Mountains of Oregon. I expected soil moisture would be influenced by the horizontal redistribution of water following surface topography. Contrary to expectations, I found persistent spatial patterns in soil moisture which were weakly related to topography with divergent hillslopes being, on average, wetter than convergent hollows. Soil moisture was more strongly related to soil properties—specifically, the rock content and the amount of water stored in the soil after draining to field capacity. Soils at the site were relatively deep ($\bar{x} = 2.3$ m), well-drained, and underlain by porous, highly weathered saprolite. Our results suggest that these subsurface conditions prevent the horizontal redistribution of water at shallow depths, but additional research is needed to mechanistically describe the spatial organization of soil properties, which were strongly related to soil moisture in the upper soil profile (< 1 m). To that end, I recommend that future research test the spatial extent and depths at which soils and topography interact to modify hydrological processes in steep, complex topography. This is especially challenging in mountainous terrain where we lack detailed information on soil properties and their spatial variability at hillslope to watershed scales. Investigations of subsurface water storage across topographic gradients at multiple spatial scales may benefit from geophysical tools (Flinchum et al., 2018), which could provide insight into scale- and depth-dependent physical, chemical, and/or biological processes that regulate soil moisture available to vegetation.

In Chapter 3, I examined the sensitivity of latewood growth in Douglas-fir trees to interannual climate variability in the West Cascades of Oregon. I expected latewood growth to be more sensitive to vapor pressure deficit (VPD) than to precipitation because subsurface water storage in this region is replenished in both wet and dry winters suggesting a reliable water supply for plants during the dry season (Hahm et al., 2019). I found that latewood growth of Douglas-fir was highly sensitive to the average daytime VPD from mid-June to mid-July and less sensitive to the timing and amounts of precipitation. Moreover, I found that the soil moisture deficit over the growing season varied across sites located along a steep hillslope gradient, and that moisture status mediated the effect of early summer VPD on seasonal growth. These results demonstrated that amount of precipitation that is stored in the soil for plant use over the growing season may influence spatial patterns of forest sensitivity to atmospheric water stress (e.g., increased temperature and VPD). Future research should focus on mechanistic understanding of localized processes that affect the spatial patterns of Douglas-fir growth under increased VPD. Additionally, tree ring analysis of carbon stable isotopes could be a more sensitive indicator of the stomatal limitations of Douglas-fir during periods of water stress. I recommend that future studies investigate the response of carbon isotope signatures in latewood to climate variables to further understand physiological water stress in Douglas-fir. It is possible that stable carbon isotopes signatures may be more sensitive to climate later into the summer when the majority of cellulose is incorporated into the latewood during the phase of cell wall thickening (Belmecheri et al., 2018).

In Chapter 4, I used a process-based model to investigate the relative effect of increasing VPD versus decreasing rainfall on physiological water stress in Douglas-fir. Summer temperatures in the Pacific Northwest are projected to warm by 1.2 to 4.7 °C from 2014–2070

under the Representative Concentration Pathway 4.5 while spring and summer rainfall is projected to decline by as much as 34% (Mote et al., 2013). I found that precipitation-based drought is likely to have a minor effect on forest productivity relative to increasing VPD. For example, cumulative GPP declined by 6% under a 5 °C warming in the summer but declined only 1% due to a 30% reduction in rainfall. Our results demonstrated that heat-driven increases in VPD are likely to reduce forest productivity regardless of soil moisture availability. In contrast, decrease in rainfall will have a negative effect on cumulative transpiration, which we found declined by 11% under prolonged spring and summer drought. While most of the soil water in the upper meter was depleted by late summer without spring and summer rainfall, the availability of soil water in deep soils (>1 m) mitigated plant hydraulic stress. This demonstrates that decreases in rainfall will reduce transpiration over the growing season but may not induce additional water stress on Douglas-fir if deep water storage is accessible. Heterogeneity in subsurface storage in steep, complex terrain, as highlighted in Chapter 3, could create a range of physiological and growth responses in Douglas-fir. Water stored in the matrix and fractures of weathered rock, below the lower boundary of most field investigations, can be a significant source of water for vegetation in mountain ecosystems with a Mediterranean climate (Klos et al., 2018). Future research that links deep subsurface structure to water availability for vegetation and integrates climate feedback across the soil-plant-atmosphere continuum will greatly improve our understanding of how forest vegetation will response to a changing climate.

Collectively, these results support findings that climate change poses increased risks for water stress in Douglas-fir forests in the West Cascade Mountains of Oregon. Specifically, local soil properties are a greater control than topography on shallow soil moisture and latewood growth is highly sensitive to VPD between June and July. In addition, I found that elevated VPD

significantly reduced gross primary productivity independent of soil moisture stress. Overall, this work contributes to a growing body of literature on the relative controls on subsurface water storage and mechanistic understanding of forest water stress with critical implications for management practices aimed at creating more drought resilient forests.

5.2 References

- Allen, C.D., Breshears, D.D., McDowell, N.G., 2015. On underestimation of global vulnerability to tree mortality and forest die-off from hotter drought in the Anthropocene. *Ecosphere* 6, 1–55. <https://doi.org/10.1890/ES15-00203.1>
- Anderegg, W.R.L., Hicke, J.A., Fisher, R.A., Allen, C.D., Aukema, J., Bentz, B.J., Hood, S., Lichstein, J.W., Macalady, K., McDowell, N.G., Pan, Y., Raffa, K., Sala, A., 2015. Tree mortality from drought, insects, and their interactions in a changing climate Research review Tree mortality from drought, insects, and their interactions in a. <https://doi.org/10.1111/nph.13477>
- Flinchum, B.A., Holbrook, W.S., Grana, D., Parsekian, A.D., Carr, B.J., Hayes, J.L., Jiao, J., 2018. Estimating the water holding capacity of the critical zone using near-surface geophysics. *Hydrol. Process.* <https://doi.org/10.1002/hyp.13260>
- Grant, G.E., Tague, C.L., Allen, C.D., 2013. Watering the forest for the trees: An emerging priority for managing water in forest landscapes. *Front. Ecol. Environ.* 11, 314–321. <https://doi.org/10.1890/120209>
- Hahn, W.J., Dralle, D.N., Rempe, D.M., Bryk, A.B., Thompson, S.E., Dawson, T.E., Dietrich, W.E., 2019. Low subsurface water storage capacity relative to annual rainfall decouples Mediterranean plant productivity and water use from rainfall variability. *Geophys. Res. Lett.* 6544–6553. <https://doi.org/10.1029/2019GL083294>
- Higuera, P.E., Abatzoglou, J.T., 2021. Record-setting climate enabled the extraordinary 2020 fire season in the western United States. *Glob. Chang. Biol.* 27, 1–2. <https://doi.org/10.1111/gcb.15388>
- Jiang, Y., Kim, J.B., Trugman, A.T., Kim, Y., Still, C.J., 2019. Linking tree physiological constraints with predictions of carbon and water fluxes at an old-growth coniferous forest. *Ecosphere* 10. <https://doi.org/10.1002/ecs2.2692>
- Klos, P.Z., Goulden, M.L., Riebe, C.S., Tague, C.L., O’Geen, A.T., Flinchum, B.A., Safeeq, M.,

- Conklin, M.H., Hart, S.C., Berhe, A.A., Hartsough, P.C., Holbrook, W.S., Bales, R.C., 2018. Subsurface plant-accessible water in mountain ecosystems with a Mediterranean climate. *Wiley Interdiscip. Rev. Water* e1277. <https://doi.org/10.1002/wat2.1277>
- Mote, P.W., Bethel, J., Capalbo, S.M., Dalton, M.M., Eigenbrode, S.E., Glick, P., Houston, L., Littell, J.S., Lynn, K., Raymondi, R.R., Reeder, W.S., Snover, A.K., 2013. Climate Change in the Northwest, Brief Summary. <https://doi.org/10.5822/978-1-61091-512-0>
- Tague, C.L., Moritz, M., Hanan, E., 2019. The changing water cycle: The eco-hydrologic impacts of forest density reduction in Mediterranean (seasonally dry) regions. *WIREs Water* 6, 1–15. <https://doi.org/10.1002/wat2.1350>
- Yuan, W., Zheng, Y., Piao, S., Ciais, P., Lombardozzi, D., 2019. Increased atmospheric vapor pressure deficit reduces global vegetation growth. *Sci. Adv.* 1–13.